Hydrate formation and CO2 – CH4 exchange in sandstone

–

An experimental study with emphasis on the role of initial brine saturation and salinity

Master Thesis in Reservoir Physics

by

Hans Berge

Department of Physics and Technology
University of Bergen
Norway

June 2013

Summary

Recent research activity has demonstrated the viability of producing methane from gas hydrate bearing sediments by injecting and sequestering CO_2 in a process where CO_2 replace methane in gas hydrate by a process called $CO_2 – CH_4$ exchange.

The work presented in this thesis consist of a series of ten experiments designed to increase the basic knowledge of hydrate formation and subsequent methane production by $CO_2 – CH_4$ exchange in sandstone with emphasis on the effect of initial water saturation and brine salinity. Methane hydrate was formed at 8.3 MPa and 4 °C in ten partially saturated Bentheimer sandstone cores with varying initial water saturation and salinities. The hydrate formations were reproducible and showed a strong correlation between hydrate growth rate and both salinity and water saturation, where increased salinity or water saturation resulted in slower formation and more residual water. A correlation between initial growth rate and hydrate saturation were observed where the change in growth rate were proportional to the change in saturation. Hydrate bearing sandstone core plugs with high residual water saturation were successfully obtained by using initial water saturation above 0.6.

$CO_2 – CH_4$ exchange was successfully performed on five hydrate bearing core plugs with different hydrate and water saturations. $CO_2 – CH_4$ exchange were performed by injecting liquid CO_2 and a 75 mol% N_2 + 25 mol% CO_2 mix at a rate of 0.02 ml/min and measuring the effluent composition with a GC and, for some cores, the mass flow with a mass flow meter. The highest methane recovery from hydrate was estimated at 52%.

Nitrogen was successfully used to dissolve plugging in two experiments without any resulting large scale dissociation. Co-injection of nitrogen and carbon dioxide showed excellent ability to hinder secondary hydrate formation during exchange without affecting the recovery.

One experiment was conducted by performing repeated formations and dissociations on the same core. There was observed a significant increase in formation rate when the pressure was maintained between dissociation and formation, and a significant increase in dissociation rate when the time between formation and dissociation were long.

Table of Contents

Introduction

Natural gas hydrates are solid, ice-like, crystalline compounds consisting of gas molecules (guest) encapsulated by water molecules in cage-like structures where the guest has a stabilizing effect. There are three crystalline hydrate-structures known to be formed under moderate pressure conditions (<10 MPa); sI, sII and sH, where Methane (CH_4), the most common hydrate former in nature, and carbon dioxide (CO_2) are among those who form structure sI (Sloan and Koh 2008). The driving force behind hydrate formation is called supersaturation and is dependent on how far into the hydrate stable region the formation takes place.

Gas hydrate was first discovered in the 1800 but the interest in hydrates did not begin until the emergence of the modern petroleum industry. Formation of gas hydrate plugs in petroleum pipelines and production facilities was early recognized as a problem and led to the first major research efforts on gas hydrates, spanning World War II, which were focused on hydrate prevention and removal. Hydrate as an energy resource was not recognized until 1965 when Makogen and his coworkers announced gas hydrates in the Siberian permafrost (Sloan and Koh 2008). There has been no systematic effort to map the global hydrate reserves and the estimates put forward vary widely (10^{15} – 10^{18} m^3 of gas) (Sloan and Koh 2008) but even the most conservative estimates are large and there is a consensus that the global hydrate reserve contains enormous amounts of energy. The global energy demand, the increasing focus on cleaner burning fuels and the finite nature of fossil fuels, has made gas hydrate a potential energy source which receives increasing attention both from countries, companies and universities. Research on production from gas hydrate accumulations has over the last decade moved from the laboratory to the field, where multiple successful field tests has shown the viability of production and at the same time supported the emergence of more accurate modeling tools (Sloan and Koh 2008).

Some compounds like salts, are known to inhibit hydrate growth by changing the chemical potential of water and thereby moving the hydrate stable region. Brine salinity is therefore an important parameter to consider when dealing with hydrate systems. Hydrate formation has previously been shown to be strongly dependent on brine salinity where increased salinity have been reported to limit the amount of hydrate produced (Husebø et al. 2008). Salinity are together with water saturation (S_{wi}) major controlling factors for the amount of residual water saturation (S_{wf}) in an excess-gas hydrate system (Husebø et al. 2008).

By exposing CH_4 hydrate to a more stable hydrate former, CO_2, CH_4 may be extracted while CO_2 are stored without dissociating the hydrate. This technology offers a number of advantages over the more conventional production methods which are based on dissociating the hydrate by depressurization, heating or chemical melting. The geo-mechanical integrity of the formation is maintained, water and sand production are kept at a minimum and CO_2 are stored in a way that increases the existing hydrates stability. CO_2 – CH_4 exchange in sandstone cores has been shown to be favorable (Graue et al. 2008) and a field test in the North Slope of Alaska in 2011 – 2012 has successfully produced methane by injecting CO_2

and N_2 into a hydrate formation, proving the viability of the production method (Schoderbek et al. 2012). There is still a great need for increased basic understanding of hydrates in porous sediments, especially for the CO_2 - CH_4 exchange process.

Gas hydrates and the CO_2 – CH_4 exchange process has been a focus area at the Department of Physics and technology where previous studies include the verification and validation of CO_2 – CH_4 exchange in porous sandstone (Ersland 2008, Graue et al. 2008), the investigation of the effect of variations in boundary conditions on formation and dissociation kinetics (Birkedal 2009), the development of resistivity measurement capabilities (Hauge 2011) and the investigation of initial brine salinity on fill fraction and growth pattern (Husebø et al. 2008). The work presented in this thesis takes aim to increase the basic knowledge on gas-hydrates in porous sediments and focuses around the effect of varying initial water saturation and salinity.

The content of this thesis are divided into 5 chapters. Chapter 1 contains some basic theory of gas hydrate and an overview of hydrates in nature including two case studies. Chapter 2 introduces CO_2 – CH_4 exchange and includes a small review of previous relevant laboratory work and a field trial. Experimental setups and procedures including modifications made to the setups are described in Chapter 3 while the results are presented and discussed in Chapter 4. The main conclusion and suggestions for future work are presented in Chapter 5.

Chapter 1 Fundamental Principles of Natural Gas Hydrates

1.1 Gas Hydrates

Gas hydrates are ice like, solid compounds, consisting of water and smaller guest molecules, also called hydrate formers. Water molecules surround the guest molecules in a crystalline lattice in which the guest stabilize the structure. In order to understand gas hydrates a brief review of the properties of water is presented.

1.1.1 Water and Water Properties

Water is the main component in gas hydrates. One of the most important properties of water is its ability to form hydrogen bonds. A water molecule consists of two hydrogen atoms covalently bound to an oxygen atom which forms an H-O-H angle of 104.5°. This angle in conjunction with the difference in hydrogen- and oxygen electronegativity makes the water molecule a permanent electric dipole. As illustrated in Figure 1.1a below, the water molecule can be described as having two negative poles near the oxygen atom and a positive pole near each of the hydrogen atoms. The hydrogen bond is a result of attractive (cohesive) forces between the negative and positive poles of two water molecules, illustrated in Figure 1.1 below. This bond is weaker than the covalent bonds, but is more than an order of magnitude larger than a typical van der Waals bond (Sloan and Koh 2008).

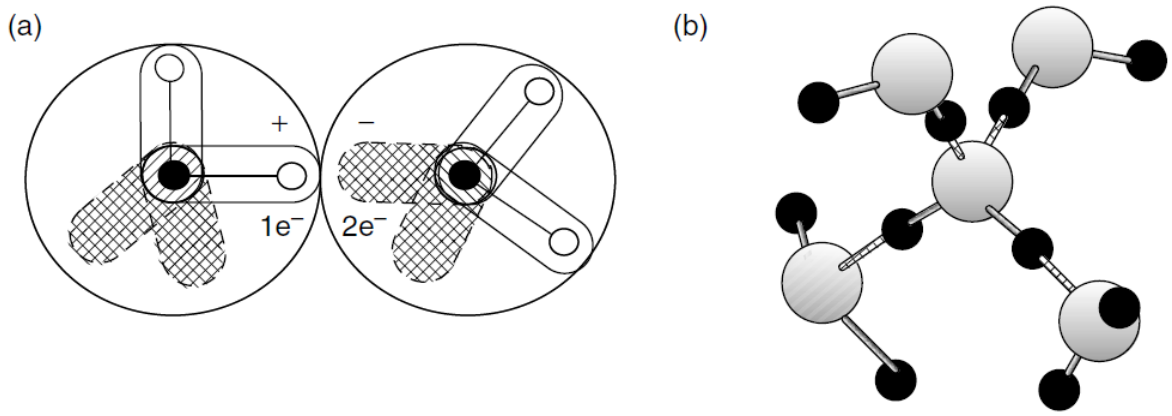

Figure 1.1: Hydrogen bonding of water molecules. (a) Between two water molecules (b) between four water molecules (Sloan and Koh 2008).

Water has a number of uncommon properties as a consequence of the hydrogen bond. It is a liquid at ambient temperature and pressure and has a boiling point 260 K higher than Methane, a non-polar molecule of comparable size. In solid state water has lower density than in liquid state. This is a direct effect of the hydrogen bonds which in addition to the cohesive force, separates the molecules rigidly. In ice and hydrates one water molecule is surrounded by four others, tetrahedrally arranged around the central molecule. This is illustrated in Figure 1.1b above. Hydrogen bonds are also present in liquid water but not to the same extent as in ice and hydrate. The polar nature of water also makes it a very good solvent for ions and polar

compounds. Other anomalous properties are its large heat capacity, thermal conductivity, enthalpy of fusion and enthalpy of vaporization (Sloan and Koh 2008).

Ice can form many different phases at different pressure and temperature conditions. The most common form is hexagonal ice (*ice Ih*), formed by freezing water at atmospheric pressure. This creates a structure of nonplanar "puckered" hexagonal rings as shown in Figure 1.2 below. This is a structural difference to sI- and sII hydrates which predominantly consist of planar pentagons.

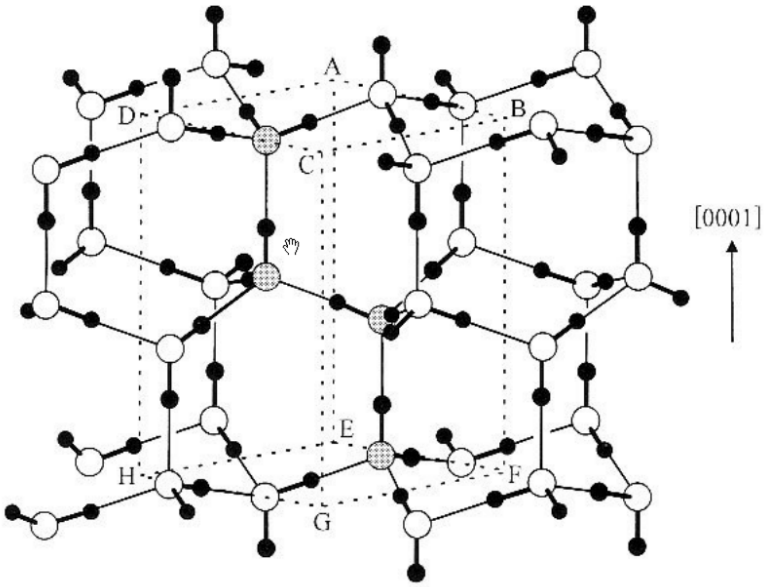

Figure 1.2: Crystal structure of ice Ih. The oxygen atoms are shown as open circles while the hydrogen atoms is shown as dark. The orientation of the water molecules are random (Travesset 2008).

Ice Ih resemble hydrates in several ways. In ice Ih, the angle between oxygen molecules is tetrahedral (109.5°) with the result of almost no geometric distortion. In the most common hydrate structures, sI and sII, this angle only deviates by 3.7° and 3.0° from tetrahedral. The H-O-H angle of the water molecules are similar, and the length of the hydrogen bond is only 1% longer in average for these hydrate structures compared to ice (Sloan and Koh 2008). A comparison of properties of ice Ih, sI- and sII hydrate are presented in Table 1.1 below. Some of the most important and characteristic properties are the dielectric and elastic properties which together with density are used to detect and evaluate hydrate deposits (Makogon 2010).

Table 1.1: Comparison of Properties of Ice and sI- and sII Hydrates (Sloan and Koh 2008). Lattice parameters for a hexagonal structure are the length of the sides (a) and the height of the structure (c).

Property	Ice	Structure I	Structure II
No. of H_2O molecules	4	46	136
Lattice parameters at 273 K [Å]	a=4.52 c = 7.36	12	17.3
Dielectric constant at 273 K	94	~58	~58
H_2O reorientation time at 273 K [µs]	21	~10	~10
H_2O diffusion jump time [µs]	2.7	>200	>200
Thermal conductivity [$Wm^{-1}K^{-1}$]	2.23	0.49 0.02	0.51 0.02
Density [g/cm^3] [a]	0.91	0.94	1.291
Compressional velocity, V_P [m/s]	3870.1	3778	3821.8
Shear velocity V_S [m/s]	1949	1963.6	2001.14
Velocity ratio (V_P/V_S)	1.99	1.92	1.91

[a] Fractional occupancy in small (S) and large (L) cavities: sI = CH_4: 0.87 (S) and CH_4: 0.973 (L);
sII = CH_4: 0.672 (S), 0.0057 (L); C_2H_6: 0.096 (L); C_3H_8: 0.84 (L)

1.1.2 Hydrate Structures

Hydrates are built up by repetitive crystal units and are generally classified on basis of this structure. There are many possible different structures but here it is focused on the most common forms of hydrates, sI and sII, shown together with sH in Figure 1.3 below. The crystal units are composed of small and large polyhedral cavities or cages, made from hydrogen-bonded water molecules. These cavities are capable of encapsulating a hydrophobic molecule, called a guest molecule or hydrate former. The repulsive force from the guest molecule is important in stabilizing the structure and keeps it from collapsing.

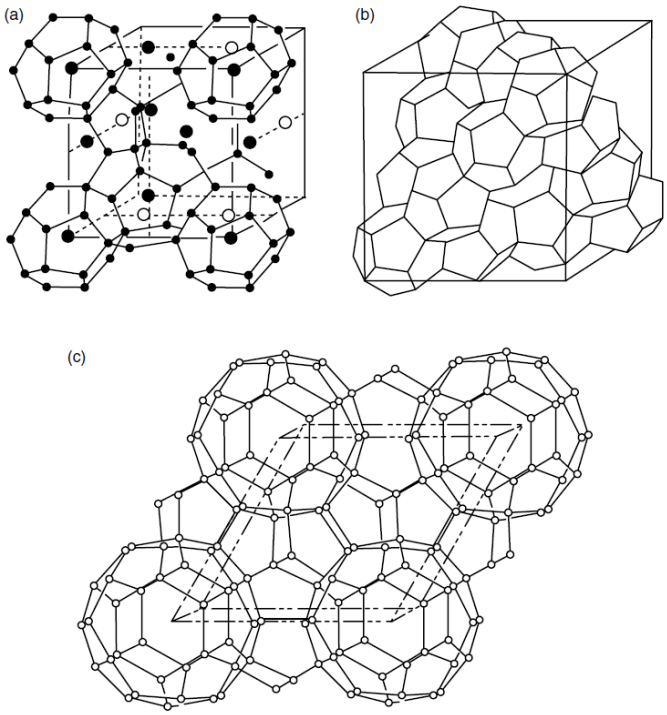

Figure 1.3: Crystal unit structures: (a), sI-hydrate, (b) sII-hydrate, (c) sH-hydrate (Sloan and Koh 2008)

There are several different polyhedrons or cages found in hydrates. The different structures consist of different combinations of small and large polyhedrons. An overview of the most common hydrate structures is described in Figure 1.4 below. The most common nomenclature for describing the polyhedrons is n_i^{mj} where n_i is the number of edges on a side and m_j is the number of sides with n_i edges.

Structure I is a cubic structure consisting of two pentagonal dodecahedron (5^{12}) and six tetrakaidecahedron ($5^{12}6^2$). This structure can be seen as linking the vertices of the 5^{12} cavities in three dimensions, resulting in eight polyhedrons consisting of a total of 46 water molecules. SI-hydrate is stabilized by guests with diameter between 4.2 and 6 Å (Sloan and Koh 2008). Some common hydrate formers for sI include CH_4 and CO_2 which is used in the experimental work for this thesis.

Structure II, also a cubic structure, consists of sixteen pentagonal dodecahedron (5^{12}) and eight hexakaidecahedral ($5^{12}6^4$). This structure can be considered as 5^{12} cavities sharing faces, arranged so that the remaining cavities are $5^{12}6^4$. This crystal unit consists of 136 water molecules. The small cavities are stabilized by guest smaller than 4.2 Å and the large cavities are stabilized by guests between 6- and 7 Å. Some common sII hydrate formers are nitrogen, propane and isobutane (Sloan and Koh 2008). The guest molecule will be discussed in more depth in the next section.

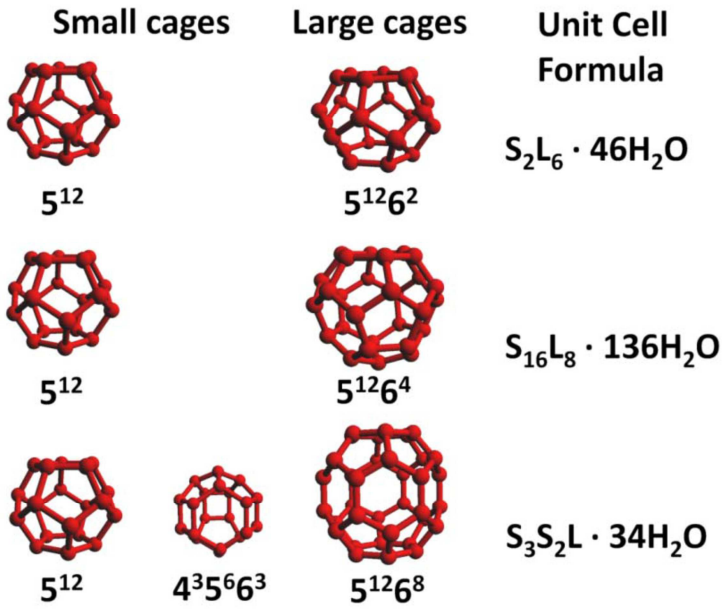

Figure 1.4: Polyhedrons in the most common hydrate structures. From the top the figure shows the crystal unit cells for SI-, SII- and SH-hydrate (Husebø 2008)

These structures are not stable as ice polymorphs. The mean diameter of the 5^{12}-, $5^{12}6^2$- and $5^{12}6^4$ cages are 7.8, 8.6 and 9.4 Å respectively. Van der Waals forces are sufficiently attractive at these distances to cause collapse of the cages. In order to stabilize the structure, some of the cages must be filled with molecules of the right size which does not interfere with the hydrogen bond. Not all the cavities are filled. The fill ratio is a function of temperature and pressure and is different for the various cages. The most common way of expressing the amount of hydrate former in hydrate is the hydration number which is the number of water molecules per guest molecule (Jeffrey 1984, Sloan and Koh 2008). In the calculations made in this thesis, the hydration number for methane hydrate was assumed to be 5.99 which is slightly higher than the theoretical maximum of the sI structure, 5.75.

1.1.3 The Guest Molecule

In order to stabilize the hydrate structures most of the cavities must be occupied by guest molecules. These molecules must fulfill a series of properties in order to have a stabilizing effect on the structure. The size of the molecule has to be right; too small and the structure will collapse, too large and the molecule will not fit the cage. Table 1.2 below shows the guest/cavity ratio for different guest molecules and cavities and indicates which can form one guest hydrates, also called simple hydrates. Sloan and Koh (2008) suggested using the guest/cavity ratio to determine upper and lower size limit for guest molecules. As can be seen from Table 1.2 the lower bound can be set at a guest/cavity ratio around 0.76 and an upper bound around 1.0 (Sloan and Koh 2008). The guest must also have a certain short range, non-polar attractive force, responsible for holding the water molecules in place. Molecules with strong hydrophilic properties cannot form hydrates since they will interfere with the hydrogen bond (Jeffrey 1984). Small polar contributions on the other hand, can be beneficial. H_2S is a

good example of this. The polar nature of the H_2S molecule gives it a positive electrostatic field outward from the molecules mass center. This is beneficial for hydrate formation because the cavities has a negative electrostatic field inwards. This field is caused by H-atoms in the water molecules pointing inwards from the cage (Kvamme 2012).

Table 1.2: Ratio of molecular diameters to cavity diameters small and large cavities in sI- and sII -hydrate (Sloan and Koh 2008).

		Molecular diameter/cavity ratio for cavity type			
Molecule	**Diameter**	**Structure I**		**Structure II**	
He	2.28	0.447	0.389	0.454ζφ	0.342ζφ
H_2	2.72	0.533	0.464	0.542ζφ	0.408ζφ
Ne	2.97	0.582	0.507	0.592ζφ	0.446ζφ
Ar	3.8	0.745	0.648	0.757ζ	0.571ζ
Kr	4	0.784	0.683	0.797ζ	0.601ζ
N_2	4.1	0.804	0.7	0.817ζ	0.616ζ
O_2	4.2	0.824	0.717	0.837ζ	0.631ζ
CH_4	4.36	0.855ζ	0.744ζ	0.868	0.655
Xe	4.58	0.898ζ	0.782ζ	0.912	0.687
H_2S	4.58	0.898ζ	0.782ζ	0.912	0.687
CO_2	5.12	1.00ζ	0.834ζ	1.02	0.769
C_2H_6	5.5	1.08	0.939ζ	1.1	0.826
c-C_3H_6	5.8	1.14	0.99	1.16	0.871ζ
$(CH_2)_3O$	6.1	1.2	1.04ζ	1.22	0.916ζ
C_3H_8	6.28	1.23	1.07	1.25	0.943ζ
i-C_4H_{10}	6.5	1.27	1.11	1.29	0.976ζ
n-C_4H_{10}	7.1	1.39	1.21	1.41	1.07

ζ Indicates the cavity occupied by the simple hydrate former.
φ Indicates that the simple hydrate is only formed at very high pressure.

As shown in Table 1.2 above, small hydrate formers that stabilize the small cavities can also occupy the large cavities, making simple hydrates that only contain one type of guest molecule. Methane, ethane, carbon dioxide and hydrogen sulfide form simple sI-hydrats, while nitrogen, propane and iso-butane form simple sII-hydrates. Larger molecules such as n-butane and benzene do not fit into the smaller- and sometimes not the larger cavities. This makes them unable to form hydrates alone. In order for these compounds to form hydrates they need small molecules such as methane or nitrogen to stabilize the smaller cavities in the hydrate structure (Sloan and Koh 2008).

Methane, which is used as a hydrate former during hydrate formation in this thesis, can occupy both small and large cavities in sI-hydrate and can make simple sI-hydrate. Larger

molecules such as iso-butane and propane only fit in the sII cavities, making hydrocarbon mixtures with these components likely to form sII-hydrate (Sloan and Koh 2008).

1.1.4 Hydrate Thermodynamic Equilibrium and Kinetics

The thermodynamic equilibrium at which hydrate are stable requires low temperature, high pressure and a sufficient concentration of hydrate former. This is often depicted as a 2D pressure-temperature diagram with the hydrate equilibrium line (AB) as shown in Figure 1.5 below, but could also be shown as a 3D plot with an additional concentration axis. In order to have a phase transition, a thermodynamically driving force is needed. This force is called supersaturation and is provided when we move away from the equilibrium line into the hydrate stable region either by sub-cooling, as illustrated by the SP line in Figure 1.5, by increasing the pressure (over-pressure) or by changing the molecular composition.

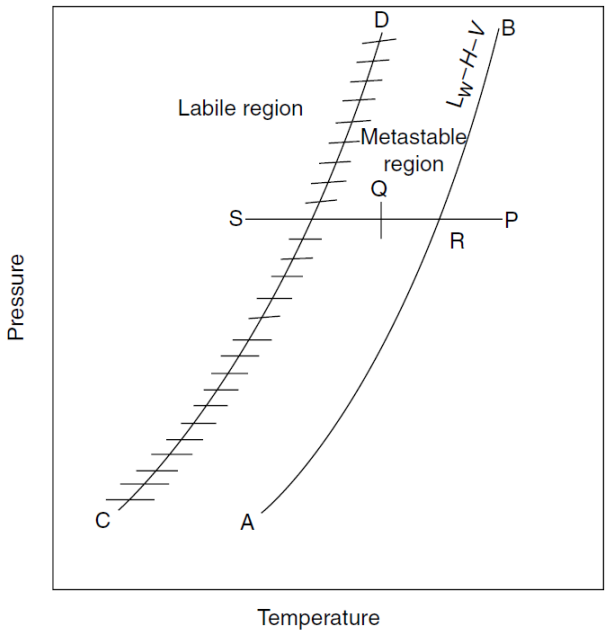

Figure 1.5: Hydrate formation by sub-cooling relative to the equilibrium line (AB) and the supersaturation limit (CD). (Sloan and Koh 2008)

Thermodynamic equilibrium for hydrates is well understood but the formation kinetics is one of the most challenging problems in regard to how hydrates form. This problem can be divided into two parts as illustrated in Figure 1.6 below: (1) How long does it take for hydrate to reach stable growth after the system has passed the equilibrium line, called the nucleation time, and (2) growth rate during stable growth. Figure 1.6 shows an example of a laboratory experiment where water and gas is brought into the hydrate stable region. The system is connected to a gas reservoir that keeps the pressure constant by supplying gas when gas is "consumed" by hydrate formation. This is the same logging method used in the experimental work for this thesis.

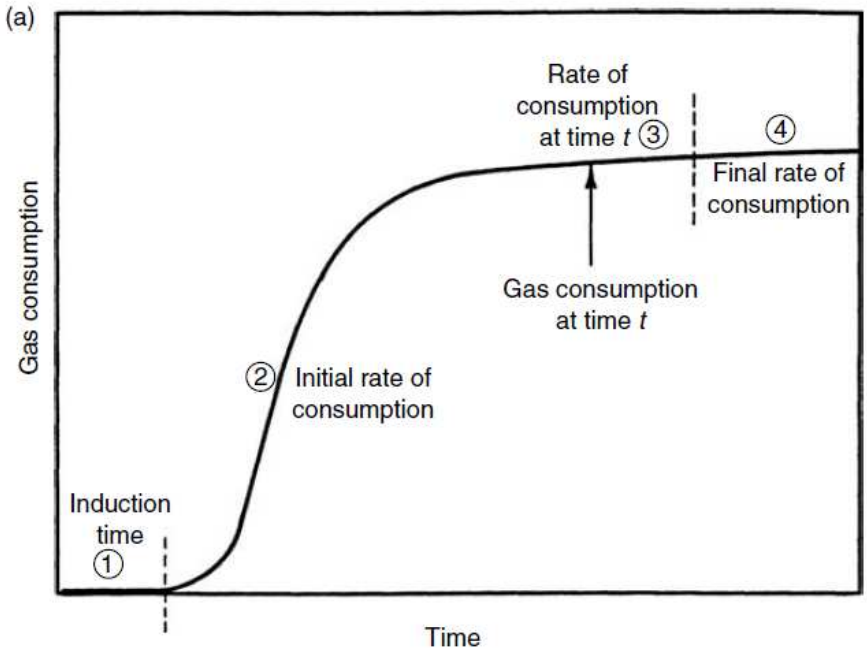

Figure 1.6: Gas consumption vs. time for hydrate formation. (Sloan and Koh 2008)

When water and gas is brought into the hydrate stable region, nucleation will begin. Small hydrate clusters spontaneously form and dissociate. This is considered a stochastic process dependent on supersaturation, external agitation, interface area, water contaminants and water history among others. In order to get a stable hydrate phase it is necessary to reach a critical cluster size, after which the hydrate will go into stable growth. From a Gibbs free energy (ΔG) perspective there are two competing contributions: (1) The energy required to displace the old phase or the "surface excess free energy" (ΔG_S) and (2) the energy gained by forming the new phase or the volume excess free energy (ΔG_V). Figure 1.7 below shows ΔG_S, ΔG_V and ΔG as a function of cluster size for spheres. The critical Gibbs free energy, ΔG_{crit}, is an energy barrier that has to be overcome in order to reach stable growth. This barrier is lowered as the driving force gets stronger. The rate at which stable clusters are formed is therefore very dependent on the amount of supersaturation (Sloan and Koh 2008, Kvamme 2012).

It is difficult to measure nucleation since it happens on a very small scale. Induction time is therefore used instead. The induction time is the time it takes from nucleation starts to the first measurable volume of hydrate is formed, and is dependent on the sensitivity of equipment and method. Despite large efforts to correlate the time of hydrate growth with different factors it has proven to be difficult. Hydrate nucleation is as mentioned stochastic, less so with high driving forces, and dependent on a number of variable factors, many of which is difficult to consider, a problem worsened if the system is dynamic (Sloan and Koh 2008).

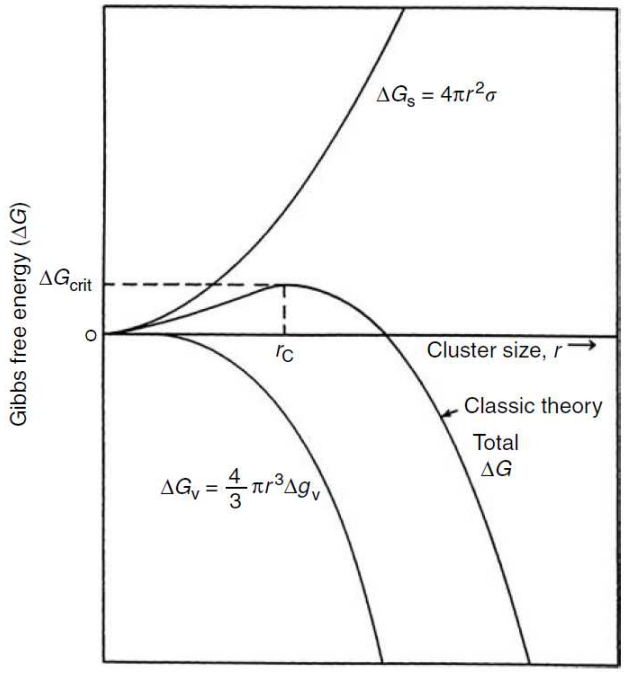

Figure 1.7: Surface excess free energy (ΔG_S), volume excess free energy (ΔG_V) and total ΔG as a function of cluster size. (Sloan and Koh 2008)

Hydrate nucleation is strongly dependent on supersaturation as a driving force. This makes nucleation in most cases more likely to occur at the gas/liquid or liquid/solid interface. At these interfaces, gas/liquid in particular, adsorption of guest molecules provides a high concentration of both guest- and host-molecules and a larger probability of reaching critical cluster size. Once critical cluster size is reached hydrate will form rapidly until there is a lack of guest or host molecules. The growth rate, (2) in Figure 1.6, is in most cases limited by mass or heat transfer, and less the intrinsic kinetics. Dissociation is an endothermic reaction that must be supplied with heat from the environment and is therefore in most cases limited by heat transfer (Kashchiev and Firoozabadi 2002, Sloan and Koh 2008).

1.1.5 Hydrate Inhibition

With the emergence of the modern petroleum industry hydrates were quickly recognized as a problem, leading to extensive research efforts in hydrate prevention. High pressure and low temperature in transportation, process and production systems can lead to hydrate formation, and if not dealt with, blockage. The economic loss caused by downtime in flow-line operations can be significant and a hydrate plug can become a high velocity projectile as it dissociates, posing a huge security risk to facilities, crew and the environment. In order to prevent hydrate formation companies try to keep the operational parameters outside the hydrate stable region but this is not always possible. As production moves to more extreme environments, such as the arctic region, longer and deeper subsea pipelines are required and it is no longer possible to keep the flowing phase outside the hydrate stable region (Koh 2002).

Hydrate growth can be slowed or completely avoided by introducing substances that in some way inhibits hydrate-formation. Hydrate inhibitors can be divided into three groups based on

how they work: thermodynamic inhibitors, kinetic inhibitors and anti-agglomerates. The early thermodynamic inhibitors have to be used in large quantities (up to 40 wt%) in order to achieve the desired effect. The economic and ecological expense of using these inhibitors led to an increased interest in the development of kinetic inhibitors and anti-agglomerates which can be used in smaller quantities (less than 1 wt%) (Kashchiev and Firoozabadi 2002, Sloan and Koh 2008).

Kinetic inhibitors typically work by postponing the time for massive hydrate growth by steric hindrance, mass-transport hindrance and by affecting the hydrogen bonds. Even though some kinetic inhibitors like PVP are water soluble, they can adsorb onto non-polar interfaces and create a relatively thick barrier. This makes them able to adsorb onto interfaces and particles that would act as nucleation sites and in this way reduce the nucleation rate (Kashchiev and Firoozabadi 2002, Kvamme 2012).

Anti-agglomerates are typically polymers with a polar and a non-polar part. The polar part of the polymer can go into the hydrate structure, leaving the non-polar part sticking out. The result is small hydrate particles covered by non-polar coatings hindering further growth(Sloan and Koh 2008, Kvamme 2012).

Thermodynamic inhibitors include alcohols, glycols, and salts. When solved in water these substances will interact with the water dipoles, weakening the attraction towards hydrate. The result is a shift in the thermodynamic equilibrium line. Glycols and alcohols have two effects that inhibit hydrate formation. The biggest effect comes from the hydroxyl groups which will hydrogen bond to water molecules. Another effect comes from the hydrocarbon part which will cause water to organize around it. Both effects are in direct competition with hydrate and contributes move the hydrate stable region. Salt ions dissolved in water will form a Coulombic bond with water molecules much stronger than the hydrogen-bond. The water molecules are more attracted to the non-polar salt ions than to the hydrate structure, resulting in a shift in the hydrate stable region. A secondary effect comes from the water molecules clustering around the salt ions causing a decrease in the solubility of the hydrate former (Sloan and Koh 2008, Kvamme 2012).

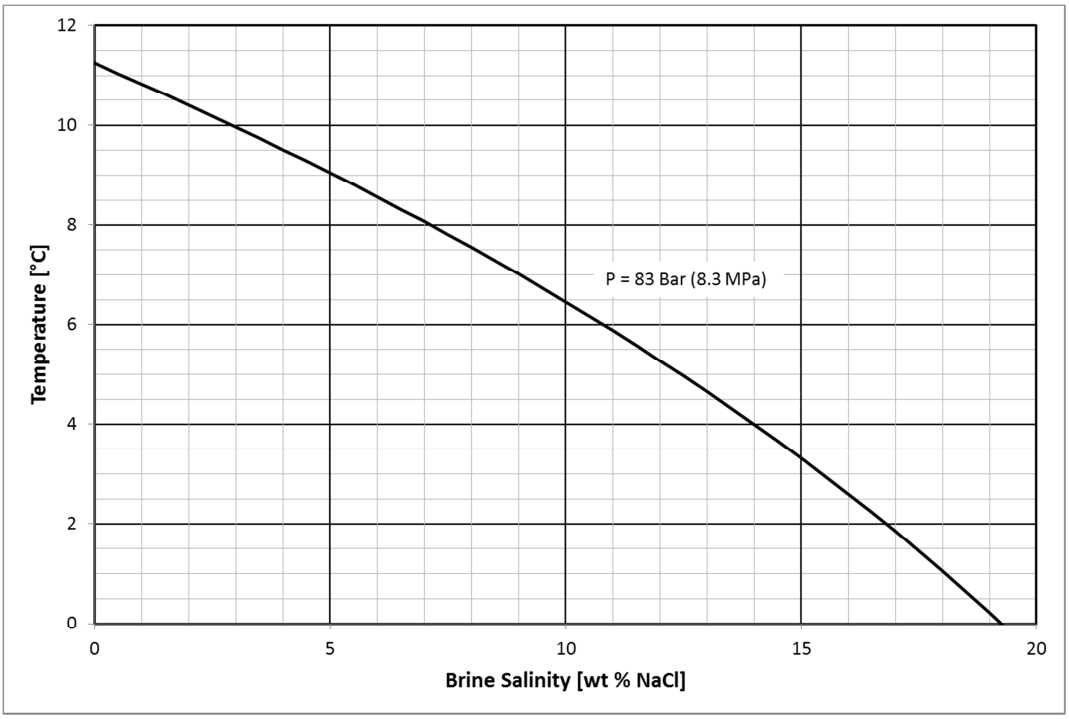

Figure 1.8: Methane-Hydrate equilibrium temperature at 8.3 MPa with varying NaCl brine salinity. Values have been produced using CSMGem software (Sloan and Koh 2008).

All the experiments in this thesis have been performed with 0.1 or 3.5 wt % NaCl brine solution. As hydrate form, the brine salinity will increase as a result of salt ions remaining in the brine while water molecules are consumed. As illustrated in Figure 1.8, the hydrate equilibrium temperature will be reduced as a result of this. At the experimental conditions used in this thesis (8.3 MPa and 4 °C), hydrate formation will stop when the brine salinity reaches 14wt%.

1.2 Gas Hydrate in Sediments

Gas hydrates which are considered for production are typically located in porous reservoirs and all the experimental work in this thesis have been performed with hydrates within porous sandstone. In order to follow the discussion on production of gas hydrates from reservoirs and the experimental results some basic concepts of porous mediums and fluid flow in porous mediums is reviewed below.

1.2.1 Porosity

Sedimentary rock is generally made up of mineral grains, cement and void space or pores. Porosity, ϕ, is a measure of the amount of void space in the rock and is defined as the ratio of void volume, V_p, to bulk volume V_b,

$$\phi \stackrel{\text{def}}{=} \frac{V_p}{V_b} \tag{1.1}$$

All off the pores in a sedimentary rock are not necessarily connected to each other. There will typically be some dead end pores and some isolated pores which don't contribute to fluid flow. In some cases it is therefore necessary to differentiate between effective- and total porosity. Effective porosity is calculated by using the volume of connected pore-space instead of the total pore-space in Equation (1.1) above.

The pore space can be filled by one or more fluids. In a gas hydrate reservoir the pores can be occupied by hydrate, gas and water. The saturation of fluid i, S_i, is given as the fraction of the total pore volume occupied by the fluid.

$$S_i \stackrel{\text{def}}{=} \frac{V_i}{V_p}, \quad i = 1 \ldots, n \tag{1.2}$$

In this thesis hydrate is treated like a pore "fluid" and not a part of the rock matrix. The hydrate saturation is given by S_H.

1.2.2 Permeability

The many interconnected pores in sedimentary rocks make it possible for fluids to flow through this pore network. How easily fluids will flow depends in large part on the effective porosity and in some cases on pore-size distribution, tortuosity and the pore-throat /pore-volume ratio. Permeability is a measure of flow capacity and can for one phase flow be considered as a constant rock property. This is called the absolute permeability, K, and can be defined by Darcy's law for linear, horizontal flow for an incompressible fluid:

$$q = -A\frac{K}{\mu}\frac{dp}{dx} \tag{1.3}$$

Where q is the volumetric flow rate, A is the cross sectional area of flow perpendicular to the flow direction, K is the absolute permeability, μ is the viscosity of the fluid and dp is the pressure differential in the flow direction, x. The flow rate is positive in the direction of falling pressure.

In the case of gas flow, Equation (1.3) is not valid since gas is highly compressible. In practical terms, at not to high pressures, the compressibility concern can be resolved by using the mean pressure, $\overline{p}$, and the fluids viscosity at this pressure, resulting in a mean volumetric flow rate:

$$\bar{q} = A\frac{K}{\mu}\frac{\Delta p}{\Delta l} \tag{1.4}$$

Where $\bar{q}$ is the mean volumetric flow rate at the mean pressure point in the sample and Δp is the pressure drop over the length, Δl.

Gas can move with minimal friction against the pore walls compared to liquids. This phenomenon, called the Klinkenberg effect, causes a higher flow rate than expected from Equation (1.4). This leads to an overestimation of the permeability. The error caused by the Klinkenberg effect is usually small but it increases with decreasing pressure and permeability (Zolotukhin and Ursin 2000). Klinkenberg proposed the following correction:

$$k_m = K\left(1 + \frac{b}{\bar{p}}\right) \tag{1.5}$$

Where k_m is the measured gas permeability and K is the absolute permeability. The constant b in the equation is called the Klinkenberg factor and is dependent on rock properties and gas type (Zolotukhin and Ursin 2000).

During the experimental work presented in this thesis there have been instances where the systems fluid flow ability has been limited by factors not connected to the sandstone core plug and its permeability. In these cases the term Injectivity has been used instead of permeability. Injectivity are a concept normally used about injection wells in the petroleum industry. The Well Injectivity Index, I_w, are defined as:

$$I_w = \frac{q_{inj}}{p_{winj} - \bar{p}} \tag{1.6}$$

Where q_{inj} is the injection rate, p_{winj} is the mean injection pressure and $\bar{p}$ is the mean formation pressure. The use of the term in this thesis however is qualitative and refers to the ability of the experimental system including tubing, valves and the core plug, to conduct fluid flow.

1.2.3 Relative Permeability

When a porous medium is saturated with multiple immiscible fluids, *i*, each fluid can be described as having a corresponding effective permeability, $k_{i,e}$, which can be defined by a generalization of Darcy's law:

$$q_i = -A\frac{k_{i,e}}{\mu_i}\frac{dp}{dx} \tag{1.7}$$

The corresponding relative permeability of the specific fluid, $K_{r,i}$, is defined as the ratio between its effective permeability and the mediums absolute permeability:

$$k_{r,i} = \frac{k_{i,e}}{K} \tag{1.8}$$

The sum of relative permeabilities is always less than unity. The relative permeability of a fluid is greatly dependent on the fluid saturation, where higher saturation gives higher relative permeability for that fluid.

1.2.4 Capillary Pressure

A solid in the presence of two immiscible fluids typically has a wetting preference towards one of the fluids defined by the fluids tendency to spread on the solid surface. The wetting preference is a result of an electrostatic force between the fluid and the solid commonly called adhesion and has great impact on how the fluids occupy the pore space in a porous medium. When two immiscible fluids are present in a capillary tube like a narrow pore channel, the adhesive force will make the wetting fluid spread along the pore wall and the interface between the two fluids curve convex towards the wetting fluid. The resulting angle towards the tube wall, Θ, is called the wetting angle. Capillary pressure, P_c, is the pressure difference over the interface between the two liquids caused by cohesive forces between the fluid-molecules and external adhesive forces. The capillary pressure will cause the wetting fluid to displace the non-wetting fluid in the narrow channels. Capillary pressure increases with decreasing tube diameter which causes the wetting fluid in a porous medium to occupy the small pores first. It is also possible for a fluid to be trapped in a pore by capillary forces.

1.2.5 Hydrate Distribution in Porous Sediment

Porous sediments where methane hydrate formation takes place typically contains five phases as illustrated in Figure 1.9 below: (1) mineral grains, (2) methane hydrate, (3) water that can form hydrate (free water), (4) equilibrium pore water and (5) free gas phase. Many surfaces (quarts, iron, iron-oxides and calcite among others) reduce the waters chemical potential and makes it incompatible with the hydrate structure. The result is a thin layer (1 – 1.5 nm) of water coating the grain surface which cannot form hydrate (Kvamme 2012). The gas will typically saturate the center of the pores while the smallest pores or pores only accessible by very narrow pore throats may be completely saturated by water as a consequence of capillary forces. Hydrates has been found to be pore filling, cementing or floating in the pore fluid depending on the sediment and phase saturations as well as other factors. Hydrate growth will

preferentially begin at the gas – water interface but can also occur from dissolved gas. There are numerous reports of hydrate at low S_H preferentially growing in the bulk of larger pores with low water saturation adjacent to an area with high water saturation (Tohidi et al. 2001, Kleinberg et al. 2003, Rees et al. 2011).

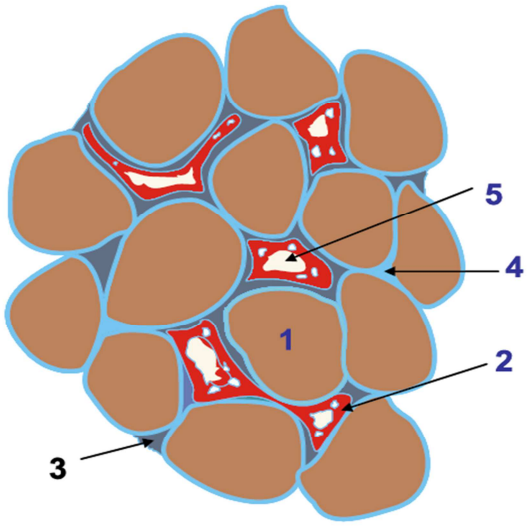

Figure 1.9: Phase distribution of gas hydrate in porous sediment. The phases depicted are (1) mineral grains, (2) gas hydrate, (3) free water, (4) equilibrium pore water and (5) gas (Chuvilin et al. 2011). The location of the different phases can vary with saturations and sediment type.

Hydrate redistribution after hydrate formation have been observed by a number of researchers (Tohidi et al. 2001, Rees et al. 2011), illustrated in Figure 1.10 below which show pictures before, right after, and 2 days after methane hydrate formation in a glass micro model. Rapid hydrate formation with a large degree of supersaturation will typically concentrates the hydrate in bulks which disperse with time. The redistribution process is a result of the dynamic nature of a hydrate system. Hydrate will continuously dissociate and form on a small scale in a process where hydrate bodies with more favorable energy consumes bodies with less favorable energy. In bulk, this typically results in larger bodies of hydrate consuming the smaller due to the more favorable energy of large structures (Kvamme 2012). Porous sediments however are a vastly more complicated system, with many additional factors influencing hydrate redistribution.

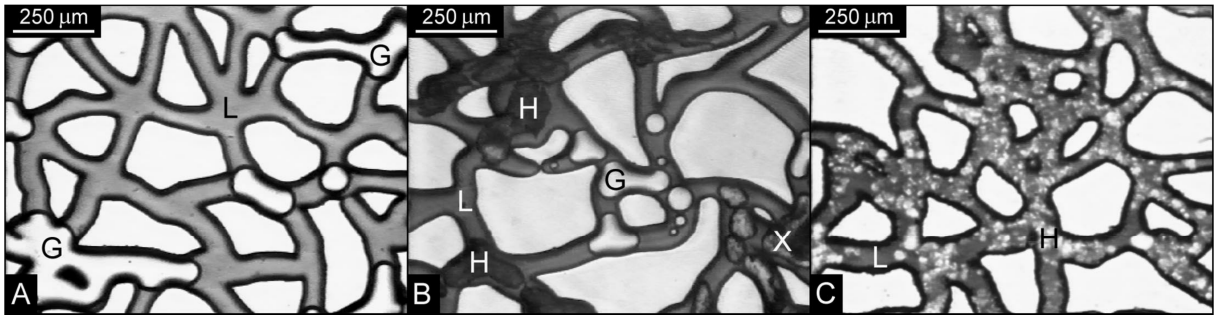

Figure 1.10: Pictures of hydrate formation in a glass micro-model where the large white areas are grains. Picture A were taken before hydrate formation and depicts gas bubbles (G) in the formation water. Picture B depicts newly formed hydrate (H) in the presence of gas bubbles in the water and some gas encapsulated by hydrate (X). Picture C shows the distribution after 2 days where hydrate is depicted as white areas in the dark liquid (Tohidi et al. 2001).

1.3 Gas Hydrate as an Energy Resource

The global energy demand is rising and the predominant energy source, fossil fuels, is finite. In order to meet the energy demand of tomorrow, it will be vital to find new sources of energy. An important part of this includes increasing the world's hydrocarbon (HC) reserves by exploiting unconventional HC sources, as recently done with shale gas and coal-bed methane in the United States. Estimates of the world's hydrate reserves vary widely, but even the most conservative estimates indicate enormous amounts of methane in hydrate (Moridis 2008). This makes gas hydrates an energy source which should be considered for the future. Natural gas burns much cleaner and releases less CO_2 compared with other HC sources. In a world faced with big environmental challenges this should further increasing the desirability of gas hydrates as an energy source.

Figure 1.11 below shows discovered gas hydrate deposits and may give an indication of the global gas hydrate distribution. The global distribution of hydrates is different from other HC-sources making hydrates a potential important resource for countries dependent on oil and gas import (India, Japan, South Korea and Kina).

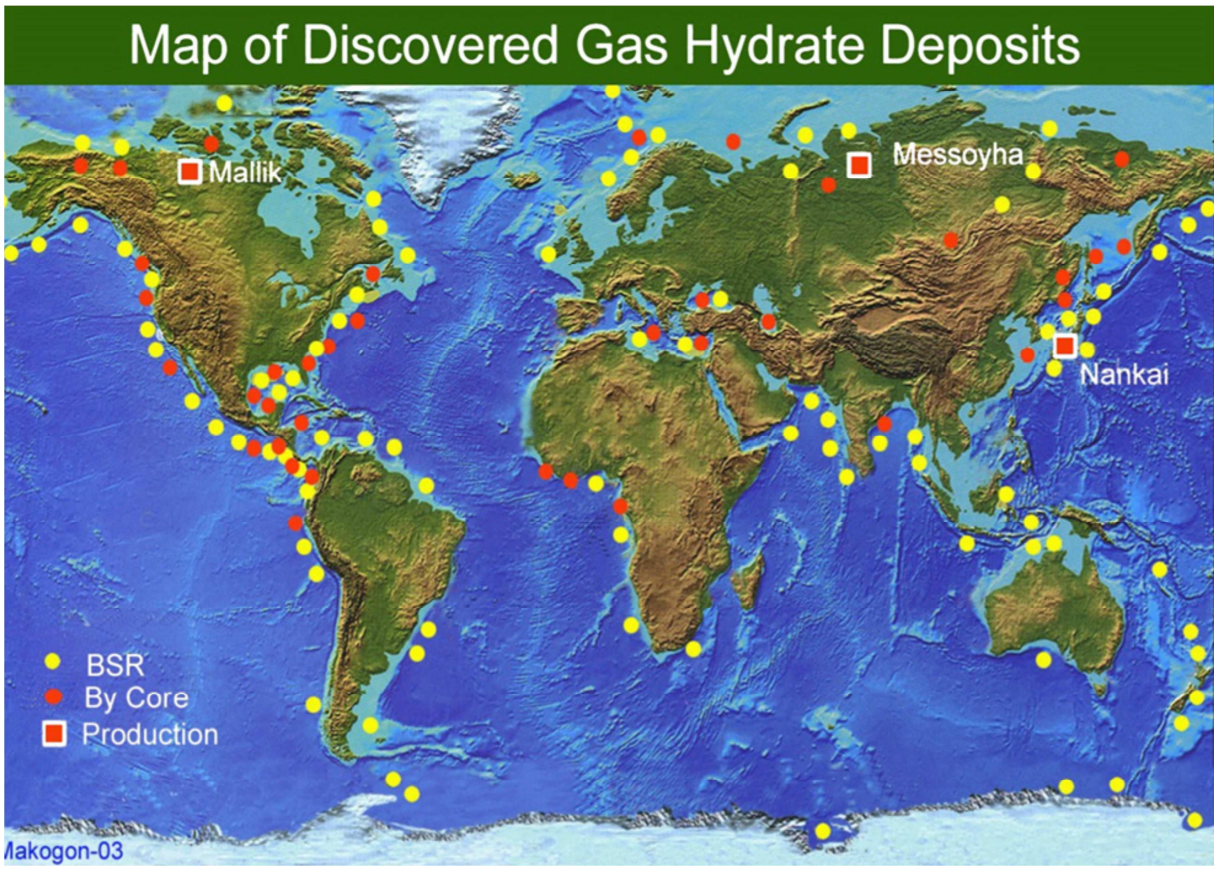

Figure 1.11: Distribution of discovered gas hydrate deposits. BSR = Bottom Simulating Reflector (Makogon 2010)

1.3.1 Magnitude and Hydrate Distribution Worldwide

Gas hydrate deposits in nature are, as indicated by Figure 1.11, generally found in sediments under the permafrost, continental margins and enclosed seas (Tréhu et al. 2006) where the amount of hydrate in marine environments is two orders of magnitude larger than on land. As previously mentioned, hydrate formation require low temperature, high pressure and presence of water and a sufficient concentration of gas.

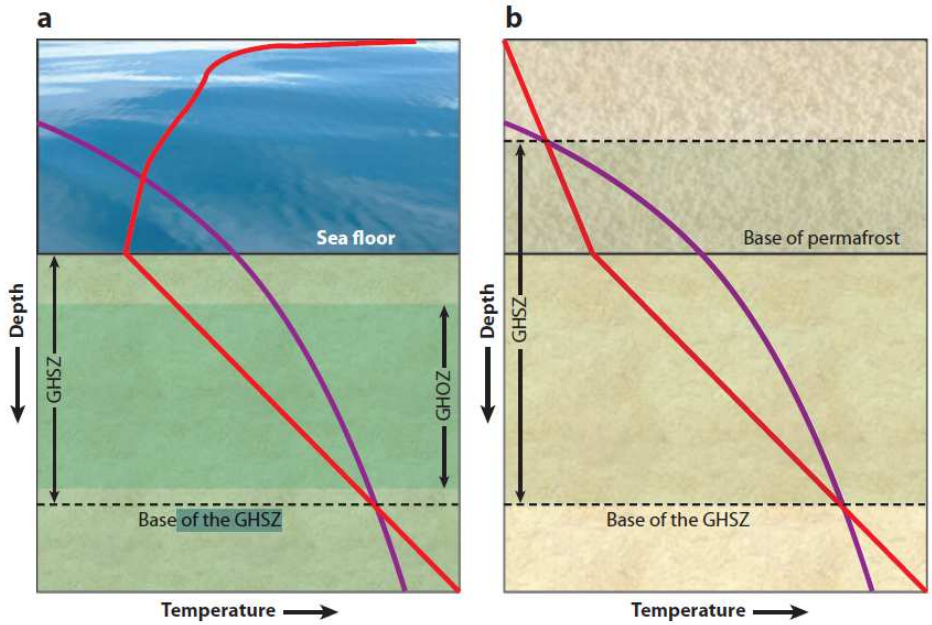

Figure 1.12: Gas hydrate stability zone (GHSZ) for (a) marine- and (b) permafrost systems. The red line represents the ambient temperature and the purple line is the hydrate stability curve. Gas hydrate is limited to the gas hydrate occurrence zone (GHOZ) due to availability of guest molecules (Hester and Brewer 2009).

The pressure and temperature conditions needed to form methane-hydrates are generally met in sediments more than 100-300m under the permafrost (Hester and Brewer 2009) and in submarine sediments exceeding 300–800 m water depth, depending on local geological- and oceanic conditions (Tréhu et al. 2006). In fact, the early estimates of the world's hydrate reserves included all of these areas, resulting in estimates in the range of two orders of magnitude higher than some of the most recent estimates. Hydrate formation is strongly dependent on guest molecule availability and the majority of these areas have a guest molecule saturation below the saturation limit which in many cases makes them unable to form a stable hydrate zone. For this reason are hydrate accumulations are generally found in the continental margins and enclosed seas. In these areas is the sedimentation rate and gas flux high enough to form hydrate bearing zones. Figure 1.12a and b show a representation of a typical gas hydrate stability zone (GHSZ) for marine and permafrost systems. The geothermal gradient in these systems allows for low temperatures at large enough depths to form hydrates. In marine systems there will typically be a gas hydrate free zone near the sea floor unless the gas flux is very high. This is in large part a result of anaerobic oxidation of methane by sulfate (Tréhu et al. 2006, Hester and Brewer 2009). In addition to the before

mention conditions, gas hydrate formation is also dependent on other factors such as the composition and phase state of the hydrate formers, the salinity of the formation water and the structure and lithology of the porous medium (Makogon 2010). If Figure 1.12 is considered in conjunction with Figure 1.8 it is clear that brine salinity alone can dramatically influence the size of the GHSZ.

Table 1.3: Estimates of in situ Methane Hydrates (Sloan and Koh 2008).

Year	CH_4 amount 10^{15} m^3 STP	Citations
1973	3053	Trofimuk et al.
1977	1135	Trofimuk et al.
1982	1573	Cherskiy et al.
1981	120	Trofimuk et al.
1981	301	McIver
1974/1981	15	Makogon
1982	15	Trofimuk et al.
1988	40	Kvenvolden and Claypool
1988	20	Kvenvolden
1990	20	MacDonald
1994	26.4	Gornitz and Fung
1995	45.4	Harvey and Huang
1995	1	Ginsburg and Soloviev
1996	6.8	Holbrook et al.
1997	15	Makogon
2002	0.2	Soloviev
2004	2.5	Milkov
2005	120	Klauda and Sandler

There have been made several attempts to estimate the amount of hydrate in the earth, listed in Table 1.3 below, but a lack of direct evidence makes them uncertain. The estimates vary widely from Soloviev (2002) of 0.2 x 10^{15} m^3 to Trofimuk et al. (1973) of 3053 x 10^{15} m^3 with the most cited estimate at 20 x 10^{15} m^3 of methane (STP) of Kvevolden (1988). Gas hydrates store methane very effectively where 1 m^3 of hydrate can contain 164 m^3 CH_4 (STP) and the amounts of hydrate worldwide are large even when taking the most conservative estimates into account.

1.3.2 Deposit Classification

There is a wide variety in the gas hydrate deposits found in nature and because of this a clear need to classify them. The methane that forms hydrates can have a biogenic or a thermogenic origin. Biogenic methane has been produced by biological conversion of organic matter in relatively shallow and cold burial depths. This process can occur in situ, in the GHZS, and over large areas where it typically results in low hydrate saturations not suitable for production. High sedimentation rates and high carbon content promotes the production of

biogenic methane, making it more common in marine environments. Thermogenic methane has been produced by high temperature processes and usually originates from deeper sources before it migrates up to the GHSZ through fractures or channels.

The way that methane migrates to the GHZS can be vital to the properties of the resulting hydrate accumulation and can be used to classify the deposits. The two extremes are high gas flux- (HGF) and low gas flux (LGF) hydrate. HGF hydrate are typically formed when gas migrate through faults into the GHSZ, often resulting in more localized accumulations. The high gas flux makes it possible for gas to displace formation water and create a free gas phase and possibly an underlying gas cap. LGF hydrates typically form slowly from dissolved methane. The solubility of methane changes as the lighter methane rich formation water migrates upwards and hydrate formation is precipitated. The gas is typically almost pure biogenic methane and no free gas phase is formed (Sloan and Koh 2008, Hester and Brewer 2009).

The variation in hydrate saturation and the wide range of geological settings of hydrate accumulations makes only a small fraction of the gas hydrate accumulations producible with today's technology where a large fraction is considered unfit for production even with technological advances. Boswell and Collett (2006) recognized this and presented a Gas Hydrate Resource Pyramid, shown in Figure 1.13 below, where hydrate accumulations where categorized with respect to their prospect for future production. The top of the pyramid represents the resources closest to commercial production including accumulations with large hydrate saturations in quality reservoir rock under existing artic infrastructure and are estimated to $9.4x10^{11}$ m^3 STP of gas in place (Moridis 2008). The next tier represents the same kind of accumulations, but away from existing infrastructure. The third most challenging accumulations represent hydrate in high-quality reservoirs in marine settings. The deep water will make these accumulations expensive to produce, making existing infrastructure as in the Gulf of Mexico favorable (Boswell and Collett 2006).

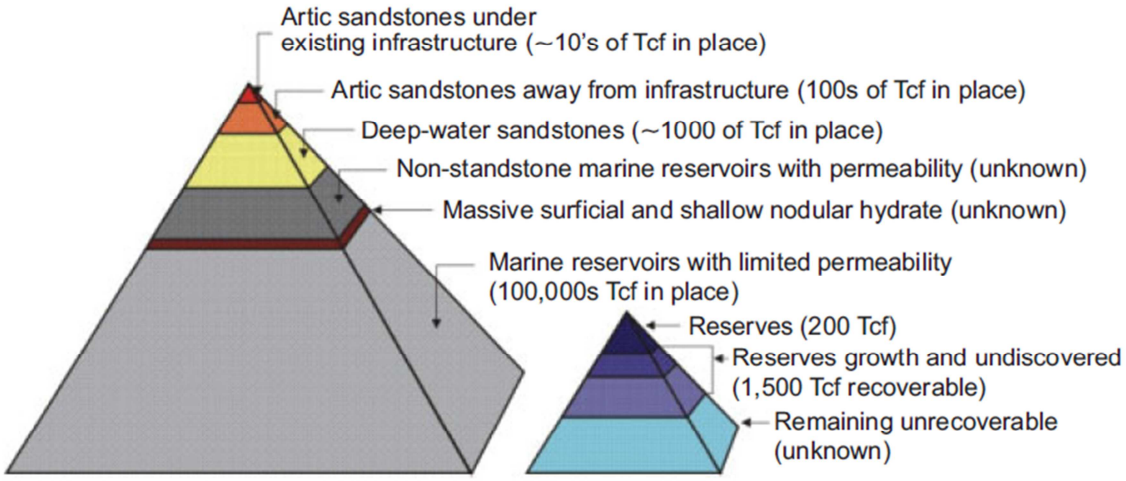

Figure 1.13: Gas hydrate resource pyramid (larger) and gas resource pyramid for all non-gas hydrate resources (smaller). (Boswell and Collett 2006)

Moridis and Collett (2003) divided the accumulations into three classes based on their geological and initial reservoir conditions. Class 1 deposits consist of two zones, a hydrate bearing interval and an underlying two phase zone with free gas and water. The class is denoted 1W or 1G dependent on whether the hydrate bearing interval has free water or gas present. For both cases the GHZS often coincide with the bottom of the hydrate zone. Class 2 also consists of two zones, but with an underlying aquifer. Class 3 has no underlying zone of mobile fluids and only consists of a hydrate zone. Class 1 is considered the most desirable in terms of gas production. These accumulations are very close to the hydrate thermodynamic equilibrium and only small changes in pressure or temperature are required to dissociate the hydrate. Class 2 and 3 on the other hand can be far into the hydrate stable region making production a bigger challenge (Moridis and Collett 2003). There is a forth class of hydrate deposits which consists of large areas with widespread, low hydrate saturations without any confining strata. This class is generally not considered a target for production (Ersland 2008).

1.3.3 Dissociation Production Strategies

Figure 1.14 below illustrates the three main production strategies that involve dissociating gas hydrate and producing the resulting gas phase. The strategies are (1) depressurization, (2) thermal stimulation and (3) injection of inhibitors.

There have been done numerous numerical simulations on production strategies for the different hydrate deposit classes. Class 1 deposits have been reported (Moridis 2008) to be the most promising target for production. The reason for this is the proximity to hydrate equilibrium, which minimizes the required pressure drop in order to dissociate the hydrate and the existence of a free gas zone which guarantees gas production. Of the two types of class 1 deposits, type 1G is reported to be the most promising. Moridis and Collett (2003), Moridis (2008) reported depressurization as the most promising production strategy for this type of deposit and considers it within the reach of conventional technologies. Problems may arise with secondary hydrate choking the well if the well is not located sufficiently far away from the initial hydrate interface and the well may have to be continuously heated to avoid hydrate formation (Moridis 2008).

Class 2 and 3 deposits are reported to be a viable production target by depressurization. By completing the wells partly in the water zone for class 2 deposits there will be a good pressure response along the bottom of the hydrate interface. Production from this class is characterized by high production rates but long lead time with very little gas production. Class 3 deposits may have earlier gas production but at lower rates. There may also be problems creating pressure response in the early phase of production due to the lack of mobile phases (Moridis 2008).

Depressurization has been reported to be the best production strategy independent of deposit class. Thermal stimulation is expensive and heat flux is slow compared to pressure and should only be considered for use locally around and in the wellbore to hinder secondary hydrate formation. The use of inhibitors is reported to be expensive and potentially damaging to equipment and should only be considered for hydrate prevention in the wellbore (Moridis 2008).

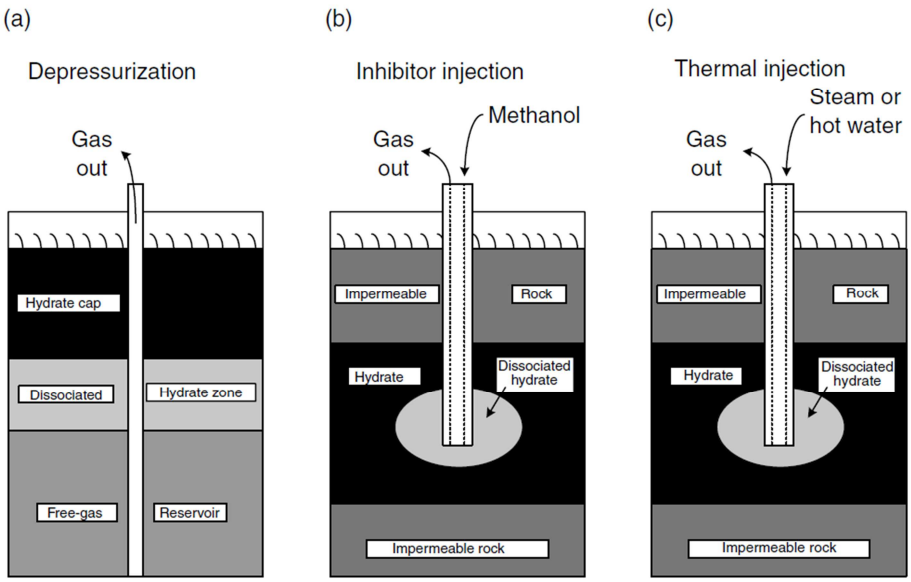

Figure 1.14: Illustration of the three dissociation based production strategies (Makogon 1997)

1.4 Case Studies

Two case studies are presented below; Messoyakha which was the first reported case on production from gas hydrates and acted as a catalyst for research on gas hydrates as an energy resource, and Mallik which are one of the world's largest hydrate accumulations where multiple important field tests has taken place.

1.4.1 Messoyakha – Hydrate Production in Permafrost

The Messoyakha gas field is a conventional gas field located in the northern part of the West Siberian basin and is regarded as the first example of gas production from a permafrost hydrate accumulation. It started gas production in 1969 and by mid-1971 the pressure response from the field began to deviate from the expected values. According to Makogon (2010) this was caused by the dissociation of an overlying hydrate zone.

A cross section of the field is shown in Figure 1.15. The field is located under 450 m of permafrost and is characterized as having an effective pay-zone of about 25 m with initial reservoir pressure of 7.8 MPa, an average porosity of 25% and permeabilities varying from 10 mD to 1 D with an average of 125 mD. Over the gas zone there is a hydrate zone with an average hydrate saturation of about 20% and presence of free gas. This will classify the field as a Class 1G and put the deposit on the top of the gas hydrate pyramid in Figure 1.13. The

initial gas in place excluding hydrate was 24 x 10^9 m^3 with an additional 12 x 10^9 m^3 (STP) of gas in hydrate (Makogon 2010).

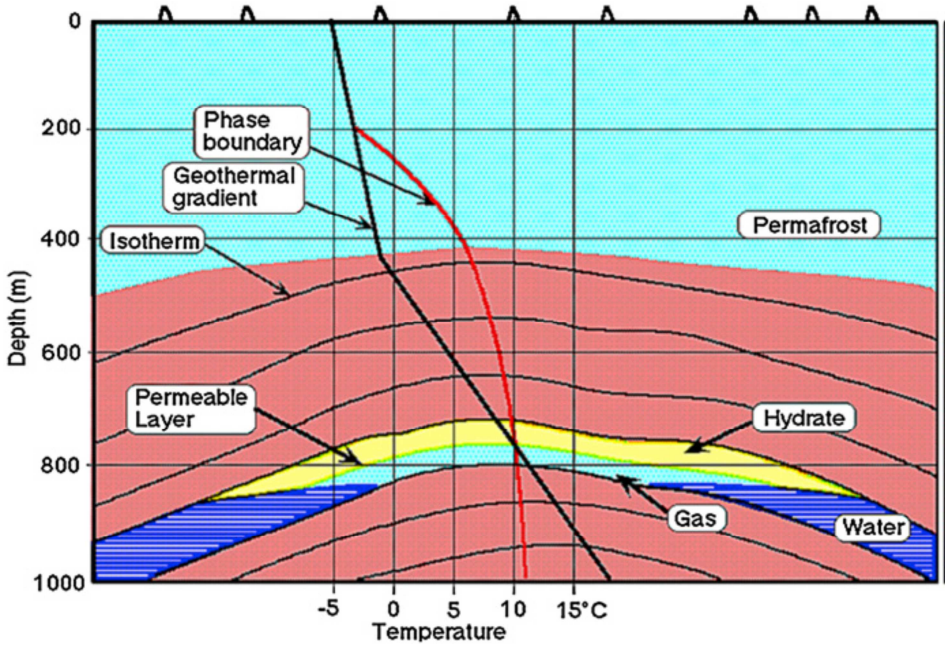

Figure 1.15: Cross sectional illustration of the Messoyakha gas field (Makogon 2010). The bottom of the hydrate bearing zone coincides with the bottom of the GHSZ illustrated by the phase boundary crossing the geothermal gradient.

The field was shut in between 1979 and 1982. In this period the pressure increased from 5.0 to 6.0 MPa indicating dissociation of hydrate. By December 31st 2008 the total gas production had reached 13.3 x 10^9 m^3. According to Makogon (2010), 6.9 x 10^9 m^3 of this comes from dissociated hydrate. This is supported by the reservoir pressure which after 35 years of development had reached 6.0 MPa in contrast to the expected 3.6 MPa if no hydrate was present. The field has also been produced by inhibitor injection. Inhibitor test data from the field where methanol was used show large production increases over short time. In later years the field has been produced at lower rates resulting in an almost constant pressure. It should also be noted that the gas water interface did not move as gas was produced (Sloan and Koh 2008, Makogon 2010).

The discovery of this field acted as a catalyst for hydrate research, but lacking available data and the existence of alternative theories based on cross flow of gas in conjunction with the heterogeneity of the reservoir (Collett and Ginsberg 1998), calls the role of hydrates into question (Moridis 2008, Xiuli Wang 2011).

1.4.2 Mackenzie River Delta: The Mallik Gas Hydrate Accumulation

The Mackenzie River delta in Canada was originally explored for conventional resources but has since then become the site of maybe the best characterized gas hydrate accumulation worldwide. The exploration of the Mallik Gas Hydrate Accumulation started on the basis of well logs made when searching for conventional HC-recourses. Three drilling programs were

executed in order to gain a better understanding of the hydrate accumulation, to prove the viability of gas production from hydrates and support modeling efforts. The field is overlain by 600 meters of permafrost and results from the drilling programs has revealed 10 significant hydrate bearing layers in the 900 – 1100 m interval, some with hydrate saturation over 80% (Moridis 2008). Estimates indicate a total of 5.19 x 10^7 m^3 of gas in hydrate over an area of 10 000 m^2, making the Mallik field one of the largest hydrate fields in the world (Sloan and Koh 2008).

During the Malik 2002 drilling program, conducted from December, 2001 until March 14, 2002 two observation wells were completed, 48 wire-line cores were obtained with over 150 m of gas hydrate bearing sediments, three successful pressure- and one thermal stimulation test were performed and multiple well logs obtained. The pressure stimulation tests successfully produced hydrate by depressurization and gave valuable information on the amount of hydrate through the pressure response in the formation as well as geo-mechanical and geothermal measurements at production pressures. The thermal stimulation test was performed by circulating hot brine in a 17 m section with high S_H, heating the formation to over 50 °C. The result was a continuous gas production over 125 hours, peaking at 1500 m^3/day. These tests proved the concept of gas production from gas hydrates and provided valuable information which was used to calibrate existing gas hydrate reservoir models. Results from modeling showed much better promise for the depressurization method, in large parts due to a much higher effective permeability than first expected. This led to a series of production by depressurization tests in 2007 and 2008.

The JOGMEC/NRCan/Aurora Mallik production program conducted two production tests; one in the winter of 2007 and one in the winter of 2008. The 2007 test had major problems with sand production which interfered with pumping operations. The result was that the test was terminated without achieving the desired bottomhole pressure (BHP). During the test an estimated total of 830 m^3 of gas and 20 m^3 of water were produced (Kurihara et al. 2010).

In the 2008 test a sand-screen was installed before the bottomhole pressure was stepwise reduced to 4.5 MPa in three stages and a longer production test was carried out, without problems with sand production. The first pressure reduction took the pressure from 11 to 7.4 MPa where it was held for 39 hours. Gas production started slightly above 7.4 MPa with an initial rate of 4000 m^3/day which decreased to about 1500 m^3/day at the end of the stage. The second stage took the pressure down to 5.2 MPa where the production rate increased to 3000 m^3/day before it decreased to 1500 m^3/day again. The third stage took the pressure down to 4.5 MPa where the production rate stabilized at 2500 m^3/day with water production at 15 m^3/day. This was the first time methane was produced to the surface by depressurization from a methane hydrate reservoir (Kurihara et al. 2010), excluding Messoyakha, and is an important step in the process of realizing gas hydrate as an energy source.

Chapter 2 CO_2 - CH_4 Exchange

When methane hydrate is exposed to a more stable hydrate former, CO_2, there is a release of methane and subsequent sequestration of CO_2 in a solid state process called CO_2 - CH_4 exchange. As illustrated in Figure 2.1 below, CO_2 hydrate is thermodynamically more stable than CH_4 hydrate at low temperatures. This in conjunction with the under saturation of methane caused by CO_2 injection provides a driving force for the exchange process (Hester and Brewer 2009). CO_2 and CH_4 produces sI hydrate both alone and together. Both molecules can occupy the large and small cages, but as shown in Table 1.2, the CO_2 molecule is larger with a molecular diameter/cavity ratio of 1 for the small cages, making CO_2 prefer the large cages. This makes the fill ratio of CO_2 in the small cages strongly dependent on pressure (Jung et al. 2010). The energy released from CO_2 hydrate formation is larger than the energy required for CH_4 dissociation, making the CH_4–CO_2 exchange process endothermic which possibly accelerates the exchange process.

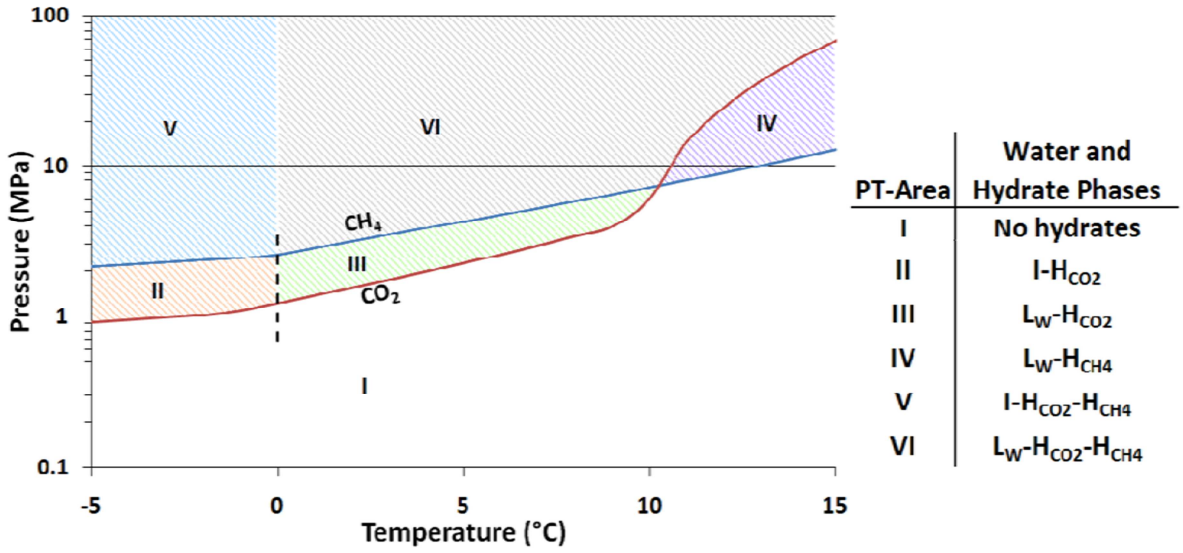

Figure 2.1: Phase diagram of both CO2 and CH4 hydrates. The diagram is divided into six PT-Areas. The table to the right shows the water phase as well as which hydrate is stable within each area (I= Ice, Lw= Liquid Water, HCO2= CO2-Hydrate, HCH4= CH4-Hydrate). (Husebø 2008).

2.1 Previous Experimental Investigations on CO_2 – CH_4 exchange

Ebinuma (1993) submitted a patent that described a method of producing methane out of- and storing carbon dioxide in hydrate formations. Based on the knowledge of CO_2 hydrate's larger thermodynamic stability it was hypothesized that injection of heated CO_2 into an existing natural gas hydrate accumulation would dissociate the existing hydrate and simultaneously form CO_2 hydrate. The endothermic nature of the methane hydrate to carbon dioxide hydrate reaction was recognized and this would supply additional energy to the process. Since then numerous investigations of CO_2 – CH_4 exchange has been carried out leading to a field test carried out in 2011 – 2012.

2.1.1 CO2 –CH4 Exchange in Bulk

Ota et al. (2005a), Ota et al. (2005b) studied the kinetics of the replacement process by exposing methane hydrate to CO_2 at 3.25 MPa and 275.2, 273.2 and 271.2 K in three different experiments where the hydrate composition was monitored by Raman spectroscopy. They observed a very high initial exchange rate which they attribute to surface replacement. They also observed a temperature-dependence with higher temperatures giving higher exchange rates. The rates at the later stages (>10 h) was successfully correlated with a model with constant surface area and a driving force proportional to the fugacity difference between the hydrate and gas phase.

Park et al. (2006), (2008) studied the effect of nitrogen on recovery by exposing methane hydrate powder to CO_2 and a 20 mol% CO_2 and 80 mol% N_2 mixture at 274.15 K and 3.5 and 12 MPa respectively. The hydrate structure and guest distribution was measured by NMR and Raman spectroscopy. They found that 64% of the methane was replaced when exposed to pure CO_2 while 85% was replaced when exposed to the CO_2 and N_2 mixture. Nitrogen would compete with methane for the small cages and replace 23% of the total methane while CO_2 would replace CH_4 in the large cages replacing 62% of the methane. They also performed the same experiment on sII- and sH hydrate which was produced by adding ethane and iso-pentane respectively. They found that the sII and sH hydrate would convert to sI hydrate when exposed to CO_2 or the CO_2 and N_2 mixture. The recoveries were found to be over 90 % in all of these four cases.

McGrail et al. (2007) investigated the rate of CO_2 - CH_4 exchange in bulk by using raman spectroscopy. They found it to be strongly temperature dependent and measured the penetration rate of CO_2 into CH_4 hydrate to be 0.22 and 1.3 mm/h at 0 and 4.5°C respectively. They concluded that the penetration rate was to slow for practical application in porous sediments, but no investigation of CO_2 - CH_4 exchange in sediments was performed. They instead investigated temperature dissociation and subsequent CO_2 hydrate formation by injection of temperate L_{CO2} – L_w emulsion. No energy demand estimate for this method was presented and it will not be further discussed here.

2.1.2 CO_2 – CH_4 exchange in pours medium

Zhou et al. (2008) studied the replacement of CH_4 from hydrate in quartz sand using carbon dioxide-in-water emulsions and liquid CO_2 at 281 K and 5 MPa. They correlated the exchange rate of the liquid CO_2 experiments with Ota et al. (2005b) and fond a good match despite the very different experimental procedures. They observed highest initial replacement (after 24h) with the 50:50 emulsion followed by 70:30, 90:10 and lowest with the liquid CO_2. After 96h the 90:10 emulsion had the highest replacement percent followed by 70:10, 50:50 and liquid CO_2. This was attributed to favorable mass and heat transport. They conclude that emulsions are advantageous compared to liquid CO_2.

Graue et al. (2008) studied methane hydrate formation, dissociation and CO_2–CH_4 exchange in partially saturated Bentheimer sandstone cores by MRI imaging. Hydrate was formed by pressurizing with methane to 8.16 MPa, injecting water and letting it imbibe until a saturation of 50% was reached, and then cooling it to 3.6 °C. The CO_2–CH_4 exchange was performed on a fractured core by injecting pure liquid CO_2 into the fracture and let stand to react with the hydrate. They observed methane being produced into the fracture with the MRI. After 3 CO_2 flushes they estimate the total methane recovery to be 50 – 85%. No liquid water was observed during the experiment indicating that no large scale dissociation took place. These experiments demonstrated favorable exchange kinetics in porous sandstone due to the large hydrate surface in such a system.

Hester et al. (2011) studied exchange rate and -extent in a fractured Bentheimer sandstone core at different initial water saturations while imaging with MRI. Hydrate was formed as an excess gas system by the same method used by Graue et al. (2008) before CO_2 was injected at a constant rate for a given duration. After injection, the hydrate was depressurized stepwise to find the hydrates dissociation pressure, which was used to find the hydrate composition. All of the experiments except one had the hydrate dissociated during a single pressure step, indicating a uniform hydrate composition throughout the core. The exception had a heterogeneously distributed water phase before formation which created a zone with very high hydrate saturation in the core. The exchange in this experiment showed significantly slower and less exchange, indicating that high hydrate and water saturation may be mass transfer limiting. The water distribution in this core was observed to be uniform after dissociation. They did not observe a significant difference in exchange for cores with initial water saturation of 0.3 and 0.6 which both reached a high CO_2 fraction in hydrate (60-80%). An experiment was also performed by flushing with CO_2 and shutting it inn to let the CO_2 diffuse into the core halves and react with the methane hydrate. After nine days the exchange was less than for two days of flushing.

2.2 CH_4 - CO_2 Exchange as a Production Strategy

The goal of all the previous mentioned experimental work was to evaluate the CO_2 – CH_4 exchange process as a production strategy. This production strategy has a number of advantages over the strategies involving dissociation of hydrate. Water and sand production is kept to a minimum while the sequestration of CO_2, gives an almost carbon neutral energy source, where CO_2 is stored in a way that will keep the hydrate stable even when the methane hydrate would have dissociated. Large scale dissociation of hydrates in marine sediments has been linked to catastrophic failure of marine sediments in the past, as the Storegga slides (Sloan and Koh 2008). By replacing methane hydrate with a more stable CO_2 hydrate the geo-mechanical stability is maintained.

An obvious downside of this technology is the extra expenses associated with CO_2 injection on this scale. Equipment must be able to withstand the corrosive nature of CO_2, and the general cost of this type of injection – production operation is expected to be significantly higher than for a simple pressure depletion operation. Gas hydrate fields are typically located in remote areas without nearby infrastructure where transportation of CO_2 and CH_4 to and from the site will be a challenge.

2.2.1 Field Test: Ignik Sukumi

ConocoPhillips executed a field test in 2011 - 2012 on CO_2 – CH_4 exchange based on a series of experimental results on CO_2 – CH_4 exchange in sandstone cores and sand-packs (Graue et al. 2008, Stevens et al. 2008), which demonstrated the viability of CO_2 – CH_4 exchange as a potential production method (Schoderbek et al. 2012).

In 2011 a well was drilled in the Alaska North Slope at a site selected for a high probability of gas hydrates in conditions similar to the laboratory experiments. Well logs revealed four hydrate bearing sandstones in the target formation. The well was perforated in an interval with thick, homogenous sandstone saturated with approximately 75% hydrate and 25% water. Due to concerns about loss of injectivity caused by secondary hydrate formation, and operational concerns around a liquid carbon dioxide injection, a series of laboratory experiments were performed and a phase behavior model developed. The solution was to inject a 77mol% N_2 + 23mol% CO_2 gas mixture which was predicted to be the optimal ratio for forming the least secondary hydrate and ice in the formation while still giving a sufficient exchange rate (Schoderbek et al. 2012).

In 2012 the project resumed. A sand screen was installed and a total of 5950 m^3 at 9.7 MPa of the gas mix was injected over 13 days. Production from the reservoir started after reconfiguration of the surface equipment, and was carried out in four phases: unassisted flow-back, jet pumping above methane hydrate stability pressure, jet pumping near methane hydrate stability pressure and jet pumping below methane hydrate stability pressure. The produced volumes of N_2, CO_2 and CH_4 are displayed against time in Figure 2.2 below. The well produced a total of 620 m^3 carbon dioxide, 4390 m^3 nitrogen and 23250 m^3 methane

where over half of the CO_2 injected, were stored in the formation. The test demonstrated the viability of CO2 – CH4 exchange as a production method (Schoderbek et al. 2012).

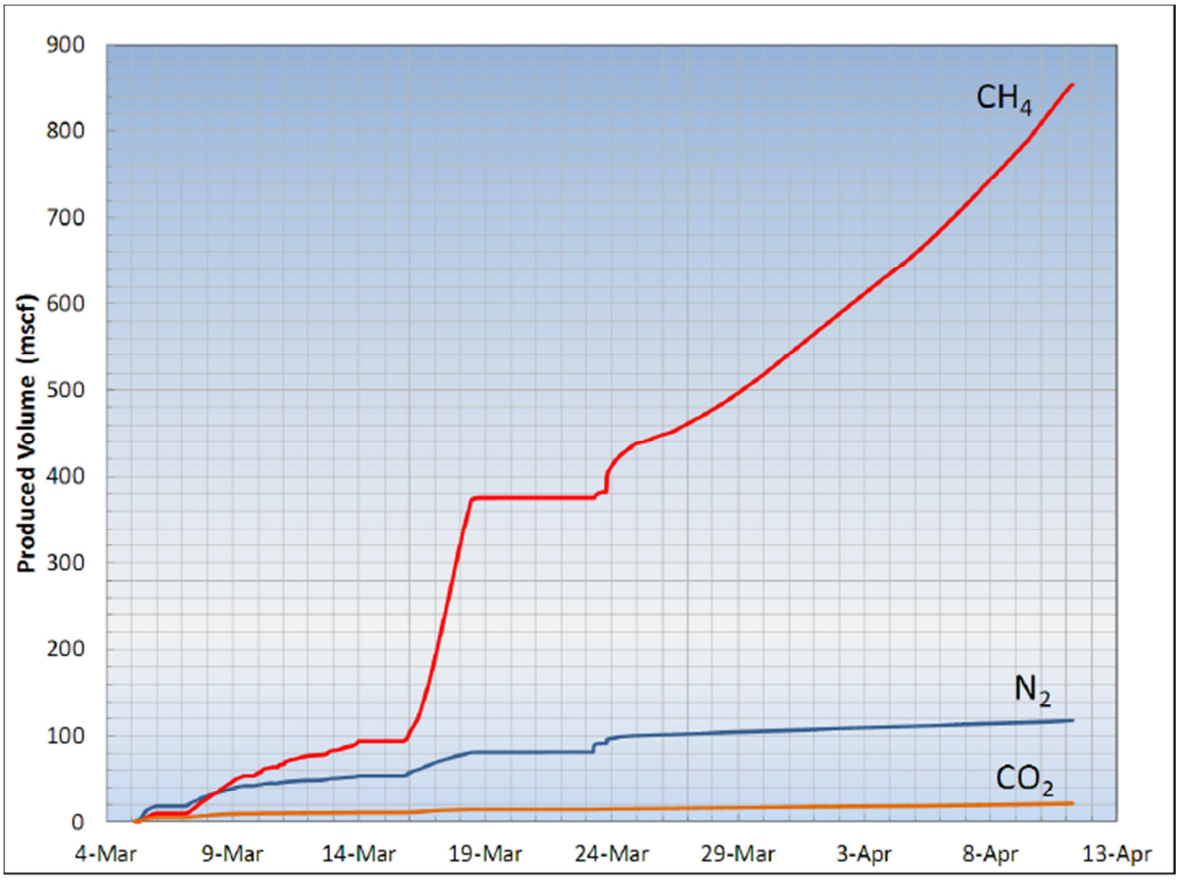

Figure 2.2: Produced volumes of each gas during production from Ignik Sukumi.

Chapter 3 Experimental Setups and Procedures

The majority of the experimental work in this thesis has been based on experimental procedures and setups developed at the Institute of Reservoir Physics over years of work on gas hydrates in sandstone core plugs. Hydrate formation, CO_2 – CH_4 exchange and dissociation experiments was conducted using three preexisting setups which were modified to improve the reliability of the data and decrease the failure rate. Most of the presented results have been performed on Setup A which was able to measure the core plugs resistivity. All the experimental work has been performed in collaboration with Christian Hågenvik.

This Chapter presents the experimental procedures and setups with modifications done to them and gives a short introduction to resistivity measurements and some basic premises behind the calculations.

The porous medium used for all the experiments for this thesis was sandstone cores from the Bentheimer quarry in Germany. Bentheimer sandstone is high permeable and very homogenous with porosity around 0.24. The mineralogy is 99% quartz with trace amounts of kaolinite, giving it an average grain density of 2.65 g/cm^3 (Graue et al. 2008).

3.1 Experimental Setups

There have been done extensive experimental work on gas hydrates in sandstone cores at the University of Bergen previous to the work presented in this thesis. Three pre-existing experimental setups (A, B and C) were therefore available which have been used in the experimental work. Setup A was able to measure resistivity and all setups logged PVT data which were used for mass balance calculations. The need for better reliability, flexibility, mass balance control and pore pressure control has made extensive modifications necessary, resulting in a redesign of all setups. All connections and valves were replaced and a mass flow meter (MFM) was implemented and tested as part of the later stages of the experimental work.

3.1.1 Setup A

Setup A was originally designed and built at the University of Bergen by Birkedal (2009), Hauge (2011) in an effort to gain resistivity measurements during gas hydrate formation, dissociation and CO_2-CH_4 exchange. Figure 3.1 shows a diagram of the original setup and

Figure 3.2 shows a cross sectional diagram of the core holder.

The core holder, a Temco EHCH resistivity core holder, was mounted in a cooling jacket connected to a Thermo Neslab RTE-17 refrigerated bath filled with antifreeze. An air driven Haskell MS-188 pump, connected to the confining pressure port, could pressurize and control the confinement by injecting hydraulic oil. The pore pressure system consisted of a high pressure pump connected to the core holder with 1/8'' steel tubing through a port in each end piece. A 4-way connection allowed a thermocouple to measure temperature at the core surface

without compromising the pore pressure system. The production/mass balance part of the pore pressure system was shared by all the setups and will be described later in a separate section.

Electrical resistivity could be measured over the whole core by connecting a LCR-meter producing a 1000 KHz current to the steel tubing on each side of the core holder. Non conducting material where used to hinder current from going through the pore pressure line and bypassing the core holder. Problems with noise when the LCR-meter was connected to a computer made it necessary to use a camera to log the resistivity. The system was able to perform 4-pin resistivity measurements by using a special sleeve with wiring and metal rings as illustrated in

Figure 3.2, but this feature has not been used in the work for this thesis as CO_2 destroys the sleeve and leaks into the confinement.

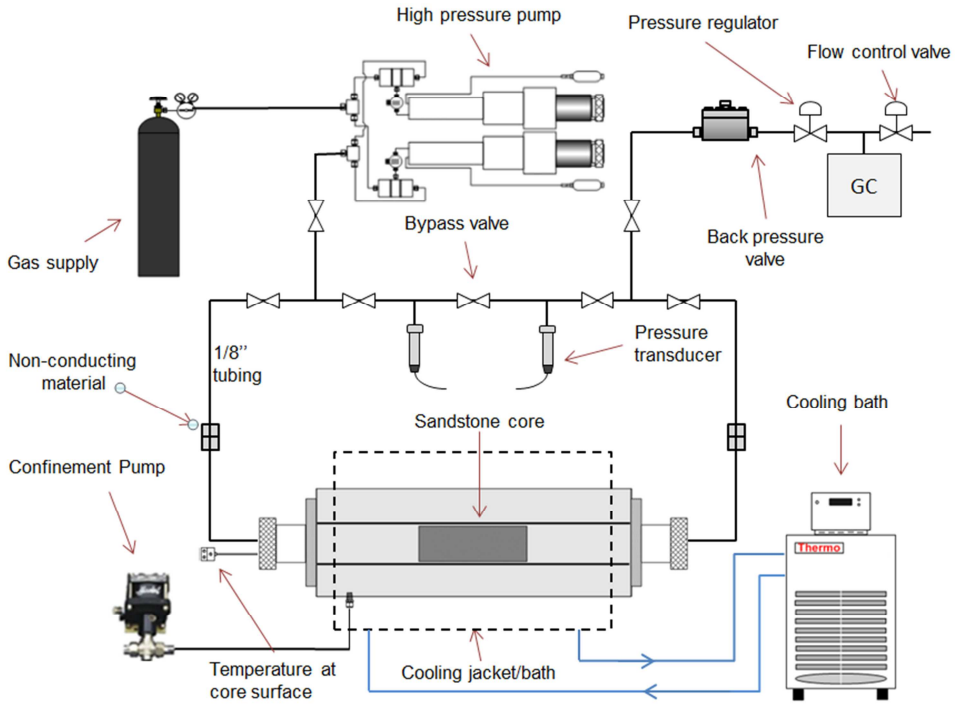

Figure 3.1: Schematic diagram of setup A before modifications where implemented. Tubing between system and BPV had to be disconnected if one of the other systems was to produce through the GC and Pressure Transducers gave no control over core pressure if system was closed.

Figure 3.3 below shows a diagram of setup A after the modifications were made. The original arrangement of valves and pressure transducers made it impossible to know the pressure in the core if the core was isolated (valves closest to the core holder closed). This could lead to water blowing into the line when the valves were re-opened or in worst case loss of core pressure and dissociation of the hydrate due to undiscovered loss of pressure. The new system solves the problem mentioned above and still allows for disconnection of the pressure transducers if calibration was needed.

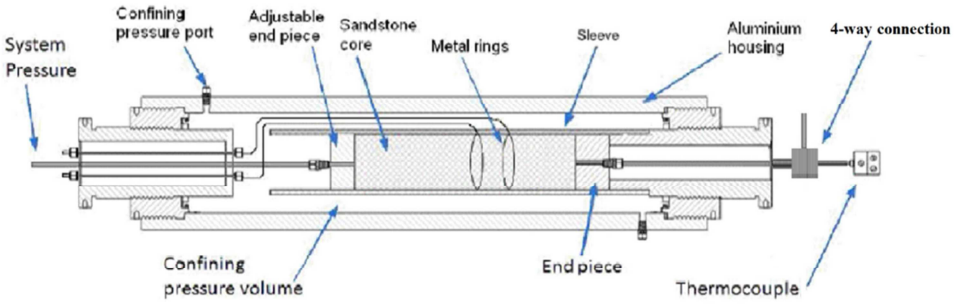

Figure 3.2: Floating en piece core holder. When confinement is applied, the adjustable (floating) end piece is pressed against the core plug and the confining sleeve is pressed against the end pieces. This provides a good connection for the resistivity measurements and isolates the pore pressure system from the confinement system and the environment.

The old confinement system was highly unstable. Small leaks of confinement oil caused confinement pressure to drop in the range of 1.4 MPa over a single night and the air driven pump would increase the pressure in the same range by a single stroke. The pump was also highly inconsistent in when it would start re-pressurizing if it worked at all. This caused the confinement pressure to fluctuate wildly in the duration of an experiment and the complete loss of confinement was always a threat. The resistivity measurements are highly dependent on confinement pressure, resulting in large fluctuations caused by varying confinement. The lack of confinement pressure logging made it difficult to interpret these fluctuations. On this basis the confinement system was redesigned as a part of the work for this thesis.

The new confinement system is shown in a simplified diagram in Figure 3.3. To solve the problem of fluctuating confinement pressure a buffer with nitrogen was connected to the system. Small leaks of confinement oil which previously caused significant pressure drops would with the new system be effectively buffered by the expansion of the nitrogen gas. The buffer could be pressurized with oil by the newly implemented ISCO pump or by Nitrogen directly from the cylinder. The confinement was pressurized with the pump and then switched over so the pressure was held by the buffer. Two manometers provide pressure measurements at the buffer and at the core holder so the pressures could be matched before switching over. Another big advantage of the new system is the ISCO pumps ability to draw oil out of the confinement, making it possible to draw down the confinement pressure with the pump. This was not possible with the air driven pump where the confinement had to be tapped by carefully opening a valve leading to an oil container. This procedure was generally considered to dangerous to perform as gas could have diffused into the confinement.

The modified system connected the confinement systems for setup A and B and only required one pump and one buffer. This was a necessity due to the limited space and equipment available. One potential weakness is the inability to hold different confinement pressures for the two systems.

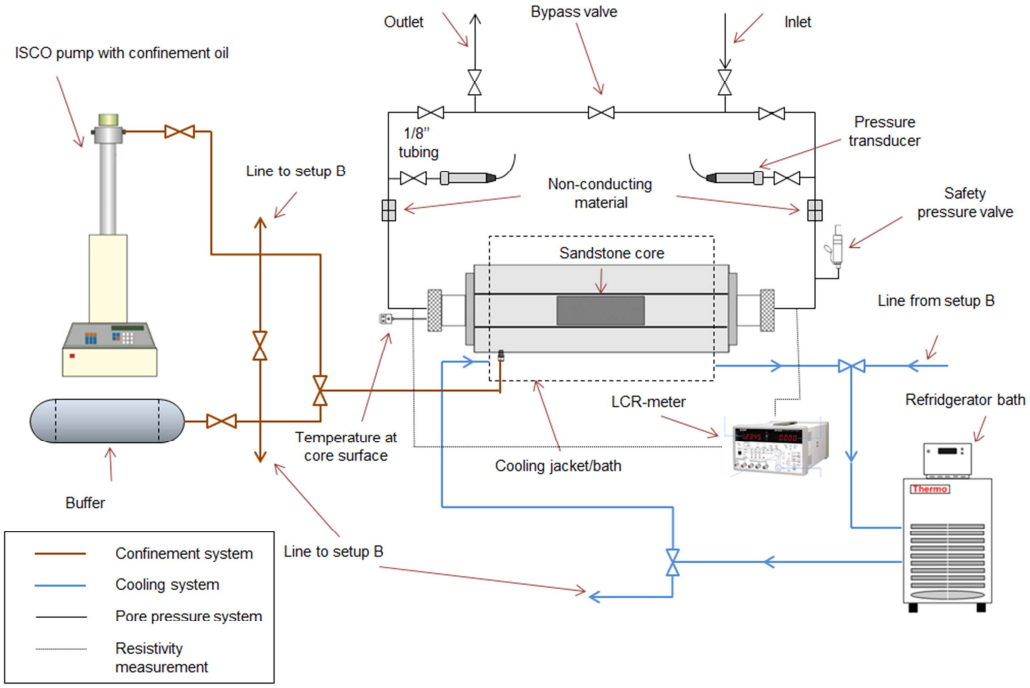

Figure 3.3: Schematic over Setup A with cooling and confinement systems. A buffer with nitrogen hinders large confinement pressure fluctuations and the new arrangement of the pore pressure system gives the opportunity to monitor pressure in the core when isolated. Safety pressure valves were also added.

3.1.2 Setup B

This setup was designed and built by Birkedal (2009) in response to flooding problems encountered with the open bath cooling system described under Setup C below.

Figure 3.4 shows a cross sectional diagram of the core holder used in setup B. This high pressure Hassler core holder was mounted in a cooling jacket connected to the same Thermo Neslab RTE-17 refrigerated bath as setup A. An air driven Haskell MS-188 pump was used to pressurize and control the confinement in the same way as the original setup A. A thermocouple was connected to one of the ports with a high pressure pass in order to be able to measure the surface temperature of the core plug.

The pore pressure system was connected through one port in each end piece and is thus able to pressurize the core from both sides simultaneously, avoiding having water blown into the tubing. The original setup was the same as for setup A with exception to the core holder, the non-conducting material and the LCR-meter.

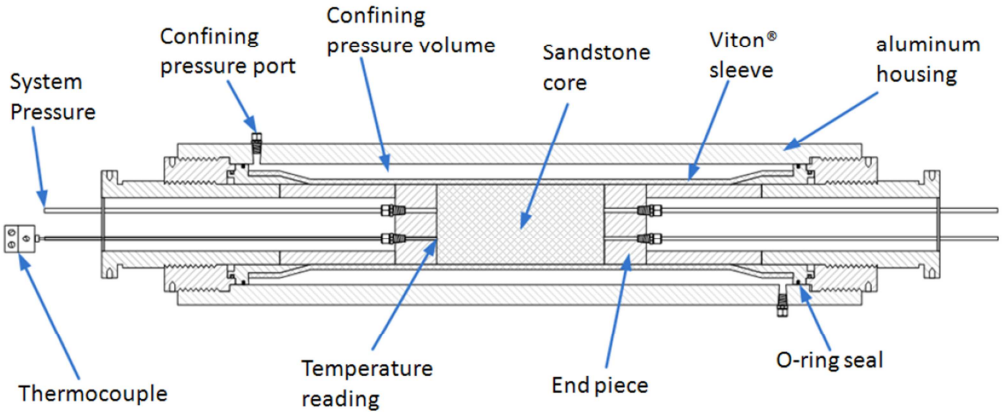

Figure 3.4: Cross sectional diagram of core holder used in setup B and C (Husebø 2008)

Due to the advantages of the modifications made to system A and to avoid confusion there was made a decision to standardize the setups. Setup B was modified after setup A as seen in Figure 3.3, with exception for the LCR-meter and the non-conducting material. Thermocouples were installed at inlet, outlet and confinement in order to support numerical simulations and to check the thermal gradient in the core.

The cooling system for setup A and B consist of a single Thermo Neslab RTE-17 refrigerated bath filled with antifreeze and connected to both systems by insulated hoses. The flow can be directed to one, both or none of the systems by valves. A weakness of this system is the inability to finely tune the temperature of both systems simultaneously.

3.1.3 Setup C

Setup C consisted of a Hassler type core holder which could be completely submerged in an open cooling bath filled with antifreeze. A Thermo Neslab RTE-17 refrigerated bath circulated antifreeze through the open bath where the flux of antifreeze in and out of the bath was controlled by two valves.

This setup had some major drawbacks compared to the cooling jacket setups. A minor error in the adjustment of the valves could lead to shutdown of the refrigerated bath due to low levels of antifreeze and subsequent flooding. This could also happen due to water evaporating out of the open bath if not refilled on a regular basis.

Setup C was later fitted with a cooling jacket and configured in the same way as setup B, but with a separate buffer-confinement system and a separate cooling system.

3.1.4 Pore pressure and mass balance system

The outlet sides of the pore pressure systems could be connected to a backpressure valve (BPV), connected to a nitrogen cylinder via a pressure regulator in order to control the BPV's opening pressure. This was connected to the Gas Chromatograph (GC) via a pressure

regulator, regulating the pressure down to about 0.15 MPa. A flow control valve could be adjusted to get a steady flow through the system.

This system had severe problems with mass balance calculations which were done by PVT analysis based on the injection rate. The large difference in liquid carbon dioxide and methane gas densities as well as effects of mixed molar mass made these calculations very uncertain. During production, the BPV would let effluent through in bulks with large periods of pressure build up before more gas would be let through. This creates major problems for the PVT-type analysis, potentially causing large errors in calculations.

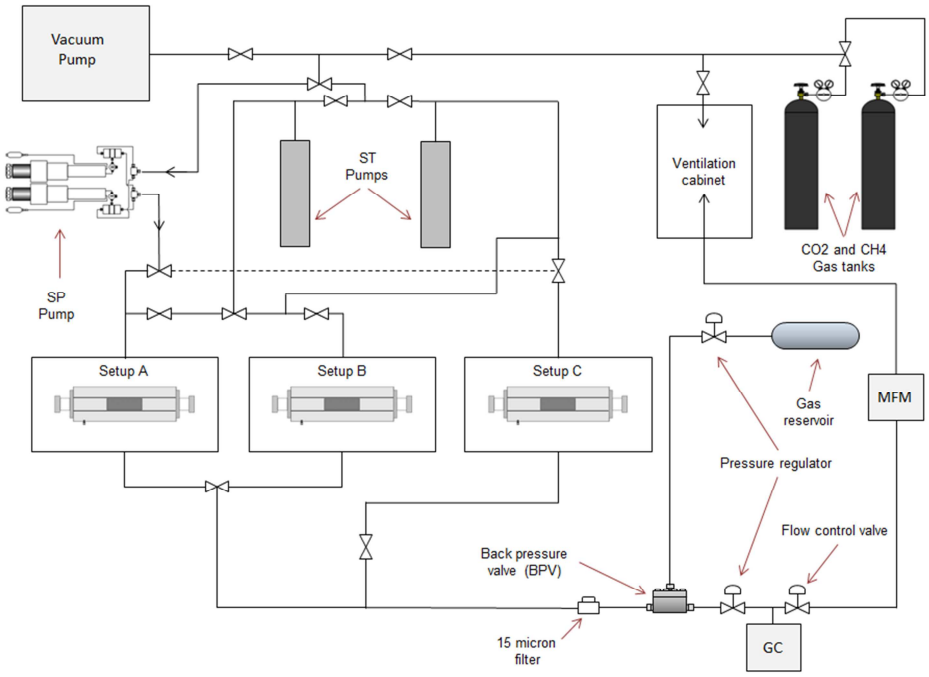

Figure 3.5: Overview of the experimental system after modifications was made. The three setups have an interconnected pore pressure system which makes it possible to quickly change pumps between setups. The production part of the system can be switched between setups with valves and consist of a gas chromatograph (GC) which measures the effluent composition and a mass-flow meter (MFM) which measure the mass flow.

Figure 3.5 shows a diagram of the final pore pressure and mass balance system excluding the details in the individual setups illustrated in Figure 3.3. Two Sanchez high pressure ST-pumps were connected in such a way that they could independently deliver gas to any of the three systems. Together with a third pump, a Quizx 5000-SP, this allowed for co-injection of two substances to any single system while an experiment was ongoing on a second system. It also became possible to perform formation experiments on all three setups simultaneously. The great flexibility offered decreased the work required to perform experiments and provided a much higher experimental output rate by removing the necessity of waiting for other experiments to be completed and reducing the planning required.

The outlet sides of all setups were connected to a single BPV which could be switched between the different setups by valves. This removed the necessity of disconnecting and

connecting tubing often causing leaks. The BPV pressure was controlled by a gas reservoir filled with nitrogen. The composition of the produced gas was measured by a GC as and a MFM measured the mass flow rate before the gas was led to a ventilation chamber.

The implementation of the MFM provided the ability to measure effluent gas flow and predict recoveries with much better precision. The gas volume flow however, still needed to be controlled by a flow control valve, which is a weakness of the system due to the varying volume flow caused by the vaporization of liquid CO_2 when passing through the pressure regulator.

3.2 Experimental Procedures

The experimental procedure have been designed to produce hydrate bearing sandstone cores with a uniform hydrate saturation where CO_2 could be injected in order to study the exchange process. The procedures were based on the significant experience accumulated in-house in the course of years of research on gas hydrate bearing sandstones. It was desired to achieve varying hydrate saturations as well as cores with hydrate and active water present in order to study the effect on formation and exchange. There were expected to be injection problems due to loss of permeability in the higher S_{wi} cores and the use of N_2-gas was prepared to counter it.

3.2.1 Core Preparation

The core plugs were cut to approximately 14 cm diameter and milled to 5.05 cm diameter then left in a heating cabinet at 80 ° C for 24 hours to dry before they were weighed. The porosity was calculated on the basis of the core weight and average grain density.

In order to partially saturate the cores and achieve a homogenous saturation, the cores were put vertically in a box with a small amount of brine. The brine, consisting of distilled water and NaCl, was allowed to spontaneously imbibe through the whole core. The cores were then wrapped in paper towels and put into a vacuum chamber. The lowered pressure caused brine to be drawn out of the core and into the paper towel. The cores were taken out and weighed. If the desired saturation wasn't reached the cores were turned upside-down and vacuumed again.

In order to obtain cores with more active water and higher hydrate saturations some cores were saturated above S_{wi} of 0.7. To achieve this, dry cored were put in a vacuum-glass beaker with the brine in a beaker on top. Both beakers were vacuumed, carefully not to have water evaporate, before the brine was let into the bottom one to imbibed into the core. To reduce the saturation to the desired level the cores was wrapped in paper towels and vacuumed as described above.

When the desired saturation was reached the cores were wrapped in plastic then aluminum foil. The aluminum foil was fastened by aluminum tape in order to avoid problems when mounting it in the sleeve. This was done to protect the rubber sleeve in the core-holder against the CO_2 and reduce the amount of CO_2 escaping in to the confinement oil. They were then put into the core-holder and sealed to prevent water from evaporating and changing the water saturation and salinity. The plastic spacers that can be seen between the end pieces and the

core in Figure 3.6C are wrapped in aluminum foil with the core in experiments with high water saturations. This was done in order to hinder water from going into the lines and form hydrate plugs.

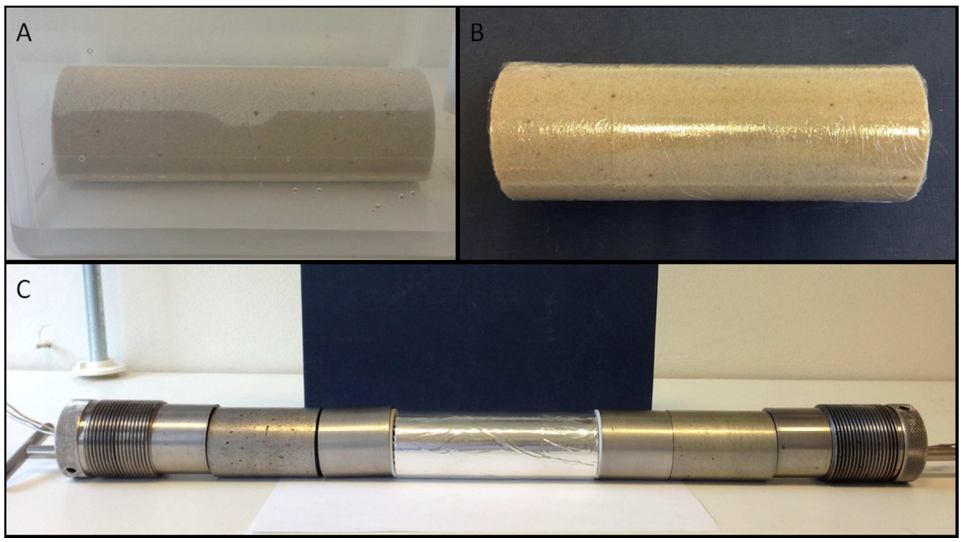

Figure 3.6: Core preparation. Core in the process of imbibing brine (a), Core wrapped in plastic foil (b) and core wrapped in aluminum foil laid out between two end pieces as it would in the core holders of setup B and C.

Some of the experiments were performed with an artificial fracture held open by a spacer as seen in Figure 3.7A and B. These cores were cut in two down the length of the plug. The two halves were then treated in the same manner as the whole core but with a plastic spacer between them when wrapping in plastic and aluminum foil. The main goal was ensuring permeability during CO_2 injection, but it also provides the opportunity to study the effect of a fracture on both formation and exchange.

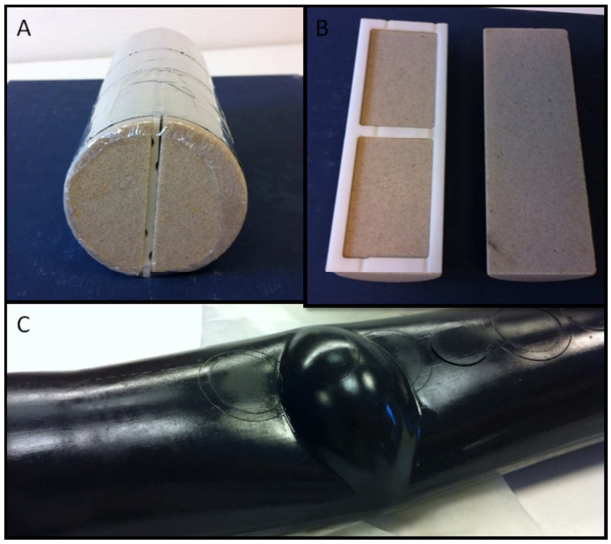

Figure 3.7: Core plug readied for spacer experiment. (A) Shows the assembled core with spacer ready to be mounted in sleeve while (b) shows the core cut in half and displayed with the spacer. (C) The resulting damage on a sleeve from expanding of CO_2 diffused into it during the experiment.

3.2.2 Hydrate Formation

Hydrate formation was performed as an excess gas system, with a limited amount of brine in the sandstone core and an unlimited supply of methane being provided by the pump. Before pressurizing the system, the prepared core plug was mounted in the core holder, isolated from the system and a small confinement pressure was applied (~1 MPa). The tubing and pump volume was then vacuumed in order to remove unwanted air before beginning the pressurization process.

The pore pressure system was pressurized directly from the methane cylinder via the pump. The pressurization process started by slowly opening the pressure regulator at the methane cylinder and opening to the core at both sides the moment the pressure hit 0.1 MPa. A big pressure difference between the core and the pore pressure system at this stage could disturb the brine distribution and in worst case water could be blown out into the tubing and potentially form hydrate plugs later it the experiment.

The pore and confinement pressure was then increased in 1 MPa increments until they reached 8.3 and 12 MPa respectively. The confinement was kept at least 1 MPa above the pore pressure at all times. In the later experiments with confinement buffer, the confinement pressure was matched to the buffer pressure before being switched over.

The pump was set to hold a constant pressure of 8.3 MPa and the system was then checked for leaks. When no more leaks were found, the system was let stand for 24 hours to stabilize. The pump data logged during this period were used to calculate the leak rate which was used in the mass balance calculations.

Hydrate formation was initiated by engaging the cooling system, cooling the core to about 4 ° C and taking the system into the hydrate stable region. Cumulative volume of methane

consumed, core plug temperature, pore pressure and in the case of setup A, resistivity where logged.

3.2.3 CO_2 – CH_4 Exchange with Methane Production

A pump was vacuumed, filled with CO_2, pressurized to 8.3Mpa and let stand overnight to stabilize. The core was then isolated and the pore pressure system was vacuumed and pressurized with CO_2 to the set BPV pressure. This made it possible to produce gas through the BPV immediately and the residual nitrogen in the core could be used as a marker to that showed when gas from the core reached the GC.

When the pressure had stabilized the core was pressurized to the BPV pressure in order to avoid a sharp pressure drop when the outlet was opened. When the BPV pressure had been reached the bypass valve was closed, the outlet valve opened and CO_2 was injected at a constant rate. The gas was produced through the pressure regulator, regulating the pressure down to about 0.15 MPa so the GC could make measurements before it was produced out into the ventilation cabinet. In later experiments the gas was produced through the MFM before venting.

Injecting pure CO_2 in the whole cores that had high initial water saturation were considered a problem as secondary hydrate formation could reduce the permeability sufficiently to stop the injection. In order to resolve this, a co-injection of 25 mol% CO_2 and 75 mol% N_2 were used. The ratio were decided based on the work done before and during the Ignik Sikumi field trial (Schoderbek et al. 2012) which had similar pressure and temperature conditions as the ones used in the experimental work for this thesis.

In the CO_2 - N_2 co-injection experiments a second pump was filled and pressurized with nitrogen gas. Nitrogen was typically used instead of CO_2 to pressurize before injection start. This made it possible to have better mass balance control of CO_2. Nitrogen was injected simultaneously as CO_2 with a rate calculated for the desired N_2/CO_2 mol-fraction.

The fractured cores would have problems with CO_2 bypassing the sandstone by going through the fracture. CO_2 would have to diffuse from the fracture into the core halves which were expected to take a significant amount of time. One experiment was performed using diffusion driven injection where CO_2 was injected at a higher rate to flush out the gas in the spacer before the core was shut-in. The core was then let stand to give the CO_2 time to diffuse into the core halves and react with the methane hydrate. Previous experiments by (Graue et al. 2008) show that this procedure causes methane to be produced out into the fracture. The injection procedure was to be repeated until there was no more methane production.

3.2.4 Dissociation

The CO_2 had a tendency to diffuse through the sleeve and into the confinement making it hard to make mass balance calculations on CO_2. This made it useful to perform a controlled

dissociation of the hydrate after $CO_2 - CH_4$ exchange which could give an estimate of the amount of gas in hydrate and the thermodynamic equilibrium of the hydrate. The dissociations were performed either by temperature increase or by depressurization. Methane was used to flush out the free CO_2 before dissociation was initiated.

The depressurization was performed by lowering the pressure to a pressure slightly above the expected equilibrium. When the system had stabilized the pressure was quickly lowered to a set value and the pump set to hold constant pressure. The procedure was repeated until no further dissociation was observed.

Dissociation by temperature was simply performed by setting the temperature of the cooling bath to 20°C while the pump held a constant pressure.

3.2.5 Depressurization

In order to support an ongoing simulation effort on dissociation of methane hydrate an experiment was performed by repeated formation and dissociation of methane hydrate on a whole core. Thermocouples were installed in the confinement as well as both sides of the core. The experiment could give insight into the memory effect, show if there were a significant thermal gradient across the core and give a baseline for the dissociations performed after CO_2 exchange. Hydrates formation and temperature dissociation were performed by the procedures described in the previous section. The depressurizations were performed by lowering the pressure quickly from 8.3 to 3.33 MPa. When no more dissociation were visible, the pressure was taken down to 2.0 MPa. The core was heated to 20°C between dissociation and formation.

3.3 Resistivity

Resistivity logging is in conjunction with other logging methods a well-established method for estimating fluid saturations in the geological formations. The method can among other things be used to detect hydrate bearing intervals and estimate hydrate saturations. In the experimental work it can give indications of growth patterns and saturations distributions in the core plug as well as indications of permeability.

3.3.1 Basic Concept

Resistivity, R, is a measure of a mediums specific electrical flow resistance measured in ohm-meter (Ωm) and is defined for a resistor of uniform cross section by Ohm's law:

$$R = r\frac{A}{L} = \frac{E}{I}\frac{A}{L} \tag{3.1}$$

Where r is the objects total resistance, I is the electrical current, E is the applied voltage, A is the cross section and L is the length of the resistor.

Resistivity for a porous medium is dependent on the geometry of the pore space, the resistivity of the matrix, the resistivity of the pore fluids, the saturations and the saturation

distribution. The matrix generally conducts electricity very poorly with exception for some clay minerals but the Bentheimer sandstone contains very small amounts of clay and could be considered nonconductive. In order to characterize the electrical properties for a pours medium a series of empirical equations defined by Archie are used. The formation factor, F, is a rock property relating the resistivity of the porous medium 100% saturated with brine, R_0, to the resistivity of the brine, R_w. The formation factor is defined as:

$$F = \frac{R_0}{R_w} \tag{3.2}$$

Based on experimental data, Archie related formation factor to porosity:

$$F = \frac{a}{\phi^m} \tag{3.3}$$

Where *a* is related to how tortuous the pore network is, also called tortuosity, and the pore size distribution. The cementation exponent, m, relates to the relation between pore size and pore throat size and the number of closed channels. Archie also defined the resistivity index, RI, as:

$$RI = \frac{R_t}{R_0} \tag{3.4}$$

Where R_t is the measured resistivity. The resistivity index is related to the brine saturation with the empirical equation:

$$RI = bS_w^{-n} \tag{3.5}$$

Where b is a function of tortuosity and n is called the saturation exponent dependent on the microscopic distribution of fluids and the amount of conductive clays.

3.3.2 Resistivity measurements on core plugs

Resistivity measurements made on Setup A does in reality measure the impedance, Z, related to the resistivity by the phase angle ϕ:

$$R = Z\frac{A}{L}\cos(\phi) \tag{3.6}$$

The 2-pin method used in the experimental work is unable to measure the phase angle. Previous experimental work has however shown the phase angle to be stable and small (Birkedal et al. 2011) and the resistivity can still be used qualitatively. When hydrate form, salt ions are excluded increasing the overall salinity and possibly forming a concentration gradient in the brine. The resistivity of the brine is highly dependent on salt concentration,

decreasing with increasing salinity. The formation of hydrate can also severely increase the tortuosity of the conductive brine phase and hereby increases the mediums resistivity.

3.4 Calculations

Some basic premises for the calculations are presented below.

3.4.1 Formation

All saturation changes during formation were calculated based on the amount of methane consumed and the initial water saturation, where a hydration number of 5.99 and an expansion factor of 1.26 for water going into hydrate were used. The hydration number was based on work done by Circone et al. (2005) were a number of experiments on the composition of methane hydrate in bulk were reported to give a hydration number of 5.99(±0.07).

Induction times were measured from the moment the temperature measurements reached 9.3 °C to the time where a clear consumption of gas where visible. This may be inaccurate on shorter induction times as the bulk core temperature may differ from the core surface temperature during cooling and the rate of cooling differed between experiments.

Final brine salinities were calculated based on the assumption of a non-changing amount of salt and the calculated change in saturation during hydrate formation.

3.4.2 Recovery

The recovery factor, RF, is defined as:

$$RF = \frac{N_p}{N} \tag{3.7}$$

Where N_p is the amount produced [mol] and N is the amount originally in place [mol]. The recovery can either be presented as a fraction or as a percentage. Two different types of recovery are presented in this thesis; total methane recovery ($RF_{CH4,tot}$) where N represents all the methane in the core (both free and in hydrate), and methane recovery from hydrate ($RF_{CH4,H}$), where N represents the methane in hydrate. There are currently no way to differentiate between methane from hydrate and free methane. The calculations on $RF_{CH4,H}$ has for this reason assumed that all the free methane and the methane in the line volume were produced first and are set to zero until that amount were produced. The total recovery assumes all the methane in the line volume was produced first and was set to zero until the estimated amount of methane in the lines were produced. The calculated recoveries come later than expected because of this and it gives a pessimistic estimate for $RF_{CH4,H}$.

The recoveries presented were based on two different types of data sets. The earlier experiments assumed that the volume produced was equal to the volume injected and the mixed molar mass of the measured effluent composition was used together with GC-data to estimate the amount of each component produced. The later experiments have direct measurements of mass flow through the MFM which the recovery calculations were based on.

Chapter 4 Experimental Results and Discussion

In this chapter the results of the experimental work are presented and discussed in three main sections; hydrate formation, dissociation of pure methane hydrate and CO_2 – CH_4 exchange. The experiments are named after the inn-house practice where they are divided into three categories based on the experimental method used. CO_2 – CH_4 exchange experiments performed on setup B or C without resistivity measurements are denoted CO_2_#, CO_2 – CH_4 exchange experiments performed on setup A with resistivity measurements are denoted HR_# and depressurization experiments where methane hydrate are dissociated and produced by depressurization are denoted DEP#_n where n a number referring to the formation – dissociation cycle (how many times the formation-depressurization has been performed on the same core).

There have been performed a total of nine experiments designed to investigate how initial saturations influence formation and subsequent CO_2 – CH_4 exchange and one experiment (DEP5) which investigated formation and dissociation kinetics. An experimental overview with some key values is presented in Table 4.1 below.

HR_47 and HR_48 can for comparison purposes be considered baseline experiments, since the low salinity experiments have initial water saturation (S_{wi}) in the same range and the higher S_{wi} experiments have the same salinity.

Table 4.1: Experimental overview.

		Pre Formation		Post Formation		CO2 - CH4 exchange	
Name	**Core**	**Salinity [wt%]**	**S_{wi}**	**S_H**	**S_{wf}**	**Injection**	**$RF_{CH4,tot}$ [%]**
DEP_5	Whole	0.1	0.43	0.46	0.06	CO2	-
CO2_20	Whole	0.1	0.42	0.53	0.00	CO2	-
CO2_25	Whole	0.1	0.41	0.51	0.00	CO2	45
HR_47	Whole	3.5	0.42	0.38	0.12	CO2	-
HR_48	Whole	3.5	0.40	0.42	0.08	CO2	23
HR_49	Whole	3.5	0.64	0.46	0.29	CO2 + N2	26
HR_50	Whole	3.5	0.65	0.47	0.28	-	-
HR_51	Whole	3.5	0.67	0.51	0.27	CO2 + N2	61
HR_52	Fractured	3.5	0.74	0.35	0.47	CO2	29
HR_53	Fractured	3.5	0.81	0.41	0.50	CO2 + N2	-

4.1 Hydrate formation

Hydrate was formed 13 times during the work for this thesis where the initial water saturations used roughly can be divided into three categories; low saturation (S_{wi}~0.4), high saturation (S_{wi}~0.6) and very high saturation (S_{wi}>0.7), where the cores with very high saturation were fractured based on results from Ersland et al. (2009) which reported significant loss of gas permeability in cores with high hydrate saturation (S_H>0.6). All of the experiments with high and very high initial water saturation were performed with 3.5 wt% NaCl brine while the CO2- and DEP experiments were performed with 0.1 wt% NaCl brine. The goal with this approach was to study the effect of varying initial water saturation and salinity on formation while at the same time obtain cores with high residual water saturation and varying hydrate saturation to be used for study of the effect on $CO_2 – CH_4$ exchange.

Hydrate formations are presented as cumulative methane consumed against time. As hydrate form, gas in the pore space is consumed and the pump, set to hold constant pressure, supplies new methane to the system. Cumulative volume gas consumed can be considered a direct measurement of hydrate growth rate and total amount of hydrate formed.

An overview of the experiments with some key figures related to hydrate formation is presented in Table 4.2 below. Figure 4.1 and Figure 4.3 are hydrate-formation comparison plots for low water saturation with two different salinities and high salinity experiments with varying initial water saturations respectively. The x-axis of these plots represents the time from start of massive hydrate growth, where the induction time has been removed for simpler comparison. No clear correlations in induction times were observed but higher saturations tended to have longer induction times.

Table 4.2: Overview of hydrate formation experiments. The salinity of the CO2- cores were considered unknown as the saturation calculations becomes uncertain at low residual water saturations (<0.01).

		Pre Formation			Post Formation		
Name	**Core**	**Salinity [wt%]**	**S_{wi}**	**Induction time [h]**	**S_H**	**S_{wf}**	**Salinity [wt%]**
DEP5_1	Whole	0.1	0.43	1.2	0.46	0.06	0.7
DEP5_2	Whole	0.1	0.43	0.6	0.45	0.07	0.6
DEP5_3	Whole	0.1	0.43	0.5	0.44	0.09	0.5
DEP5_4	Whole	0.1	0.43	0.5	0.42	0.10	0.4
CO2_20	Whole	0.1	0.42	1.1	0.53	0.00	-
CO2_25	Whole	0.1	0.41	0	0.51	0.00	-
HR_47	Whole	3.5	0.42	0.7	0.38	0.12	11
HR_48	Whole	3.5	0.40	0.3	0.42	0.08	15
HR_49	Whole	3.5	0.64	0.3	0.46	0.29	7
HR_50	Whole	3.5	0.65	27.0	0.47	0.28	8
HR_51	Whole	3.5	0.67	10.2	0.51	0.27	8
HR_52	Fractured	3.5	0.74	1.5	0.35	0.47	5
HR_53	Fractured	3.5	0.81	9.2	0.41	0.50	6

Fluctuations in the gas consumption curves were caused by fluctuating room temperature influencing the temperature of the core and the gas in the pump. These fluctuations followed the day-night cycle to a large degree and were also dependent on the activity level in the laboratory. The fluctuations were especially big during hydrate formation in HR_53 due to a large volume of gas in the pump and a big difference in the day-night temperature. Plots where the impact of temperature fluctuations is large have in most cases been displayed with the horizontal axis divided into 24 hour intervals, for easier identification of changes caused by the fluctuating temperature. The saturations changes in HR_48 were calculated with the assumption of no leakage. The formation curve is almost completely horizontal at the end of hydrate formation which indicates that the actual leakage was small and the assumption did not lead to large errors.

The formations were reproducible and showed a strong dependence on both initial brine salinity and saturation. An exception was HR_51, where indications of a different growth pattern were observed. This is discussed separately in Section 4.1.3.

4.1.1 Effect of Salinity on Formation

Salts are as explained in section 1.1.5 a thermodynamic inhibitor and the inhibiting effect is strongly dependent on concentration. When hydrate form, salt are left behind in the brine, increasing the overall salinity. Supersaturation is the driving force in hydrate formation and salinity severely affects the thermodynamic stability-region and thereby the size of the driving force. This will cause a smaller driving force for hydrate formation with higher salinity brine and consequently a lower growth rate. The thermodynamic equilibrium for methane hydrate at the experimental conditions (8.5MPa and 4°C) is reached at 14 wt% NaCl at which point hydrate can no longer grow.

Previous in house investigations by Husebø et al. (2008) found a strong correlation between initial brine salinity and fill fraction, where the fill fraction were defined as the amount of methane in hydrate relative to the theoretical maximum of hydrate cages if all the methane were part of the hydrate structure. This correlation was unaffected by initial saturation distribution and core plug geometry. They also observed that higher salinity led to slower growth rate.

Figure 4.1 below show a comparison of all the formation experiments performed with initial water saturations in the 0.4 range. The low salinity formations were characterized by a very high initial growth rate, lasting until approximately 10 ml of methane were consumed, before they were reduced to a slower almost constant growth rate. At a later stage the growth rate decline until hydrate formation were complete. This indicates that hydrate formation in partially saturated sandstone can be divided into three growth regimes; a fast initial growth rate caused by hydrate formation on the gas-brine interface, an intermediate constant growth rate most likely limited by mass transfer and a late declining growth rate limited by the availability of hydrate former or active water. The high salinity formations declined steadily after the initial growth until formation was complete, indicating a limiting factor increasing as more hydrate was formed.

A clear indication of salinity affecting the initial growth rate as well as the later, stable, growth rate was identified. The initial growth rate was observed to be consequently higher for the low salinity cores, as seen in Figure 4.2. This may be a result of the lowered driving force in the high salinity brine.

As seen in Figure 4.1, the reduction in growth rate between initial and intermediate growth, was significantly bigger for the 3.5 wt% cores. The difference in initial growth rates are likely a direct result of salinity affecting the driving force but it can also have been affected by transport of salt ions away from the hydrate formation region.

When hydrate form and salt ions are left behind in the brine, there is expected to be an ion concentration gradient in the brine with high concentration close to the brine – hydrate interface where hydrate growth occurs. The lowered driving force will have a significantly bigger influence in the high salinity brine were the increase in salinity quickly can reach equilibrium concentration (14 wt% NaCl) locally. This indicates that diffusion of salt ions can be a limiting factor in the high salinity cores. The increasing salinity can also explain the less linear nature of the high salinity core's growth. Hydrate growth rate would slow down, due to lowered driving force and slower ion diffusion rates, as the average brine salinity increases. Growth would eventually cease when the brine reached 14 wt% NaCl.

The increasing brine salinity in the low salinity cores were expected to be negligible until very low water saturation was reached. A sharp decline in growth rates were observed before salinity reached this point and is likely a result of the combination of a local lack of active water, giving hydrate a progressively smaller area to grow in, and the increasing salinity reducing the growth rate were water is available.

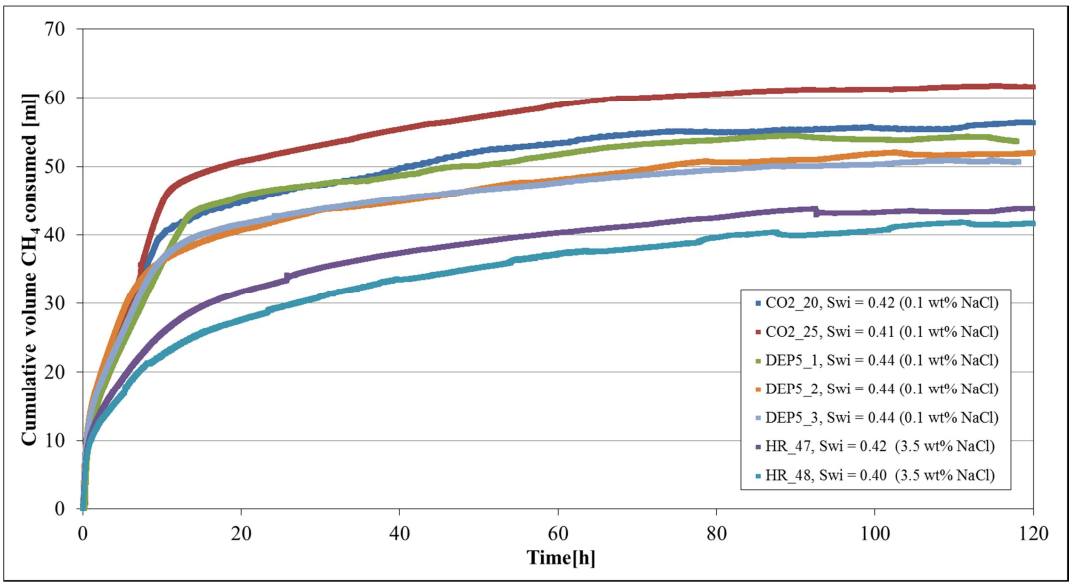

Figure 4.1: Hydrate formation for experiments with initial water saturation in the 0.4 range. The fourth formation in DEP5 has been excluded as it is a special case and will be discussed further in section 4.2.1.

The high salinity experiments also achieved significantly lower final hydrate saturation and subsequently higher residual water saturation. Mass balance calculations indicated that the

low salinity formations had close to no residual brine after hydrate formation. The experimental results also indicate that the lower hydrate saturation in high salinity cores were a result of hydrate formation being halted by increasing brine salinity, ending up at equilibrium conditions with more residual water and less hydrate. Calculations show that the two high salinity low saturation formations, HR_47 and HR_48, reached a brine salinity of approximately 11 and 15 wt% NaCl respectively. The formation curves also indicate that the hydrate formation in HR_48 was not completed which strengthens the hypothesis of brine salinity being the controlling factor of residual brine at these saturations.

The results successfully reproduces some of the results reported by Husebø et al. (2008) where the fill fractions for 0.1, 3 and 5 wt% NaCl brine were observed to be in the 0.9, 0.85 and 0.65 area. Fill fractions for calculated for the low saturation experiments are shown in Table 4.3 below. There is some scatter in the calculated fill fractions, most likely caused by the low resolution of the saturation calculations.

Table 4.3: Fill fraction for the low saturation experiments (as defined by Husebø et al. (2008))

Experiment	Initial salinity [wt%]	Fill Fraction
CO2_20	0.1	0.96
CO2_25	0.1	0.96
DEP5_1	0.1	0.83
HR_47	3.5	0.68
HR_48	3.5	0.79

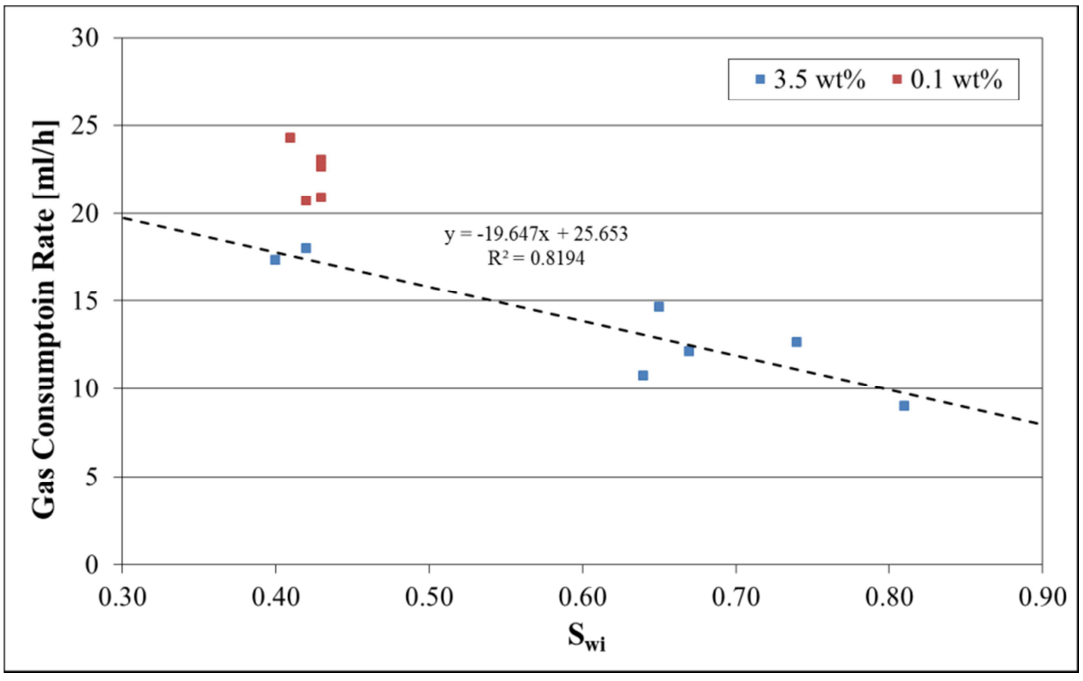

Figure 4.2: Initial gas consumption rate at different initial conditions. The growth rates presented are the maximum slope of the formation curves averaged over an hour.

4.1.2 Effect of Saturation on Formation

Bentheimer sandstone is water wet and will cause water to have a preference to coat the pore walls and completely saturate the smallest pores first. Higher initial saturations are expected to result in a larger portion of the pores being completely saturated by water, lower gas-relative permeability and smaller water–gas interface.

Figure 4.3 below shows a comparison of all the formation experiments performed with 3.5 wt% NaCl brine. These formations are characterized in the same way as the low saturation, high salinity experiments discussed above, with a high initial growth rate followed by a slower declining rate. Higher water saturation were observed to result in slower hydrate growth both in the initial and the intermediate growth regimes, and achieve higher residual water saturation with more active water.

A correlation of the initial growth rate with varying initial water saturation is shown in Figure 4.2 above. The correlation hints at an almost linear relationship where lower saturations give higher initial growth rate, but data for a wider range of saturations is needed. As mentioned above, the fast initial growth was likely a result of hydrate forming on the water – gas interface, where nucleation is most likely to occur and hydrate can grow rapidly due to an abundant supply of both hydrate former and water. Both the initial growth rates and the amount of hydrate formed during this growth regime were likely a direct result of decreasing water – gas interface area with increasing water saturation. A correlation between saturation and these parameters would then be very dependent on the pore size distribution and wetting preference of the porous medium, as it would influence the surface area of the water phase. The longer induction times observed with higher saturations supports this theory since induction time also is dependent on the surface area.

The lower growth rates observed in the intermediate regime for higher saturations can also be explained by the differences in water – gas interface area. Mass-transport mechanisms like diffusion is dependent on surface area and a smaller surface will give a thicker boundary at each a given hydrate saturation. The depth of penetration required for the limiting phase may therefore also be increased for higher saturations. This will have a great impact on growth rate if diffusion is the main transport mechanism, as a solution of Fick's law states that the depth of penetration for diffusion is proportional to the square root of time (Cussler 2009). This would greatly limit the mass-transport capability as the thickness increases. The decreased gas saturation in the high S_{wi} cores would also lead to a lower gas relative permeability which could slow down the gas flow especially to the smaller pores.

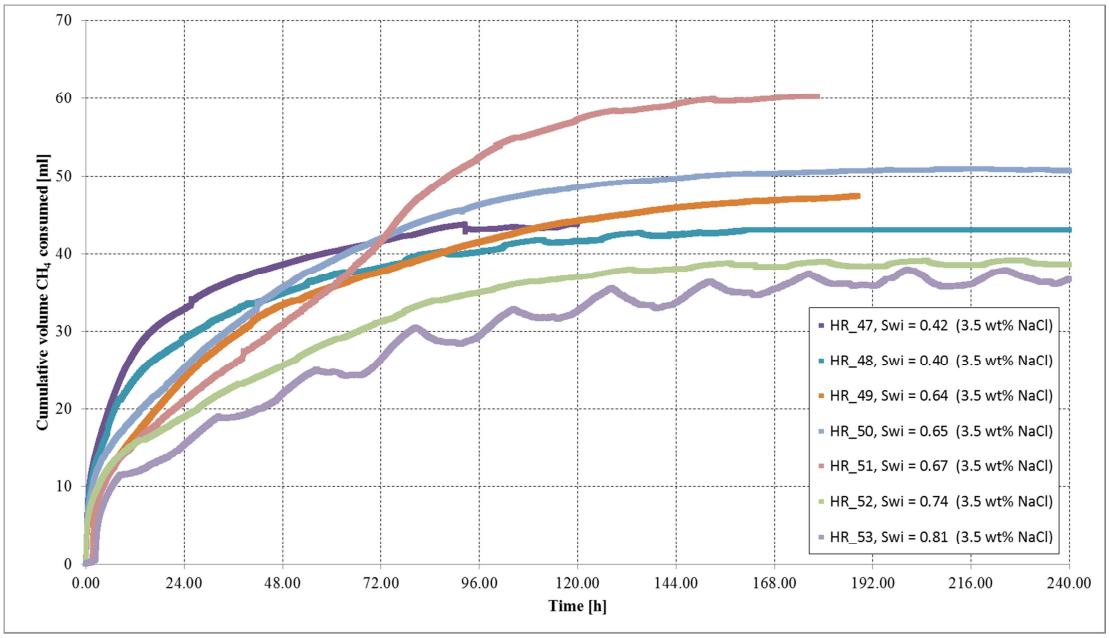

Figure 4.3: Formation curves for experiments with 3.5 wt% NaCl brine. The volume clearly fluctuates in a 24 hour cycle.

A correlation between initial water saturation and final water saturation were observed and are plotted together with a correlation between initial water saturation and final hydrate saturation in Figure 4.4a and b which includes relevant experimental data from the in-house database. The cores reached higher hydrate saturations as they moved towards a S_{wi} of 0.6 and declined again as the saturation increased further. It is clear from the experimental results that the low S_{wi} cores reached close to maximum hydrate saturation based on the amount of brine and brine salinity, illustrated for 3.5 wt% NaCl brine by the dotted line in Figure 4.4a, while the high S_{wi} cores had active water present after formation.

The only way the cores could retain active water with the experimental procedure used were if it the water became trapped without access to methane in sufficient concentration to form hydrate. Increasing S_{wi} would cause a larger fraction of the pores to be completely saturated by brine and subsequently a larger fraction of water becoming isolated from the gas phase during hydrate formation.

It is natural to expect there to be a critical S_{wi}, below which all the water will be used to form hydrate and above which the saturation distribution would cause a significant amount of water to be isolated from the gas phase during hydrate formation and cause the S_{wf} to deviate from the dotted line. More data at different saturations were needed however, in order to find a definite correlation. These correlations are also expected to be strongly dependent on pore geometry and pore-size distribution.

It must be noted, that the two cores with highest S_{wi} also were the only ones performed with fractured cores. The lack of baseline experiments with fractured cores makes it difficult to predict the effect this has on hydrate growth and comparisons can be misleading.

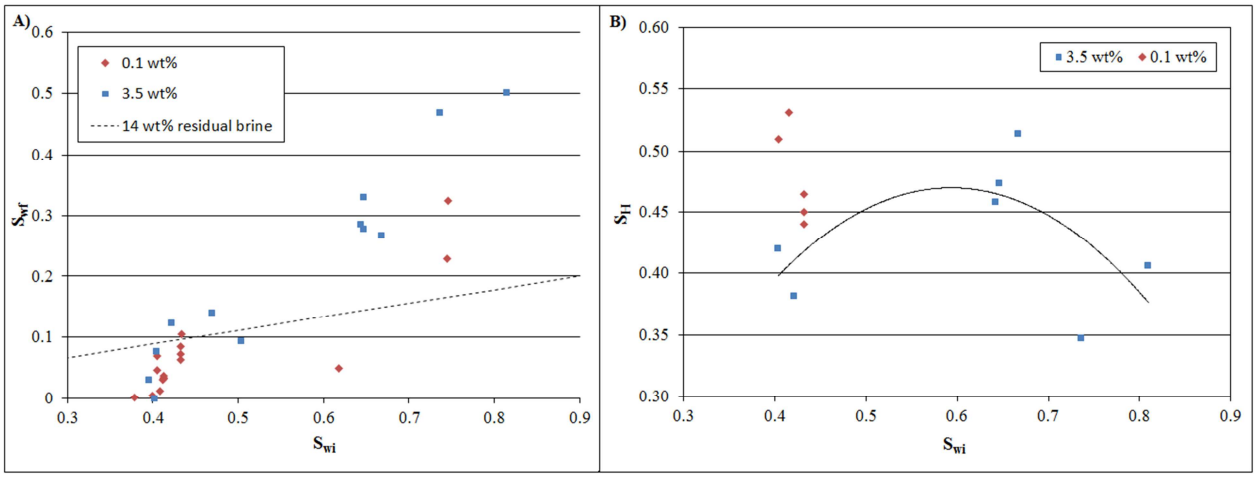

Figure 4.4: Correlation between initial water saturation and final water saturation (a) and initial water saturation and final hydrate saturation (b).

4.1.3 HR_51: Indications of a Different Growth Pattern

There are reports in the literature (Husebø et al. 2008, Ersland et al. 2010, Birkedal et al. 2011) of hydrate formation in sandstone cores occurring as both a piston-like growth, from one end of the core to the other, and as a more uniform growth throughout the entire core simultaneously. The growth behavior is among other things reported to be dependent on the initial brine saturation distribution, where a more homogenous saturation distribution results in a more uniform growth.

The resistivity measurements made during formation should be able to indicate the growth pattern. A piston-like growth would cause hydrate to consume almost all the local water in a cross section of the core, blocking the pore throats and cause a large increase in the local resistivity which in turn would have a large impact on the global resistivity. As hydrate grows through the core, the high-resistivity cross section would grow in length proportional to the hydrate growth causing the resistivity to increase almost proportionally to the hydrate growth.

A uniform growth pattern should affect the resistivity differently. A large amount of hydrate could form while retaining a continuous water phase where the increasing brine salinity would buffer the effect of a smaller area of electrical flow, causing a much small resistivity response during the early growth phase. At a certain hydrate saturation, the conductive water film would be expected to lose connectivity due to pore throats being blocked by hydrate and areas where hydrate has consumed nearly all the water. This would lead to a sharp increase in resistivity over a small saturation interval. This is supported by Birkedal et al. (2011) who measured resistivity and imaged by MRI during hydrate formation in Bentheimer sandstone.

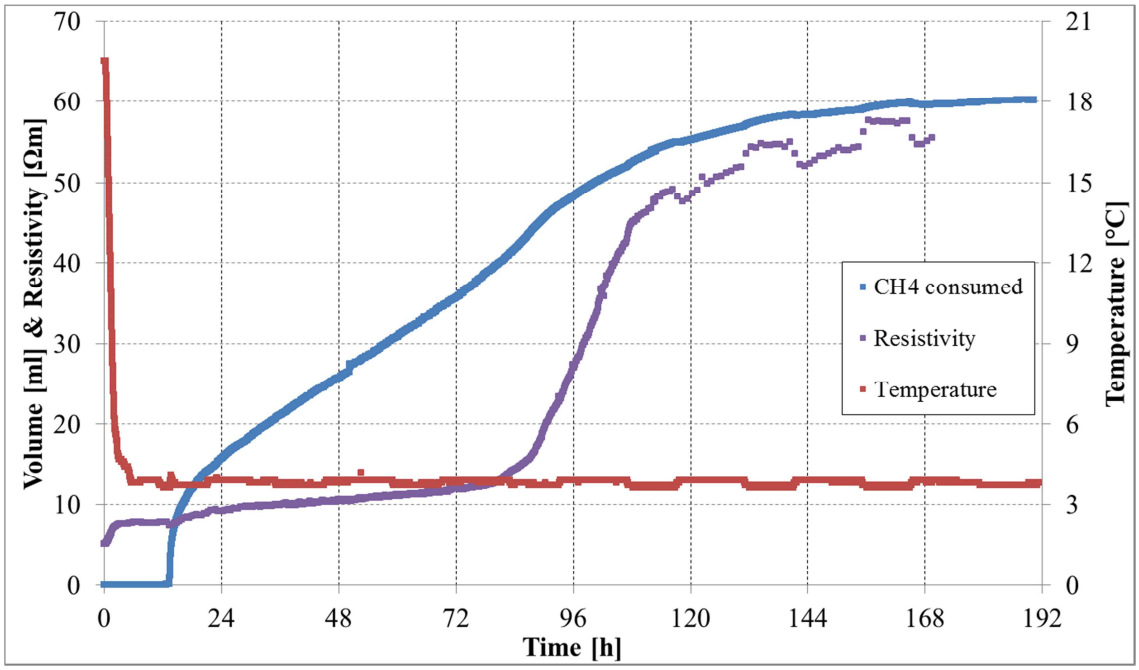

Figure 4.5: Hydrate formation for HR_51. Resistivity, temperature and cumulative volume CH_4 consumed are displayed against time, where t = 0 corresponds to the time when cool down was initiated.

The experiment was performed with the new, modified experimental setup, on a whole core with initial water saturation of 0.67. Temperature, resistivity and cumulative volume CH_4 consumed during the formation was logged and is displayed in Figure 4.5 above. Figure 4.6 is the same graphs but closed inn around the initial growth area.

The resistivity measurements are highly temperature dependent since the increased activity of ions with increasing temperature leads to a decrease in resistivity. This effect can clearly be seen in Figure 4.5 above, where the resistivity increases during the cool down process and fluctuate inversely with the day-night temperature variations at the later stages of formation. The effect may be bolstered by a slight increase in confinement which can occur with increased temperature, but the lack of a confinement pressure logging makes it difficult to speculate on the size of this contribution. The new buffer system is however expected to keep the confinement pressure fairly stable.

Hydrate growth initiated aproximatly10 hours after cool down and were followed by a high initial growth rate which gradually declined before reaching a somewhat stable rate after 20 hours. The growth rate increased again after about 72 hours, before slowly declining towards zero. This may be a result of temperature fluctuations or a result of water previously isolated coming in contact with methane. At approximately 80 hours the resistivity increased sharply. This is irregular in that resistivity in the other formations has tended to increase much sooner and to a large extent follow the same pattern as the volume curves. Mass balance calculations shows that the core ended up with a hydrate saturation at 0.51 which is significantly higher than the other high salinity cores. The gas consumption as well as the resistivity graph indicates that hydrate growth was not completed at 192 hours.

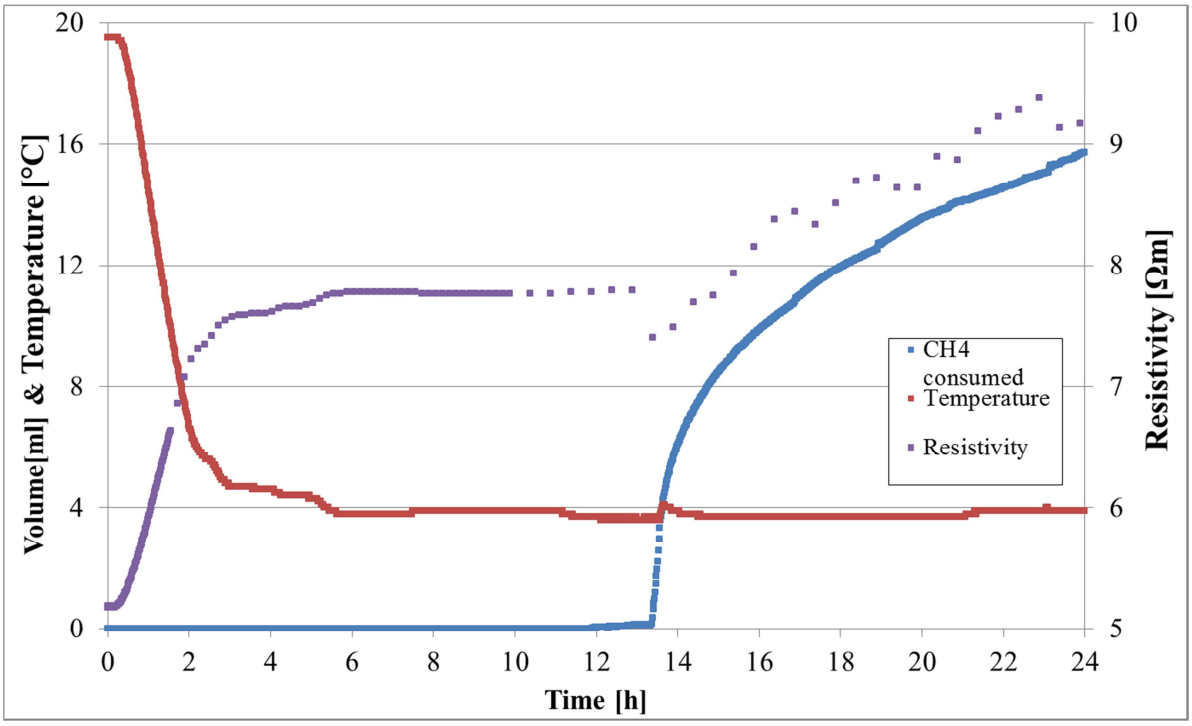

Figure 4.6: Hydrate formation for HR_51 zoomed in around the start of hydrate growth.

As seen in Figure 4.6, the temperature increased from 3.6 to 4.1 °C in the course of 0.10 hours during the initial formation. This is a strong indication of rapid hydrate growth as a result of the exothermic nature of the hydrate formation process, where the heat flux is unable to transport the excess energy away quickly enough which results in a temperature increase. The temperature increase is most likely higher in the bulk of the core where the heat flux is lower, and if true this may be a factor influencing growth at the initial stage. There was also observed a small drop in resistivity during the initial growth, most likely caused by a combination of increasing salinity and increasing temperature. These phenomena were expected and were observed during all the formations.

The hydrate formation in HR_51 was distinctly different from the other cores with an increase in growth rate late in the process and ending up at significantly higher hydrate saturation. Figure 4.7 below show a comparison of resistivity measurements over time for different experiments. The observed resistivity response for HR_51 was atypical with a late and abrupt increase. There were also indications of very slow hydrate growth 1.5 hours before the massive hydrate growth started. This was not observed in any of the other experiments and may together with the atypical resistivity response and the high final S_H indicate a uniform formation pattern. The observed resistivity response coincides well with the response observed by Birkedal et al. (2011) during uniform growth. HR_47 and HR_48 showed a response expected from a piston-like formation while the other cores had a response somewhere in between.

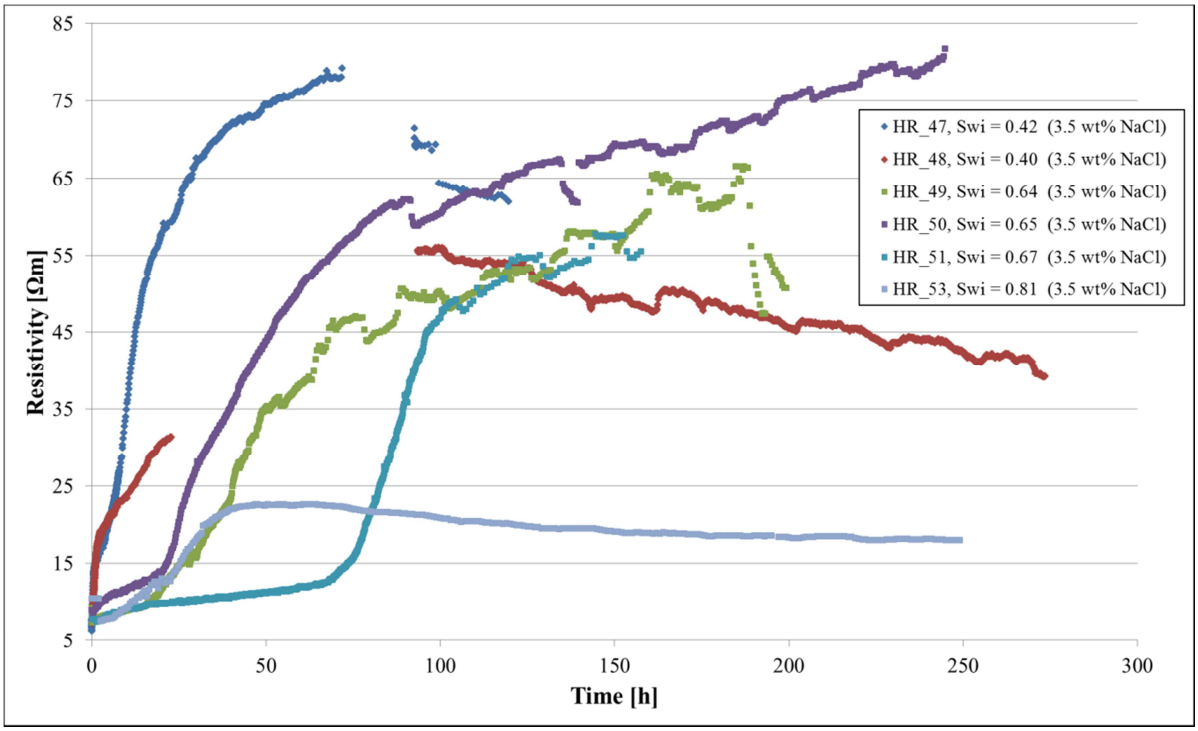

Figure 4.7: Resistivity over time for all experiments

4.2 Dissociation of Pure Methane Hydrate

One experiment was performed by forming and dissociating hydrate repeatedly on the same core. The core was a whole core saturated to a S_{wi} of 0.43 with 0.1 wt% NaCl brine. The experimental procedures are chronologically listed in in Table 4.4 below. The time between the different procedures (lag time) were varied in order to study the effect of lag time on formation and dissociation rates.

Table 4.4: Overview of phase-transition times. Time delay is the time from completion of the previous procedure to initiation of the current.

Procedure	Induction time [h]	Dissociation time [h]	Time delay [days]
Formation 1	1.2	-	-
Pressure Dissociation 1	-	29	5
Formation 2	0.6	-	3
Pressure Dissociation 2	-	12	32
Formation 3	0.5	-	2
Temperature Dissociation	-	1.4	5
Formation 4	0.5	-	4

Figure 4.8 below shows the formation curves of all four formations. The results from the formations were relatively similar with exception of the fourth, which were significantly faster than any other formation previously observed including the formations in the in-house database. This is discussed further in the Section below. There was observed a decline in the final volume of methane consumed for each consecutive formation indicating a small loss of brine for each formation-dissociation cycle.

Figure 4.9 below shows pressure, temperature and cumulative volume received by the pump during the two depressurizations. When hydrate dissociated, methane was released and the pump had to retract in order to hold a constant pressure. The cumulative volume received is a direct measurement of the amount hydrate dissociated as long as the pressure is constant. The dissociation for the first and second depressurization took approximately 30 and 10 hours respectively where the first dissociation was observed to release more gas. The different amount of gas received at the end of the dissociations is evidence for more hydrate being produced in the first formation. This was, as mentioned above, likely caused by loss of water during the first dissociation. The increase in volume received after the pressure was reduced to 2.0 MPa were likely caused by expansion of gas and gas going out of solution, not hydrate dissociation. The difference in rates will be discussed in Section 4.2.2.

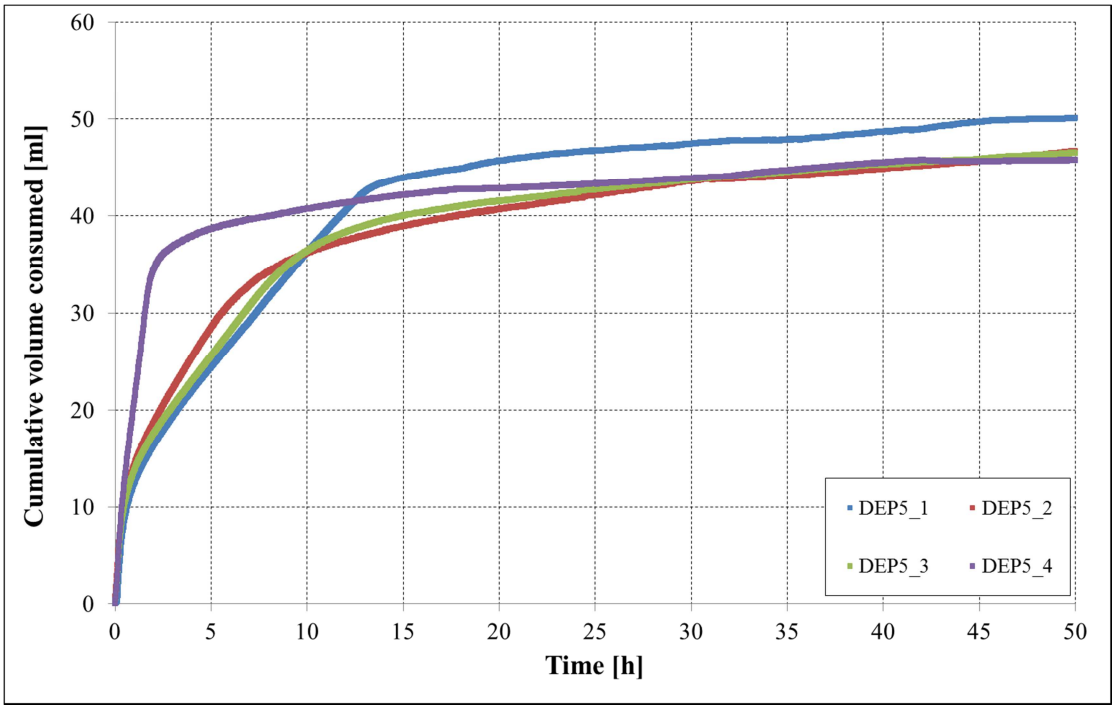

Figure 4.8: Comparison of the four formations performed during DEP5. The fourth formation clearly stands out with a faster rate. The pump delivered gas for up to an additional 100 hours but the plot is zoomed in around the first 50 hours to accentuate the differences in early growth.

Figure 4.10 below show temperature, volume received and pressure during the temperature dissociation. The rate of dissociation were observed to be much faster than during depressurization with dissociation finished approximately 1.5 hours after heating start and the dissociation itself taking around 1 hour. The reason for this is that the amount of supersaturation (the driving force) is more sensitive towards temperature than pressure. In other words, the temperature dissociation took the hydrate farther outside the hydrate stable region than the depressurizations.

The pressure curve indicates that the pump were unable to keep up with the large amount of methane released. This experiment illustrates well the sensitivity of hydrate equilibrium to temperature compared to pressure.

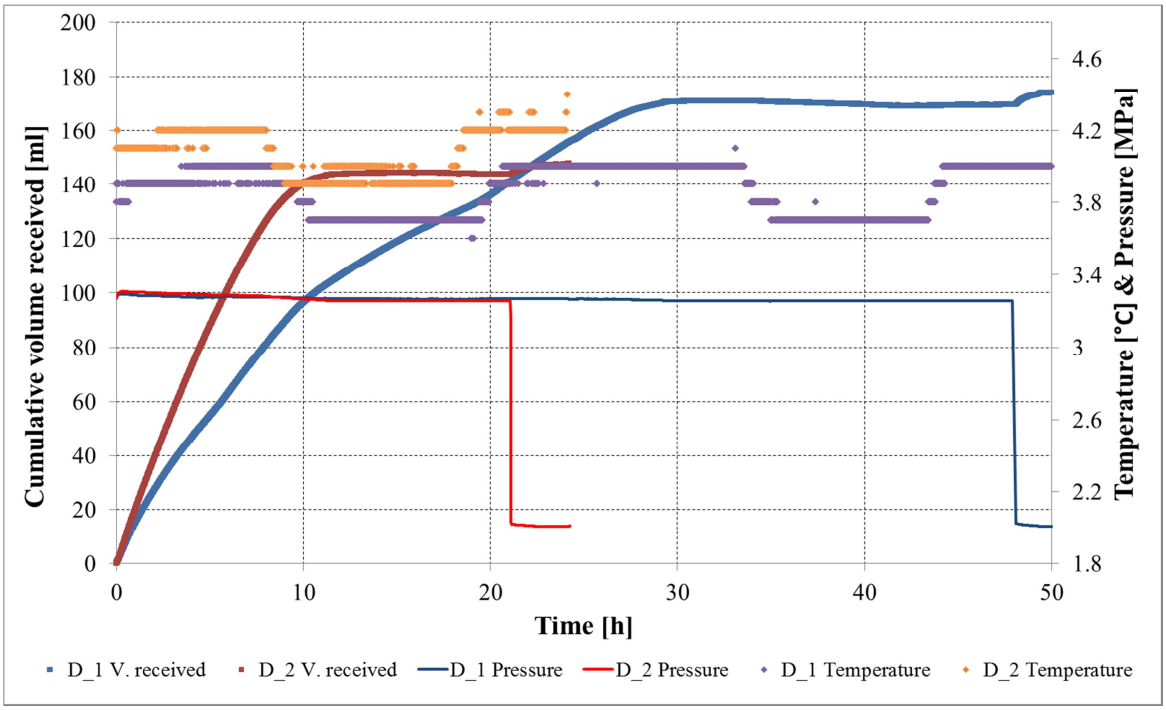

Figure 4.9: Volume received temperature and pressure during depressurization. The second depressurization was significantly faster at the same pressure.

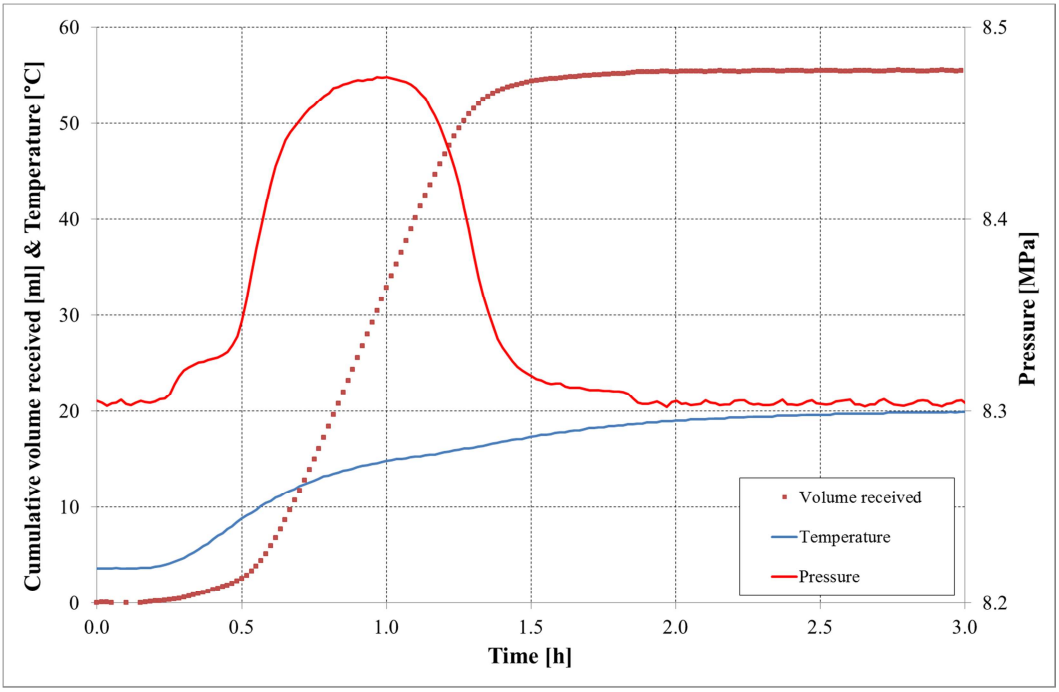

Figure 4.10: Volume received, temperature and pressure during temperature driven dissociation. The pump has not managed to compensate for the large volume of gas released.

4.2.1 The "Memory Effect"

Hydrate researchers has observed that hydrate forms more easily from water and gas obtained by melting hydrate than fresh water and gas. This "memory effect" is reported to affect induction time and morphology among others and the effect are dependent on the time between dissociation and formation, and the temperature of the water during this time. There are two different hypotheses explaining this effect. One states that the arrangement of water molecules around the guests persisting after dissociation and one states that the gas remains in solution after dissociation (Sloan and Koh 2008).

The induction times were very consistent with around 0.5 hour for the re-formations and 1.2 hours for the first formation. This may have been a result of the memory effect but more likely an effect of the water distribution becoming more uniform after a formation – dissociation cycle.

The fourth formation stood out with a significantly faster growth rate but no correlation with lag times was observed. The main difference between this and the two other re-formations were the temperature dissociation preceding it. The temperature dissociation was significantly faster than the pressure dissociations and may have caused a major redistribution of water in the core. This however cannot explain the difference in growth rates alone. Another perhaps more significant difference was the pressure and temperature between dissociation and hydrate re-formation. The temperature was increased to 20°C during the temperature dissociation and the pressure was maintained at 8.3 MPa the whole time between the dissociation and re-formation. In contrast were the pressure reduced to 2.0 MPa and the temperature increased only a short time before re-formation in the depressurizations. Since the temperature should have had the opposite effect from the one observed were the pressure the most likely suspect.

The solubility of gas in a liquid is strongly dependent on pressure, with increasing solubility with increasing pressure. The amount of methane solved in the formation water may therefore have been much higher before the fourth formation and it's even possible it had retained a level of oversaturation as one of the hypotheses for the "memory effect" suggests. Lowering the pressure as done in the two other cases would cause more methane to go out of solution and at a much higher pace. There would also be a large likelihood of under-saturation of methane in the brine when the core was re-pressurized and cooled as the pressure were not held at 8.3 MPa for a long period before cooling.

The growth rate observed for the fourth formation is almost as high as the fast initial growth rate. This suggests that the mass-transport limitations, limiting the growth rate of the other formations, were overcome to a large degree. If methane has been available in sufficient quantities in the majority of the brine phase when formation started, it could have caused a completely different microscopic growth pattern. The "memory effect" can explain this by an elevated amount of methane in solution making diffusion through hydrate to a large extent unnecessary for hydrate growth.

4.2.2 Redistribution of Hydrate

Hydrate has, as previously mentioned (section 1.2.5), been reported to redistribute after formation both on short and long timescales. When hydrate is at equilibrium conditions there is a continuous dissociation - formation process which makes the hydrate able to "move" towards a distribution with more favorable energy. Fast hydrate formation with a large degree of supersaturation has been observed to initially cause a branch-like dendritic growth structure with a large surface area (Tohidi et al. 2001). The water wet hydrate surface can then decreases the effective pore diameter which increases the capillary forces sufficiently to draw water to the hydrate formation site, precipitating additional hydrate growth in the area. Hydrate will over time reconfigure locally to a more energy efficient structure (often a smaller surface area) which will lower the capillary forces in the area and allow hydrate to redistribute globally throughout the core. The global redistribution of hydrate have been observed to give a more uniform distribution as seen in Figure 1.10. The resulting changes may have a significant impact on the physical properties and behavior of the sediment as hydrate becomes more homogenously distributed throughout the core. Observations made during DEP5 indicate increasing hydrate surface area and maybe gas permeability for the hydrate dissociated during the second depressurization. Redistribution has also been indicated during other formations by resistivity response.

The two pressure dissociations, shown by volume received and pressure in Figure 4.9, had very different rates of dissociation. The first dissociation were performed 5 days after formation were initiated and took approximately 30 hours, while the second were performed 32 days after formation and took approximately 10 hours. The difference can best be explained by a difference in hydrate distribution at the time of dissociation where the hydrate in the second dissociation was more uniformly distributed with a larger surface area. Redistribution would also cause better pressure response throughout the core which would help speed up the dissociation. The first dissociation had a slightly lower core temperature than the second. This would have contributed to the difference in rates but were considered to small to explain the larger difference in rates.

Redistribution of hydrate is also observed in the resistivity of a number of formations (Figure 4.7), as resistivity changes without any additional gas being consumed. The dropping resistivity observed during HR_47, HR_48 and HR_53 show the formation of a more continuous water phase which indicates a more uniform hydrate distribution with fewer areas with very low water saturation and fewer blocked pore throats. The increasing resistivity observed in HR_49, HR_50 and HR_51 are likely caused by further hydrate growth. This was supported by the measured cumulative volume (Figure 4.3) which indicates that the formations were not complete.

The findings are supported by observations made by Rees et al. (2011) which showed a continuous redistribution of hydrate throughout the core towards a more homogenous distribution at both a small and long time scale.

4.3 CO_2 – CH_4 Exchange

Nine hydrate bearing sandstone cores were produced, as described in Section 4.1, with hydrate saturations ranging from 0.35 to 0.53 and final water saturations ranging from 0.00 to 0.50. After hydrate formation, CO_2 – CH_4 exchange were attempted for all the CO2 and HR cores in an attempt to study the effect of the different hydrate and water saturations. An overview of the experiments with respect to the exchange procedure is presented in Table 4.5 below, where the comments indicate problems during the exchange procedure: Loss of cooling led to dissociation of the hydrate and the procedure was terminated, loss of effluent were caused by a malfunctioning pressure regulator in front of the GC causing an underestimation of the recoveries, missing GC-data were caused by the GC losing its connection to the computer and made extrapolation of some of the GC-data necessary, and leakage and plugs were caused my many factors and caused the termination of the exchange procedures. HR_49 and HR_51 also experienced plugging, but this was successfully solved by the use of nitrogen.

Table 4.5: Experimental overview for CO_2 – CH_4 exchange. The salinity is the calculated average brine salinity prior to CO_2 injection. F signifies a fractured core and W a whole core in the core column.

		Pre Injection			CH4 - CO2 Exchange			
Name	**Core**	**Salinity [wt%]**	**S_H**	**S_w**	**Injection**	**$RF_{CH4,tot}$ [%]**	**$RF_{CH4,H}$ [%]**	**Comments**
CO2_20	W	-	0.53	0.00	CO_2	-	-	Loss of cooling
CO2_25 [1]	W	-	0.51	0.00	CO_2	45	14	Loss of effluent
HR_47	W	11	0.38	0.12	CO_2	-	-	Plug
HR_48	W	15	0.42	0.08	CO_2	23	0	Missing GC-data
HR_49	W	7	0.46	0.29	$CO_2 + N_2$	26	2	-
HR_50	W	8	0.47	0.28	-	-	-	Leakage
HR_51 [1]	W	8	0.51	0.27	$CO_2 + N_2$	61	52	Missing GC-data
HR_52_1 [1 2]	F	5	0.35	0.47	CO_2	21	0	-
HR_52_2 [1 2]	F	5	0.35	0.47	CO_2	29	0	-
HR_52_3 [2]	F	5	0.35	0.47	CO_2	-	-	Plug
HR_53	F	6	0.41	0.50	$CO_2 + N_2$	-	-	Plug

[1] Recovery calculated with mass flow meter

[2] Core was flushed with CO2 in three steps with, recovery are cumulative recovery including previous flush

A comparison of total methane recovery over time for the 5 experiments where CO_2 – CH_4 exchange where successful are presented in Figure 4.11 below. Methane in the HR_52 core was produced by the diffusion driven injection method where higher injection rates over much shorter time intervals where used. This is clearly reflected in its recovery curve, where the time between the two flushes (shut-in time) has been eliminated. The five experiments differed both in initial conditions, experimental procedures and in the course of events during the exchange procedure. For this reason are all five experiments presented with a more in depth analysis of the results in separate sections below. The results are presented in the order

of increasing initial water saturation, which also were the chronological order they were performed in, with exception for CO2_25 which were performed later as a substitute for CO2_20 as it dissociated before $CO_2 – CH_4$ exchange were completed.

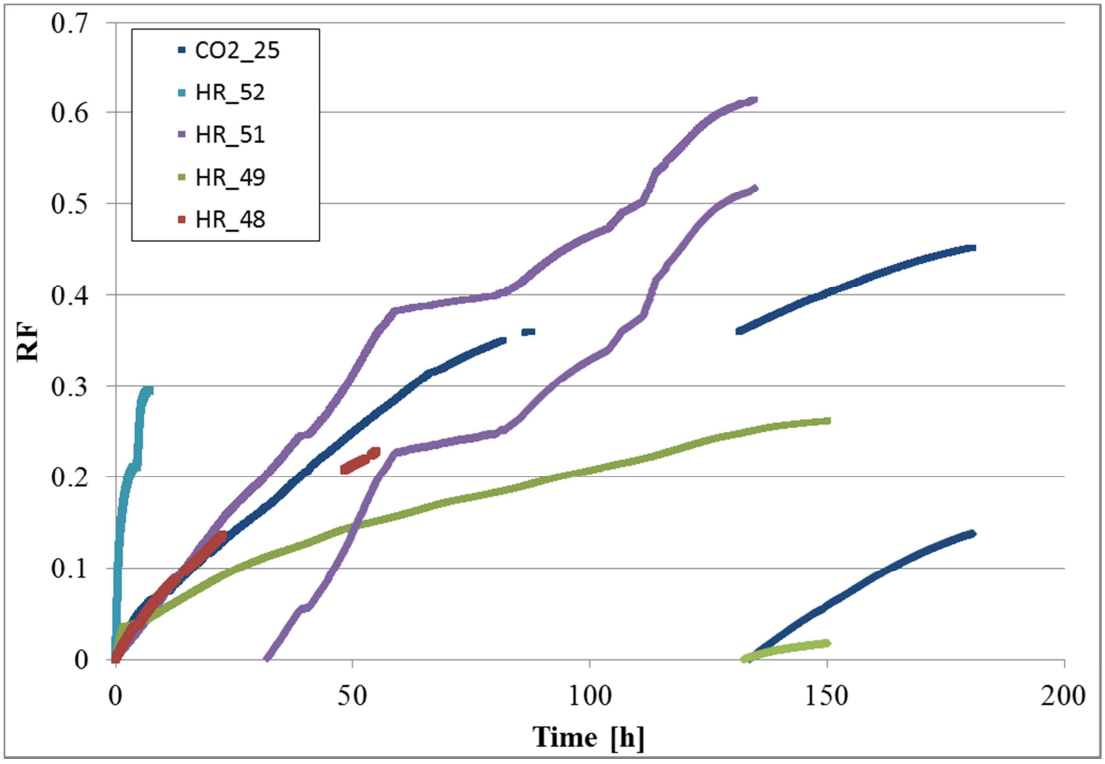

Figure 4.11: $RF_{CH4,tot}$ and $RF_{CH4,H}$ over time for all experiments. Total CH_4 recovery are plotted from t = 0 while recovery from hydrate starts when all the free methane have been produced. The GC stopped during CO_2 injection for HR_48 and HR_51 and the gas composition had to be extrapolated.

4.3.1 HR_48: Baseline

The core had a hydrate saturation of 0.42 and a water saturation of 0.08 with a salinity of 15 wt% NaCl prior to CO_2 injection. The salinity has most likely been nearer 14 wt% NaCl since methane hydrate would dissociate in the presence of 15 wt% NaCl brine. This also indicates a slight overestimation of hydrate which could be a result of the assumed absence of leakage. CO_2 was injected with a constant rate of 0.02 ml/min, with the BPV set to approximately 8.6 MPa. Figure 4.12 below show the composition of the gas produced and $RF_{CH4,tot}$ during the exchange, while Figure 4.13 show injection pressure, resistivity and core temperature over time.

The GC stopped working after 48 hours and was not restarted before 78 hours. This was not a critical part of the exchange and extrapolating the fractions was not considered a problem. Pressure and temperature were stable throughout the injection process with only minor fluctuations following the day – night cycle.

The large tubing volume and the large volume of the BPV combined with the low injection rate makes it possible for effluent fluids to mix after leaving the core. These factors made the GC measurements not completely representative for the fluids produced out of the core at a

specific time. The GC date were expected to some degree to be an average of gas compositions produced over a longer time interval as fluids diffused and mixed in the tubing and the BPV.

Nitrogen can as previously mentioned, be used as a tracer gas which marks the time when production from the free gas in the core occurs and how much of the produced gas comes from the free gas in the core. The effluent composition indicate that gas from the core reached the GC at approximately 8 hours with a peak at 20 hours. This is reflected in the methane fraction curve which peaks at approximately the same time as the N_2 fraction. The increase in recovery is also at its highest around this point, but that may be an illusion created by the way methane production was calculated without mass flow data from the MFM. The N_2 fraction in the effluent were observed to follow the CH_4 fraction closely before the GC lost connection, which can indicate that a large portion of the produced methane came from free gas during this interval.

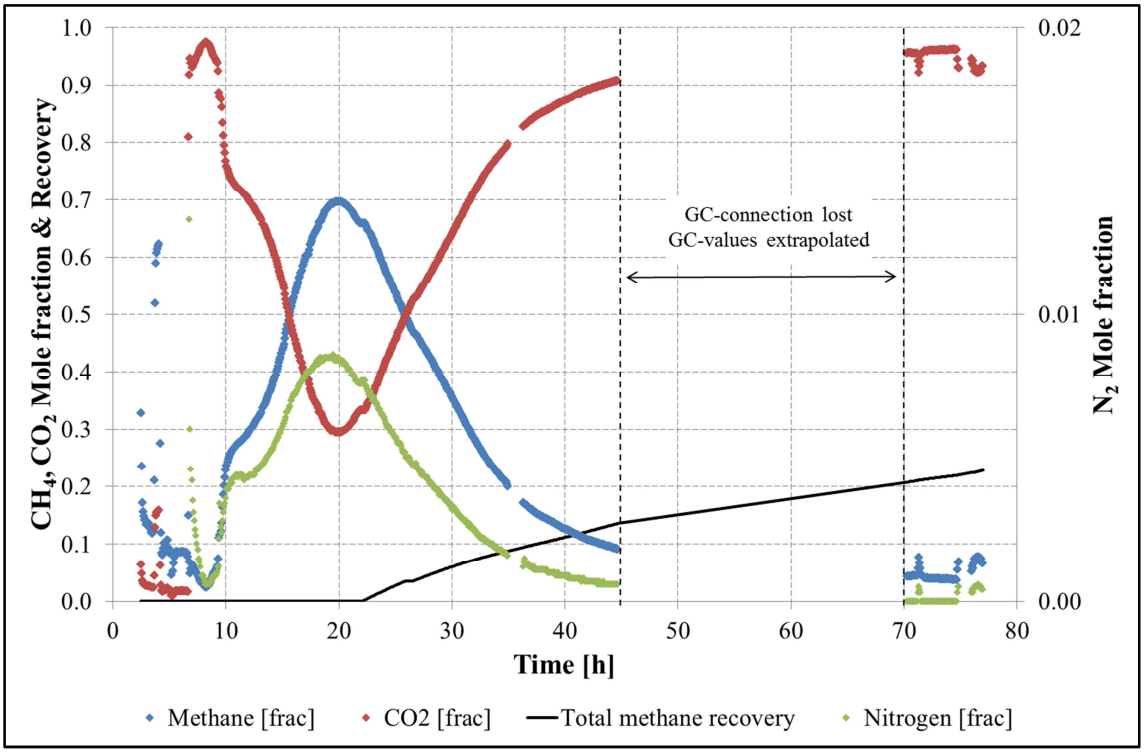

Figure 4.12: Composition of effluent gas and resistivity of the core during CO_2 – CH_4 exchange for HR_48.

After 40 hours most of the easily accessible free methane seemed to have been produced since the amount of methane in the effluent had decreased significantly. An increasing fraction of the methane produced was expected to come from the exchange process after this point. Methane extraction from hydrate was expected to start when CO_2 contacted the core and increase as the CO_2 saturation in the core increased, before slowly declining as the CO_2 fraction in the hydrate increased. The exchange process is time dependent and not strongly dependent on injection rate as long as the CO_2 concentration in the core remains stable. The

production rate of free methane from the core was expected to be strongly dependent on the injection rate since it was produced by displacement. .

The resistivity was at 40 Ωm and dropping after hydrate formation but increased steadily when CO_2 contacted the core before dropped again after approximately 25 hours. This is an indication of CO_2 forming hydrate with the residual water which disrupted the electrical flow path. Mass balance calculations show that the brine had salinity near 14 wt% NaCl after formation. This means that the residual brine was at equilibrium with methane and methane hydrate and not isolated from the gas phase. Since CO_2 hydrate are more stable than CH_4 hydrate, the CO_2 would have been able to form CO_2 hydrate with the brine as it moved through the core. Simulations on the CSMGem software gives a CO_2 hydrate equilibrium at 8.3 MPa, 4°C and 16.7 wt% NaCl. The software had some problems with the calculations however making the result less reliable. The amount of secondary hydrate formed by CO_2 are limited if the value is correct, but it was considered sufficient to give the observed resistivity response since the system would be sensitive at low water stations.

The later drop in resistivity was observed to be significantly faster during CO_2 injection than after formation. The drop may have been a result of redistribution of hydrate, since a more uniform brine distribution will decrease the resistivity. One hypothesis was that the introduction of liquid CO_2 in the core led to a less stable methane hydrate phase which accelerated the rate of the continuously ongoing dissociation - re-formation process, resulting in faster redistribution.

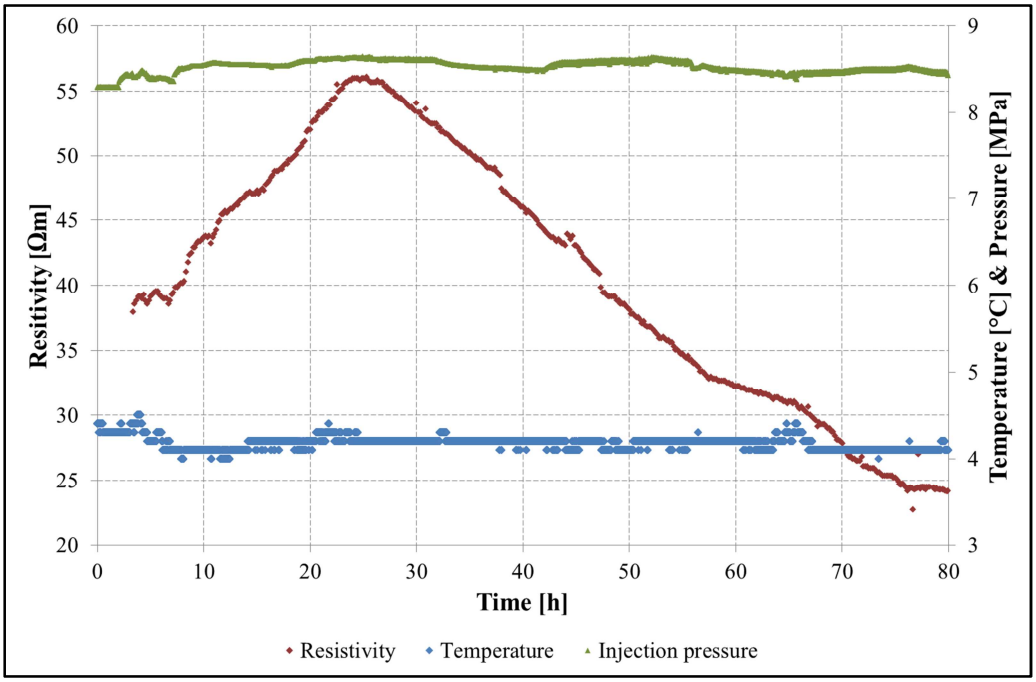

Figure 4.13: Resistivity, temperature and pressure over time.

Calculations estimate the total methane recovery at 23% with no production from hydrate. This may indicate that there was an underestimation of recovery since 23% of the methane originally in place represents less than the amount of free methane in the core and liquid CO_2

were expected to have an excellent sweep when displacing methane in a small core plug. The slope of the recovery curve suggests that the recovery would have continued to rise if production had been extended.

There could be a number of explanations for the slow and low recovery. The injection rate was very low which could have made diffusion significant. Methane could have continuously diffused in the opposite direction of CO_2 flow since there would have been a significant methane concentration gradient in the core with no methane at the inlet. The result could be a significantly slower exchange process. A more likely explanation is gravity segregation, where buoyancy forces would have caused the methane to occupy the upper part of the core while the denser liquid CO_2 only contacted the bottom part. The early CO_2 flush however should have contacted the entire core, making gravity segregation more of a problem when considering $CO_2 – CH_4$ exchange process. Some free methane may have been encapsulated by hydrate in the center of the pores or trapped in pores isolated by hydrate. This would make the CO_2 unable to contact all the free methane and would contribute to lower recovery.

The core was stepwise depressurized after $CO_2 – CH_4$ exchange in an effort to find the dissociation pressure and thereby the hydrate composition. The core was flushed with CH_4 prior to the depressurization to avoid confusing data caused by CO_2 going from liquid to gas phase. Cumulative volume received by the pump and pressure during depressurization are displayed against time in Figure 4.14 below. The volume plot indicates multiple dissociation pressures which would be the case for a heterogeneous hydrate composition.

Volume data for each pressure step between 3.17 and 2.69 MPa are plotted against time in Figure 4.15 below. The two volume plots from the dissociation indicate that dissociation started at 3.17 MPa which corresponds to a hydrate composition of approximately 60 mol% CO_2 and 40 mol% CH_4, and continued at each pressure step down to 2.69 MPa which corresponds to almost pure CO_2 hydrate. The volume fluctuations caused by fluctuating temperature made interpretation of the data difficult and the pressure steps would have to be held for a longer period if more accurate estimates were to be made. This can clearly be seen by the 2.89MPa step, where dissociation appears to be completed in Figure 4.14 but Figure 4.15 shows that gas still are being received by the pump. In order to accurately estimate the composition equilibrium has to be reached during each step, which takes time. The results from the dissociation indicates that a significant amount of CO_2 were in hydrate after the exchange procedure in contrast to the calculated $RF_{CH4,H}$.

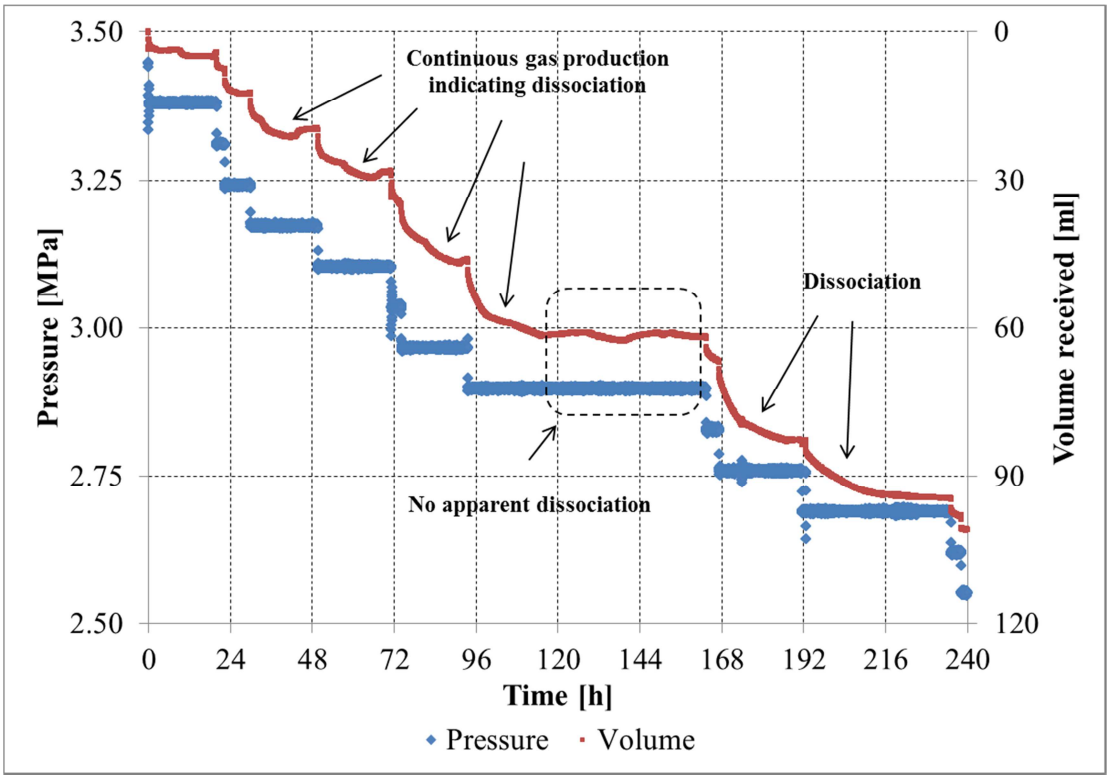

Figure 4.14: Dissociation of HR_48 displayed by volume received and pressure over time. The volume (right vertical axis) has been reversed in order to easier compare the two plots.

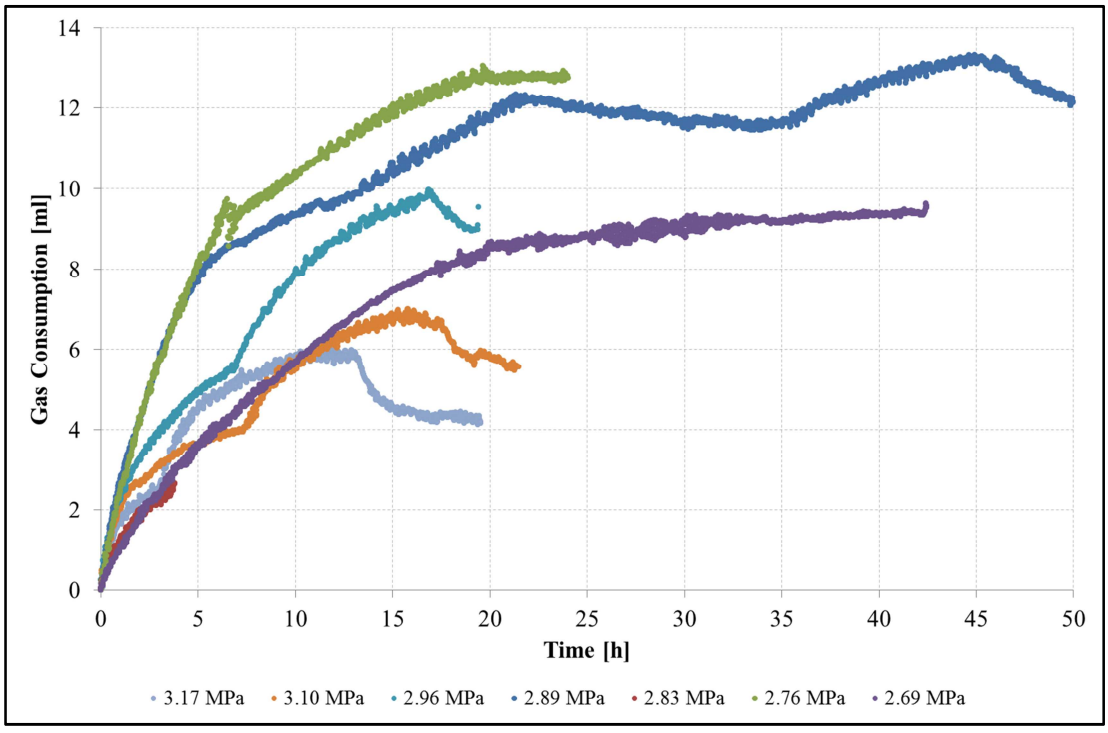

Figure 4.15: Volume consumed for each step during depressurization of HR_48.

4.3.2 CO2_25: Low Salinity

The low salinity, low saturation experiments were performed in order to study the effect of salinity on hydrate formation and CO_2 – CH_4 exchange. CO2_25 achieved a hydrate saturation of 0.51 and the calculated final water saturation was 0. This experiment was performed with the MFM.

A total of 190 ml pure liquid CO_2 were injected at a rate of 0.02 ml/min. Temperature and pressure were stable throughout the exchange procedure and no significant differential pressure were observed. Figure 4.16 below shows recovery and composition of the effluent gas during injection of pure liquid CO_2. A malfunctioning pressure regulator made it necessary to shut the core inn for a period of approximately two days while repairs were being made. Some gas escaped through a safety valve before reaching the MFM in a short period during the early production. This may have caused a slight underestimation of recovery since it happened during the period of highest methane production but it should not have significantly influenced the GC-data. There was observed a temporary increase in methane fraction in the effluent 24 hours after the shut-inn. This may have been caused by CO_2 – CH_4 exchange taking place during the shut-in interval increasing the fraction of methane and decreasing the fraction of CO_2 in the core. The time lag of 24 hours is not unrealistic as the injection rate is low. The time with elevated methane fraction however is very short indicating that it might have been a random occurrence.

The GC-data were very similar to HR_48, but with a higher fraction of methane during the initial production. The main difference between the two GC-data plots are the duration, where the effective time (discounting the shut-in) were approximately 60 hours longer for CO2_25. This corresponds to the entire calculated $RF_{CH4,H}$ in CO2_25, which were observed to still be rising when the exchange were terminated. The two GC-data plots hint at a potential for good repeatability for these experiments if problems can be avoided.

The total methane recovery and the methane recovery from hydrate were calculated to be 45% and 14% respectively. No significant differences which can be attributed to salinities were observed.

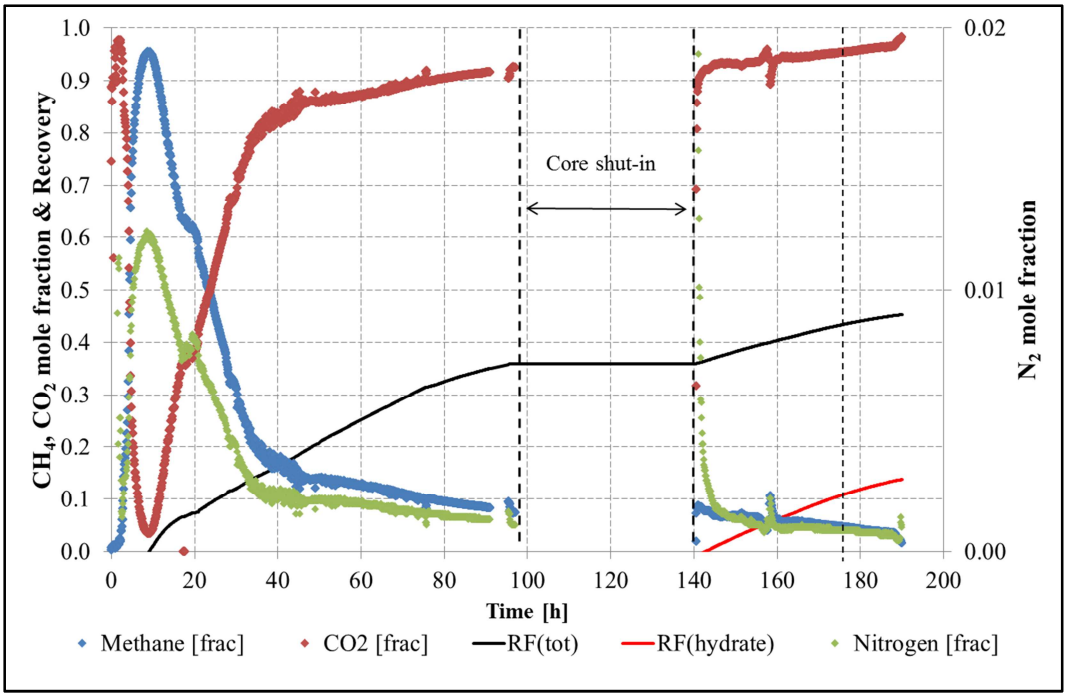

Figure 4.16: Composition of effluent gas and recovery over time. A malfunctioning pressure regulator made it necessary to suspend injection and shut-in the core for a period of approximately two days.

4.3.3 HR_49: Use of Nitrogen to Improve Injectivity

HR_49 was the first attempt to perform CO_2 – CH_4 exchange on a core with high initial water saturation. Injection problems caused by plugging and lack of permeability were successfully solved by the injection of nitrogen gas.

Before CO_2 injection was initiated, the calculated hydrate and water saturations were 0.46 and 0.29 respectively. As such the hydrate saturation was in the same range as the low S_{wi} cores but with a higher S_{wf} and a high likelihood of significant differences in hydrate distribution.

Figure 4.17 below shows resistivity and inlet- and outlet pressure during the work on injecting CO_2 in HR_49. Three attempts were first made to inject pure liquid CO_2 at a rate of 1ml/min but the injections were stopped by the pump's high pressure alarm which was set at 9.0 MPa. The inlet pressure dropped relatively quickly and a small pressure response were observed at the outlet, indicating low injectivity and a flow-barrier close to- or at the inlet.

To evaluate the injectivity further the pump was set to hold a constant pressure of 8.9 MPa after the third injection attempt. The pressure equalized over two days but the injectivity was considered too low for CO_2 – CH_4 exchange. Resistivity increased during this period indicating further hydrate formation and/or redistribution of the phases as CO_2 moved through the core.

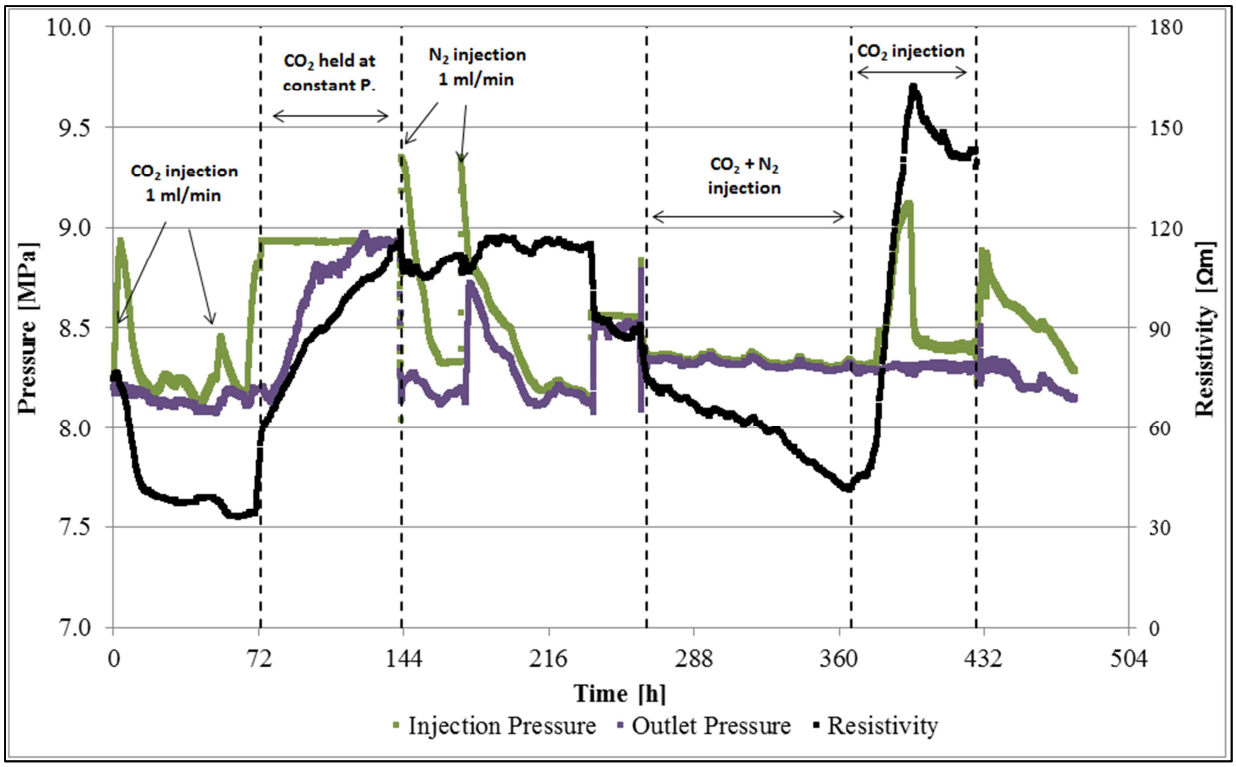

Figure 4.17: Pressure and resistivity measurements during CO_2 – CH_4 exchange in HR_49.

The outlet was opened to the BPV at 143 hours, in order to reduce the outlet pressure before pure nitrogen was injected at a rate of 1ml/min. The high pressure alarm stopped the injection after 5 min. Another nitrogen injection was attempted at 173 hours with the same result, but with a significant pressure response at the outlet indicating reestablishment of injectivity. A third attempt showed good injectivity with almost no differential pressure during injection. The drop in resistivity during the last injection attempt is a good indication of small scale hydrate dissociation which would lead to an increase in brine phase thickness and continuity. There is no indication of large scale dissociation as it would have resulted in a significant rise in pressure.

Since injectivity had been successfully restored, a co-injection of 25 mol% CO_2 and 75 mol% N_2 at a total rate of 0.02 ml/min was initiated. The effluent gas was produced out through the PBV at a pressure of 8.3 MPa while the GC measured the gas composition, shown in Figure 4.18 together with the calculated total recovery. No differential pressure were observed during this process and resistivity continued to drop.

Between 366 and 427 hours pure liquid CO_2 was injected at a rate of 0.02 ml/min. Good injectivity was observed despite a rise in differential pressure. Together with a simultaneous increase in resistivity, this indicated that some CO_2 hydrate were formed causing a decrease in core permeability. This showed that the co-injection could effectively maintain a high injectivity during CO_2 – CH_4 exchange where a pure CO_2 injection would have caused a significant reduction in injectivity. It also illustrated the resistivity's ability to detect redistribution of phases and its close relation to changes in permeability.

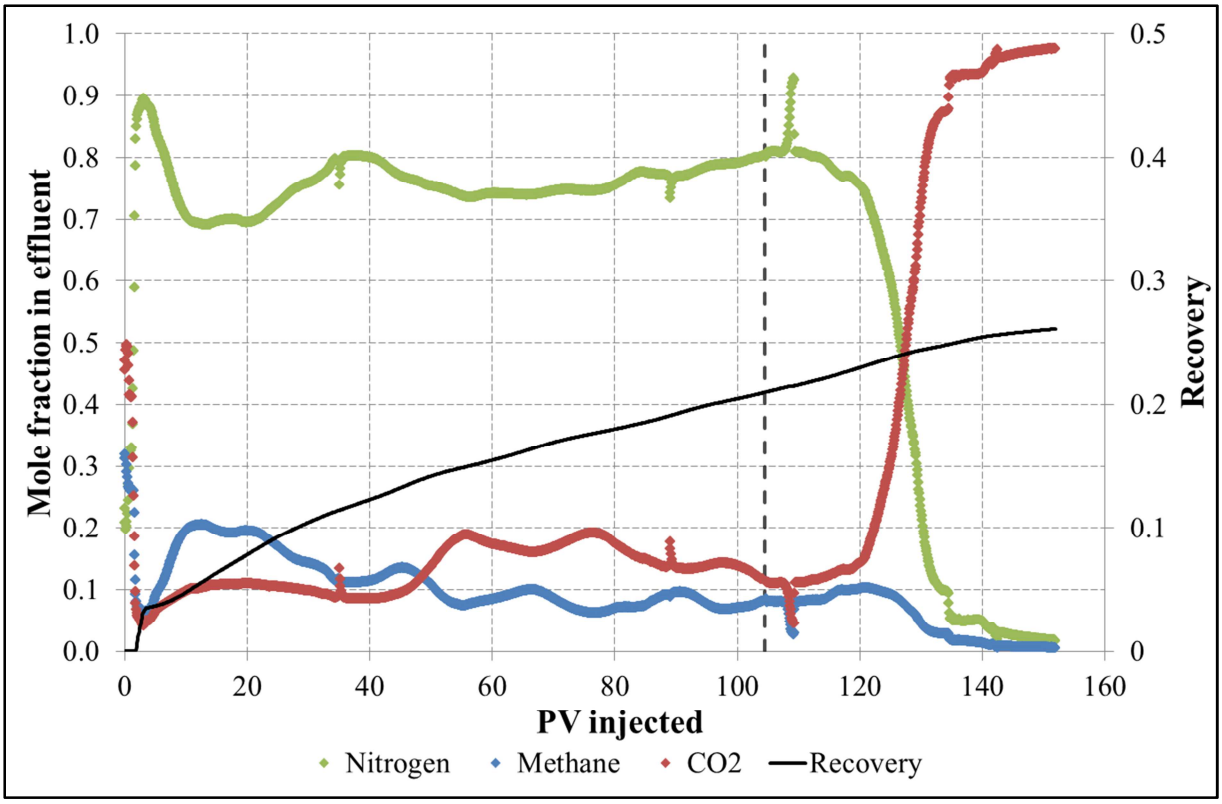

Figure 4.18: Effluent composition and calculated CH_4 recovery during exchange. Pure CO_2 was injected after 2.9 pore volumes of N_2 + CO_2 had been injected

The effluent composition and the calculated recovery of CH_4 over time are shown in Figure 4.18 above where the dotted vertical line indicates the time when pure liquid CO_2 was injected. $RF_{CH4,tot}$ and $RF_{CH4,H}$ were estimated to 26% and 2% respectively. The decline in methane fraction when the CO_2 fraction increase was caused by the high density of liquid CO_2 and does not mean that less methane was produced.

The results of this experiment show that Nitrogen can be used to remove plugging under the experimental conditions used. No indications of massive hydrate dissociation as a result of the N_2 injection were observed but the resistivity indicates a small scale dissociation or redistribution of phases leading to higher permeability. The change in resistivity was a good indicator for permeability changes during the nitrogen, CO_2 and CO_2 + N_2 injection. Direct comparison with the baseline experiment would not have given any indications of the effect of the increased water saturation since the use of N_2 and the many procedures performed before CO_2 – CH_4 exchange were initiated influenced the core beyond the expected effect of saturation differences.

The core were step-wise depressurized after CO_2 exchange were completed in an effort to find the dissociation pressure of the gas hydrate and from it, estimate the hydrate composition. Figure 4.19 below show pressure, temperature and cumulative volume gas received by the pump during the depressurization, and Figure 4.20 show cumulative volume recieved by the pump during each pressure step. The core was flushed with nitrogen before the depressurization started.

Dissociation were observed continuously from a pressure of approximately 3.45 MPa, but since the pressure were not held for a sufficient period at each interval, it were not possible to discern whether the hydrate composition were homogenous or not. A pressure of 3.45 MPa corresponds to a hydrate composition of approximately 29 mol% CO_2 and 71.5 mol% CH_4. The nitrogen gas phase however would increase the dissociation pressure which may indicate that the amount of CO_2 was underestimated. A concern with the composition estimates presented for both HR_48 and HR_49 is that the pressure were not held for a sufficient time at each interval which could have led to a severe underestimation of the dissociation pressure as the dissociation rates are expected to be low when the hydrate are close to equilibrium.

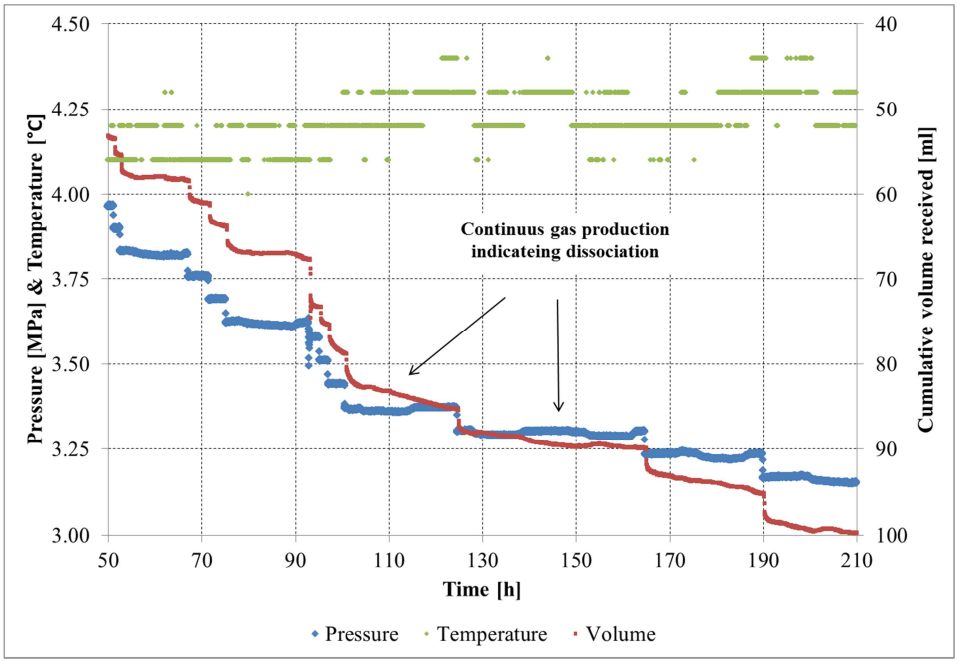

Figure 4.19: Pressure, Temperature and gas volume received during depressurization of HR_49. The

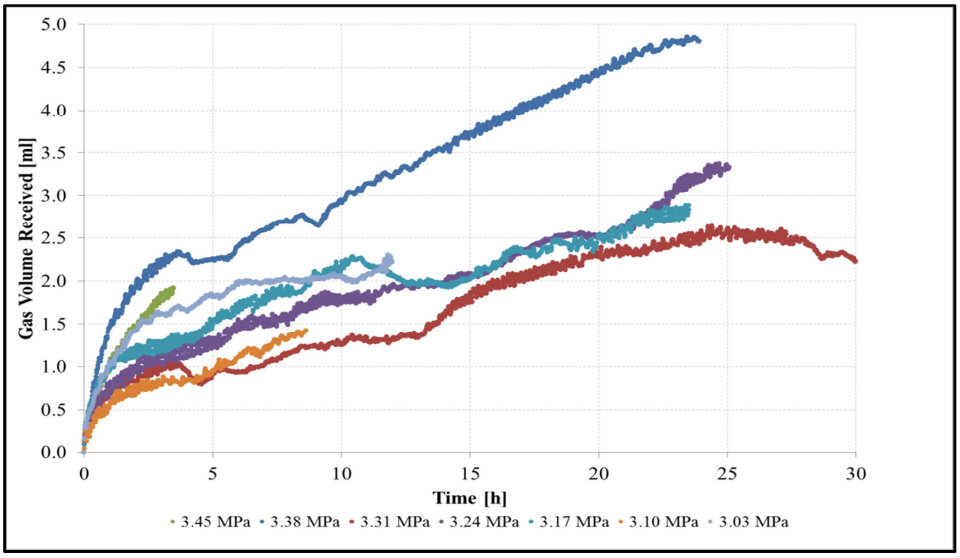

Figure 4.20: Volume consumed for each step during depressurization of HR_49.

4.3.4 HR_51: High saturation

Due to development of hydrate plugs during CO_2 injection in previous high saturation cores and the success in using nitrogen during HR_49 it was decided to continue using the co-injection with 75mol% N_2 and 25 mol% CO_2 on the cores with S_{wi} over 0.6. HR_51 had a S_H of 0.51 and a S_w of 0.27 after hydrate formation. This experiment used the MFM to measure mass flow during CO_2 – CH_4 exchange. Inlet- and outlet pressure, resistivity and cumulative volume gas injected are shown in Figure 4.21 below.

Nitrogen and carbon dioxide were initially injected for 7 hours at a rate of 0.02 ml/min before the pumps high pressure alarm, set at 9.0 MPa, stopped the injection. A pressure response was observed at the outlet which indicated some connection through the core. Resistivity dropped soon after the injection started, indicating small scale dissociation as the N_2 + CO_2 mix moved through the core. Pure N_2 was then set to hold a constant pressure of 9.0 MPa in order to ensure that injectivity was reestablished. The resistivity continued to drop and the differential pressure dropped toward zero. Co-injection was resumed after 26 hours, immediately followed by a spike in differential pressure of about 0.5 MPa which dropped to zero without any intervention. The resistivity dropped throughout the injection process as in the other experiments. The drop was not big indicating that the N_2 + CO_2 dioxide mix dissociated and/or redistributed a small amount of the hydrate phase with no large scale dissociation. Two large pressure drops, caused by an unstable BPV, were observed at 69 and 95 hours. The pressure drops were not big enough to dissociate any hydrate and should not have had any significant impact on calculations as no fluids were lost.

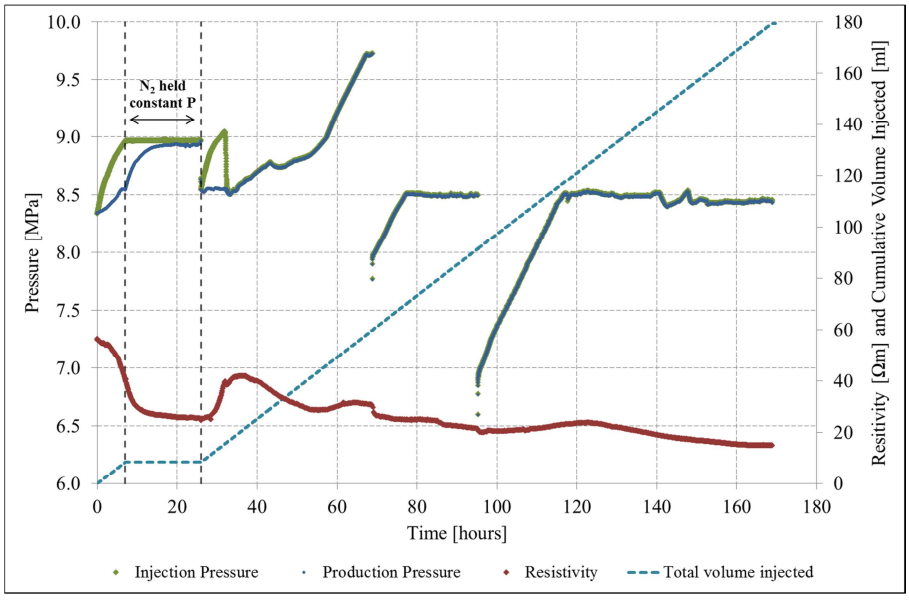

Figure 4.21: Resistivity, pressure and total volume injected during CO_2 – CH_4 exchange in HR_51. The pressure dropped abruptly twice during co-injection as a result of an unstable BPV.

HR_51 confirmed the results from HR_49 on the use of nitrogen to dissociate hydrate plugs and re-establishing injectivity, and the co-injections ability to hinder secondary hydrate formation which in very high saturation cores can lead to low gas permeability. The pressure and resistivity responses followed the same pattern.

The total methane recovery and the methane recovery from hydrate were calculated to be 61% and 52% respectively, but the GC had no connection to the computer in an 80 hour interval, as illustrated by the dotted lines in Figure 4.22 making the estimates highly uncertain.

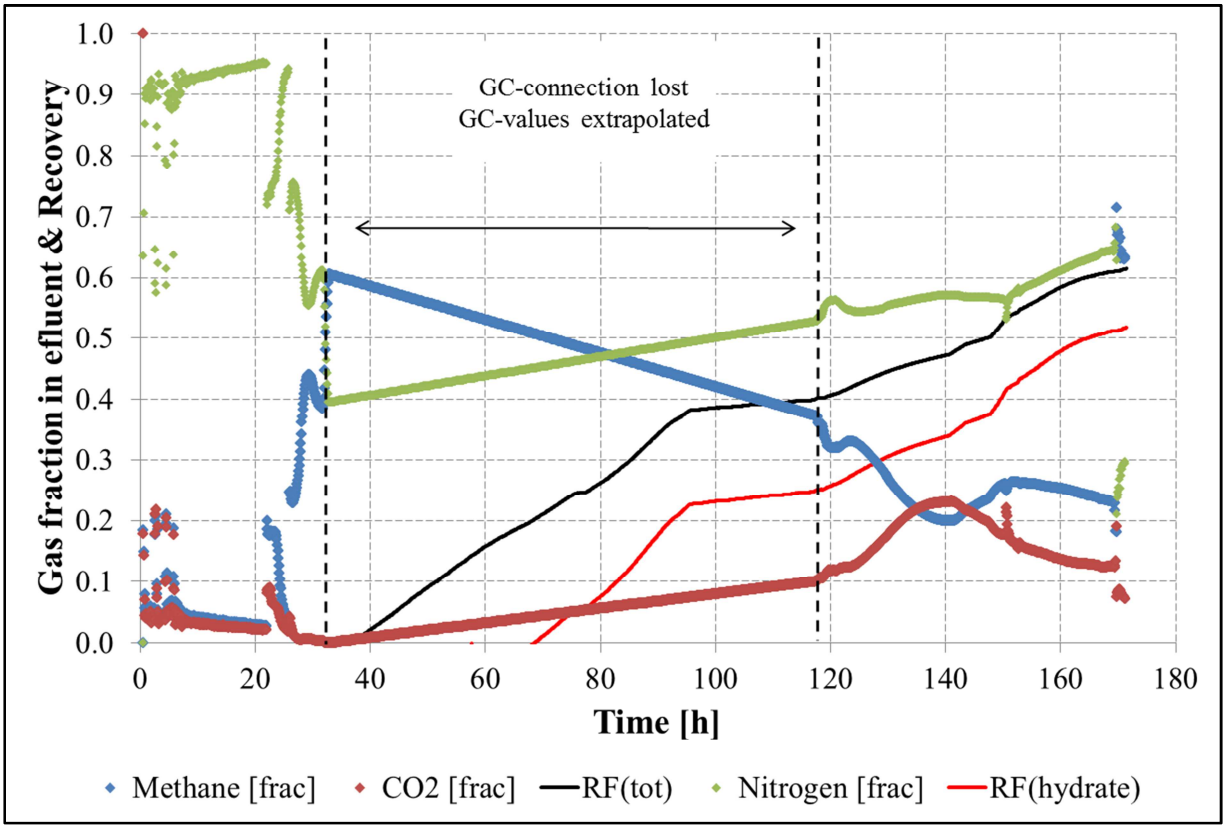

Figure 4.22: Recovery and methane fraction in effluent over time. The GC lost connection to the computer over a large time interval.

The mass flow was expected to increase as the fraction of CO_2 in the effluent decrease since liquid CO_2 has a significantly higher density compared to gases. The mass flow measurements obtained by the newly implemented MFM were lower during the 20 hours before GC-connection was reestablished indicating a low fraction of CO_2 during this interval, but the lack of similar experiments and the presence of large amounts of N_2 makes it difficult to predict the accuracy of the extrapolation. This core behaved differently than the others during formation (Section 4.1.3) were a different hydrate growth pattern was observed and an unusually high hydrate saturation was obtained. The core was therefore expected to behave differently during CO_2 – CH_4 exchange since the hydrate distribution most likely was significantly different. The effluent composition data which were obtained indicates a significant difference to HR_49 with higher methane fractions in the effluent. A possible explanation was the growth pattern which could have caused less free methane to be trapped

by hydrate and a larger hydrate surface area causing higher exchange rate. Another hypothesis was that the pure CO_2 injection in HR_49 caused a larger volume of CO_2 to be produced in the visible interval.

4.3.5 HR_52: Diffusion Driven Injection

Diffusion driven injection, where the core were shut-inn after a CO_2 flush, were performed on the fractured cores. Injecting CO_2 through a fractured core will to a large degree result in the CO_2 bypassing the core halves, making diffusion the main transport mechanism in the core halves. This method was also more time efficient with respect to the use of the mass balance system and has the potential to give a different perspective on the exchange process.

Figure 4.23 shows pressure, cumulative volume CO_2 injected and amount of CH_4 produced over time. The core was flushed with approximately 70 ml of liquid CO_2 at a rate of 0.25 ml/min. The pump was then set to hold constant pressure for approximately 20 hours before the system was isolated from the pump. The system consumed 30 ml of CO_2 during the 20 hours in a manner characteristic to hydrate formation. When the pressure support was removed, the pressure declined and stabilized at about 7.5 MPa again in a way reminiscent of hydrate growth.

A second CO_2 flush was performed after 192 hours where the system was isolated from the pump immediately after injection. The pressure dropped to 6.5 MPa over a period of 130 hours. A third flush was attempted, but plugging made injection impossible and the experiment was terminated.

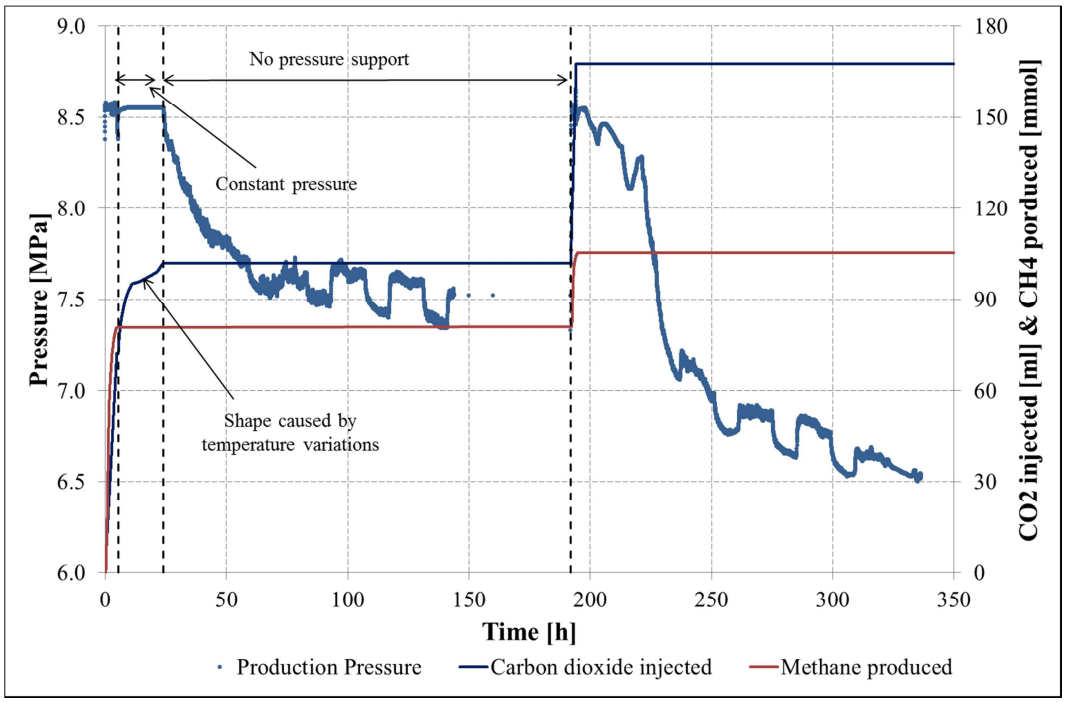

Figure 4.23: Pressure, cumulative volume CO_2 injected and cumulative volume methane produced over time.

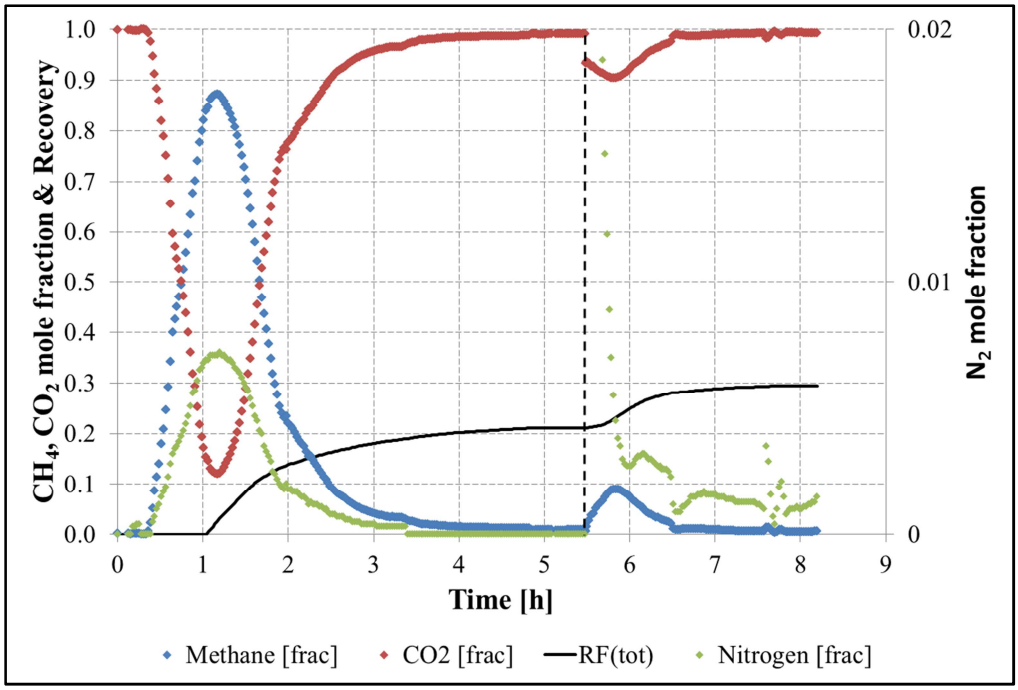

Figure 4.24: Composition of effluent and recovery during CO_2 – CH_4 exchange for HR_52. The dotted line represents the 8 days the core was shut-in between CO_2 flushes.

Effluent gas composition is plotted together with total methane recovery against time in Figure 4.24 above. The dotted line represents the shut in time and separates the two CO_2 flushes. The calculated $RF_{CH4,tot}$ and $RF_{CH4,H}$ were 45 and 14% respectively.

The first flush were observed to result in a similar effluent composition over time as to the normal injections, but much faster. The Second flush showed that a significant amount of methane had entered the fracture during the shut-in.

4.3.6 Effect of Initial Conditions

No apparent effects of varying initial water saturation or salinity were observed on the CO_2 – CH_4 exchange process. The cores with high initial saturation had problems with loss of injectivity when CO_2 injection was attempted. This was likely not caused by low permeability but rather hydrate plug formation at the end-pieces or in the tubing.

Figure 4.25 below show a comparison plot of methane fraction in effluent over time for all the continuous injections. The two experiments which were injected with pure CO_2 indicate good repeatability if the exchange procedures can be completed without problems.

The co-injections were observed to have a higher mole fraction of CH_4 in the effluent compared to the pure CO_2 injections. GC-data for HR_51 indicates a very large hydrate recovery despite the significant lack of data. This might have been an effect of a different growth pattern as it could lead to a significant difference in phase distributions. It should also be noted that the presence of N_2 could accelerate the exchange process since the amount of supersaturation would be lowered. N_2 cannot form simple hydrate at the experimental conditions, but simulations with CSMGem show small fractions of N_2 in hydrate when CH_4,

CO_2 and N_2 are in the presence of 3.5 wt% NaCl brine at these conditions. This indicates that N_2 may increase the maximum possible recovery as it would compete for the small cages in the sI structure.

A comparison of recoveries is not presented, as the time of termination, measurement methods and course of events has varied between the experiments. An observed correlation would therefore most likely be a random coincidence, not to be attributed to one of the variables studied in this thesis.

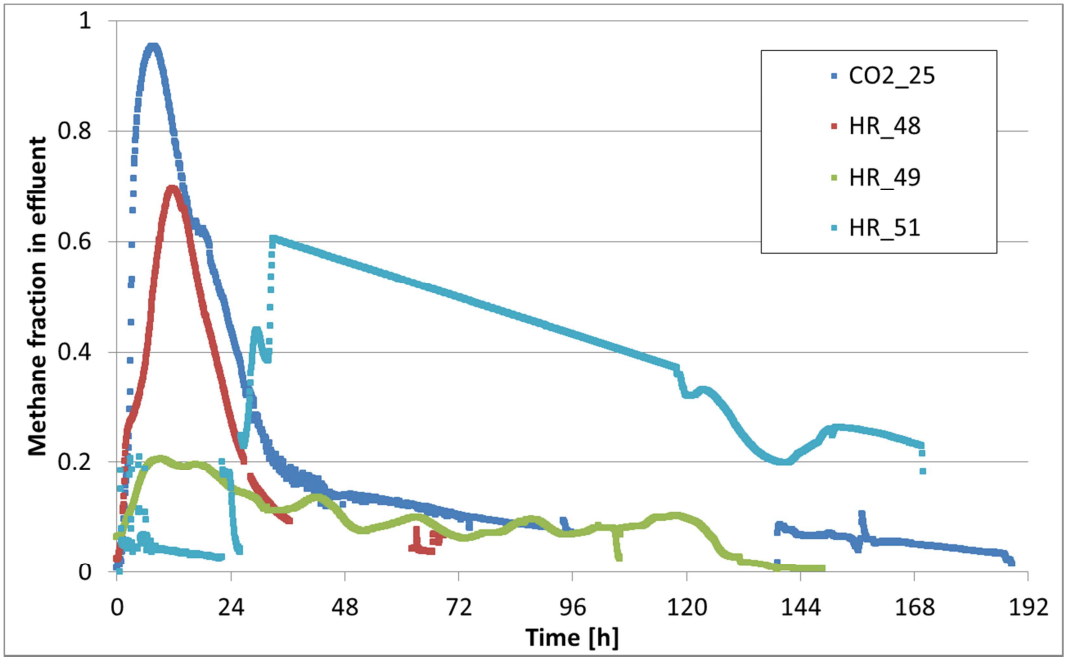

Figure 4.25: Comparison of the methane fraction in effluent over time.

4.4 Uncertainties

Calculations and measurements made during the experimental work for this thesis contain a number of uncertainties and sources of errors. The specific uncertainties are based on the margin of error in the equipment used, which is presented in Table 4.6 below. A qualitative discussion of possible sources of error is presented in the sections below.

Table 4.6: Uncertainty for equipment used in the experimental work.

Equipment	Measurement	Uncertainty (±)
Slide caliper	Length & diameter	0.005 cm
AND GF-3000 Digital Balance	Weight	0.02 g
ST Stigma 500	Flow	0.10 %
ST Stigma 500	Pressure	0.10 %
Temperature Gauge	Temperature	0.1 °C
Druck PMP	Pressure	0.08 %

4.4.1 Sources of Error in Core Preparation

During the core preparation process, there were many factors which could have led to erroneous results.

Heterogeneities in the cores were not taken into account and were considered to be a far bigger uncertainty than the Slide caliper. If the core plugs were not dried or cleaned properly it would lead to an underestimation of porosity.

Water would have evaporated out of the brine continuously after saturation of the core. A major potential source for errors was if a significant amount of water vaporized from the core prior to it being weighed. This could have been the case if the pressure were drawn to far down during vacuuming of the core or if the process of reducing the water saturation took a substantial amount of time. The result would be an underestimation of the brine salinity and a slight overestimation of the S_{wi}.

The evaporation of water could be observed when the core was on the scale by a steady decreasing weight which clearly demonstrates the insignificance of the scale uncertainty. An overestimation of the water saturation could have occurred if the core were not set into the core holder and isolated fast enough.

4.4.2 Sources of error in Hydrate Formation

The leakage rates were between 0.003 and 0.02 ml/hour and were calculated based on the amount of gas delivered to the system during a 24 hour period prior to formation where the systems were pressurized to 8.3 MPa. This was done in order to minimize the effect of temperature fluctuations. Change in leakage rates as a consequence of cooling and hydrate formation were considered insignificant as some of the rates were measured both before and after formation and gave a satisfactory matching result. The largest potential source for error

in these calculations was considered to be a possible increase in leakage rate caused by external factors, which could arise if the system were adequately disturbed. A potential significant temperature difference over the 24 hours when the leakage estimate was made, could also impact the leakage rate.

The room temperature fluctuations could have been a big source of errors since all the saturation changes are calculated based on PVT data from the pumps. The resulting density changes in the gas would cause the volume to fluctuate. The error caused by temperature would increase if the pump contained a large amount of gas.

These sources of error make the margin of error in the high precision pumps insignificant.

4.4.3 Sources of error in CO_2 – CH_4 Exchange

Calculations on the CO_2 – CH_4 exchange were considered uncertain since errors from earlier procedures would follow in addition to the probability of systematic errors being high.

Liquid CO_2 have vastly different properties than methane gas and the amount of fluids lost due to leakage was expected to increase significantly as liquid CO_2 was introduced to the system. CO_2 has previously shown a tendency to diffuse through the sleeve and into the confinement. The loss of CO_2 during exchange was considered too high for mass balance calculations on CO_2 to be used.

4.4.4 Assumptions

The hydration number used to calculate how much water was consumed during formation was found from bulk experiments at equilibrium. The impact of porous sediments is unknown but a slight decrease in hydration number was reported when methane hydrate was formed at significant supersaturation (Circone et al. 2005). A lower factual hydration number would lead to an overestimation of the amount of water going into hydrate and a subsequent overestimation of the hydrate saturation. The amount of methane in hydrate would be slightly underestimated (due to an underestimation of the gas saturation), but this error was considered to be insignificant. It should be noted that the decreased solubility of methane in water as salinity increases together with the reduction in thermodynamic driving force could impact the hydration number and cause it to change as conditions in the core changes.

Chapter 5 Conclusions and Future Work

5.1 Conclusions

- Nitrogen was found to effectively dissociate hydrate plugs without any large scale dissociation or observable negative effects on methane production.
- A 75 mol% N_2 + 25 mol% CO_2 co-injection were observed to effectively maintain a good connection through the core where pure CO_2 caused reduction in permeability.
- Hydrate formation kinetics in sandstone were observed to be strongly dependent on salinity and initial water saturation, where increasing salinity or S_{wi} led to slower hydrate growth.
- Salinity was found to be the limiting factor for final hydrate saturation in high salinity, low saturation cores.
- A linear correlation between initial water saturation and early growth rate were observed.
- Ten methane hydrate saturated cores were successfully produced from cores with S_{wi} ranging from 0.40 to 0.81 where the cores with S_{wi} above 0.6 retained an active water phase.
- CO_2 – CH_4 exchange were performed on five cores resulting in calculated methane recovery from hydrate between 0 and 52% and
- Redistribution of hydrate was observed indirectly by resistivity measurements and was found to increase dissociation rate during depressurization.
- Extremely fast hydrate growth were observed during formation in a core that five days earlier had contained hydrate which had been dissociated by temperature. This was attributed to the pressure which was held at 8.3 MPa at all times and could have led to an increased methane concentration in the core.
- An observed correlation between initial water saturation and residual water saturation after hydrate formation hints at a S_{wi} where the salinity no longer are the only limiting factor for the amount of hydrate formed.

5.2 Future work

The ability to analyze recovery with the current experimental procedure on CO_2 – CH_4 exchange can easily be improved by performing a small number of experiments which investigates the individual factors influencing the production of methane. A short list of suggestions is presented below followed by some unrelated suggestions for future work.

Production of a 100% methane saturated core with the same experimental procedures used during CO_2 – CH_4 would give a better picture of how the mass balance system behaves and increase the ability to interoperate results. Both co-injection and pure liquid CO_2 injection would be beneficial.

Results on production by gravity stable CO_2 injection would answer the question of whether the CO_2 contacts the entire core.

Depressurization of cores where exchange has been performed with pure CO_2 could give a good indication of the actual contribution to recovery from hydrate. The Depressurizations has to be done with sufficient time at each pressure step to give a usable value. GC analysis of the dissociated fluids would also be beneficial.

Performing experiments on hydrate bearing cores which has stood for a long time to let the hydrate redistribute could give a more realistic phase distribution during CO_2 – CH_4 exchange.

The newly implemented MFM has proven to be reliable and a valuable addition to the mass balance system. An effort should be made to further improve the reliability of the mass balance system. More results are needed on the exchange process, and the experiments need to be run for a longer period to obtain end-point data. This would lead to a very low experimental output rate with the current failure rate.

Nomenclature

ΔG	Gibbs free energy
ϕ	porosity
V_p	pore volume
V_b	bulk volume
K	absolute permeability
q	volumetric flow rate
A	Cross sectional area
μ	viscosity
dp/dx	pressure differential
$k_{i,e}$	effective permeability
$K_{r,i}$	relative permeability
P_c	Capillary pressure
l	length
R	resistivity
r	resistance
I	electrical current
E	applied voltage
L	length of the resistor
F	The formation factor
R_w	resistivity of the brine
RI	resistivity index
R_t	measured resistivity
b	saturation exponent
Z	impedance
ϕ	phase angle
RF	The recovery factor
N_p	produced [mol]
N	originally in place [mol]
S_{wi}	initial water saturation
S_{wf}	final water saturation
S_H	hydrate saturation
$RF_{CH4,tot}$	total methane recovery
$RF_{CH4,H}$	recovery from hydrate

References

Birkedal, K. A. (2009). Hydrate Formation and CH_4 Production from Natural Gas Hydrates - Emphasis on Boundary Conditions and Production Methods, The University of Bergen.

Birkedal, K. A., G. Ersland, et al. (2011). Electrical Resistivity Measurements of CH4-Hydrate Bearing Sandstone During Formation. 7th Conferance on Gas Hydrates. Edinburgh, Scotland.

Boswell, R. and T. Collett (2006). The gas hydrates resource pyramid: Fire in the Ice, Methane Hydrate Newsletter, U.S. Department of Energy, Office of Fossil Energy. National Energy Technology Laboratory, Fall Issue, p. 5–7. http://www.netl.doe.gov/technologies/ oil-gas/publications/Hydrates/Newsletter/ HMNewsFall06.pdf#page=5**:** 10--1039.

Chuvilin, E. M., V. A. Istomin, et al. (2011). "Residual nonclathrated water in sediments in equilibrium with gas hydrate: Comparison with unfrozen water." Cold Regions Science and Technology **68**(1–2): 68-73.

Circone, S., S. H. Kirby, et al. (2005). "Direct Measurement of Methane Hydrate Composition along the Hydrate Equilibrium Boundary." The Journal of Physical Chemistry B **109**(19): 9468-9475.

Collett, T. S. and G. D. Ginsberg (1998). Gas Hydrates in the Messoyakha Gas Field of the West Siberian Basin—A. Re-examination of the Geologic Evidence, International Journal of Offshore and Polar Engineering 8**:** 22--29.

Cussler, E. L. (2009). Diffusion: Mass Transfer in Fluid Systems, Cambridge University Press.

Ebinuma, T. (1993). Method for dumping and disposing of carbon dioxide gas and

apparatus therefor. N. Corporation. **US5261490 A**.

Ersland, G. (2008). Studies of Flow Mechanisms and Hydrate Phase Transitions in Fractured Rocks, University of Bergen.

Ersland, G., J. Husebø, et al. (2010). "Measuring gas hydrate formation and exchange with CO2 in Bentheim sandstone using MRI tomography." Chemical Engineering Journal **158**(1): 25-31.

Ersland, G., J. Husebø, et al. (2009). "Transport and storage of CO2 in natural gas hydrate reservoirs." Energy Procedia **1**(1): 3477-3484.

Graue, A., B. Kvamme, et al. (2008). "MRI Visualization of Spontaneous Methane Production From Hydrates in Sandstone Core Plugs When Exposed to CO2." SPE Journal **Volume 13**(Number 2).

Hauge, L. P. Ø. (2011). Resistivity Measurements during Gas Hydrate Formation and Subsequent CO_2 Exchange in Porous Sandstone. Department of physics and technology, University of Bergen. **Masters**.

Hester, K., J. Stevens, et al. (2011). Composition studies to determine rate and extent of CO2 exchange in a hydrate-bearing core. 7th Conferance on Gas Hydrates. Edinburgh, Scotland.

Hester, K. C. and P. G. Brewer (2009). "Clathrate hydrates in nature." Ann Rev Mar Sci **1**: 303-327.

Husebø, J. (2008). Monitoring Depressurization and CO2-CH4 Exchange Production Scenarios for Natural Gas Hydrates, University of Bergen.

Husebø, J., G. Ersland, et al. (2008). The effect of brine salinity on fill fraction and formation pattern of methane hydrates in sandstone. In: Proceedings of the Sixth International Conference on Gas Hydates.

Jeffrey, G. A. (1984). "Hydrate inclusion compounds." Journal of inclusion phenomena **1**(3): 211-222.

Jung, J. W., D. N. Espinoza, et al. (2010). "Properties and phenomena relevant to CH4-CO2 replacement in hydrate-bearing sediments." Journal of Geophysical Research: Solid Earth **115**(B10): B10102.

Kashchiev, D. and A. Firoozabadi (2002). "Nucleation of gas hydrates." Journal of Crystal Growth **243**(3–4): 476-489.

Kleinberg, R. L., C. Flaum, et al. (2003). "Deep sea NMR: Methane hydrate growth habit in porous media and its relationship to hydraulic permeability, deposit accumulation, and submarine slope stability." Journal of Geophysical Research: Solid Earth **108**(B10): 2508.

Koh, C. A. (2002). "Towards a fundamental understanding of natural gas hydrates." Chemical Society Reviews **31**(3): 157-167.

Kurihara, M., A. Sato, et al. (2010). Analysis of Production Data for 2007/2008 Mallik Gas Hydrate Production Tests in Canada. International Oil and Gas Conference and Exhibition in China. Beijing, China.

Kvamme, B. (2012). Lecture notes, PTEK 232.

Makogon, I. U. F. (1997). Hydrates of hydrocarbons, PennWell Publishing Company.

Makogon, Y. F. (2010). "Natural gas hydrates – A promising source of energy." Journal of Natural Gas Science and Engineering **2**(1): 49-59.

McGrail, B. P., H. T. Schaef, et al. (2007). Using Carbon Dioxide to Enhance Recovery of Methane from Gas Hydrate Reservoirs: Final Summary Report**:** Medium: ED; Size: PDFN.

Moridis, G. and T. Collett (2003). Strategies for gas production from hydrate accumulations under various geologic conditions.

Moridis, G. J. (2008). Toward Production From Gas Hydrates: Current Status, Assessment of Resources, and Simulation-Based Evaluation of Technology and Potential.

Ota, M., Y. Abe, et al. (2005a). "Methane recovery from methane hydrate using pressurized CO2." Fluid Phase Equilibria **228–229**(0): 553-559.

Ota, M., K. Morohashi, et al. (2005b). "Replacement of CH4 in the hydrate by use of liquid CO2." Energy Conversion and Management **46**(11–12): 1680-1691.

Park, Y., M. Cha, et al. (2008). Swapping Carbon Dioxide for Complex Gas Hydrate Structures. the 6th International Conference on Gas Hydrates. Vancouver, CANADA.

Park, Y., D.-Y. Kim, et al. (2006). "Sequestering carbon dioxide into complex structures of naturally occurring gas hydrates." Proceedings of the National Academy of Sciences **103**(34): 12690-12694.

Rees, V. L., T. J. Kneafsey, et al. (2011). "Methane Hydrate Distribution from Prolonged and Repeated Formation in Natural and Compacted Sand Samples: X-Ray CT Observations." Journal of Geological Research **2011**.

Schoderbek, D., K. L. Martin, et al. (2012). North Slope Hydrate Fieldtrial: CO2/CH4 Exchange. OTC Arctic Technology Conference. Houston, Texas, USA.

Sloan, E. D. and C. A. Koh (2008). Clathrate hydrates of natural gases. Boca Raton, Fla., CRC Press.

Stevens, J., J. J. Howard, et al. (2008). Experimental hydrate formation and gas production scenarios based on CO2 sequestration. Proceedings of the 6 th International Conference on Gas Hydrates.

Tohidi, B., R. Anderson, et al. (2001). "Visual observation of gas-hydrate formation and dissociation in synthetic porous media by means of glass micromodels." Geology **29**(9): 867-870.

Travesset, A. (2008). "The Many Phases Of Ice."

Tréhu, A. M., C. Ruppel, et al. (2006). "Gas hydrates in marine sediments: Lessons from scientific ocean drilling." Oceanography **19**(4): 124–142.

Xiuli Wang, M. J. E. (2011). "Natural Gas Hydrates as an Energy Source - Revisited." International Petroleum Technology Conference.

Zhou, X., S. Fan, et al. (2008). "Replacement of Methane from Quartz Sand-Bearing Hydrate with Carbon Dioxide-in-Water Emulsion." Energy & Fuels **22**(3): 1759-1764.

Zolotukhin, A. B. and J. R. Ursin (2000). Introduction to Petroleum Reservoir Engineering, Høyskoleforlaget AS.